Mathematical Models and Numerical Simulations of phase change in Lagrangian and Eulerian descriptions

By

Luis A. Quirós Fonseca

Submitted to the graduate degree program in Mechanical Engineering

and the Graduate Faculty of the University of Kansas

in partial fulfillment of requirements for the degree of

Master of Science.

_____

Dr. Karan S. Surana, Chairperson

_____

Dr. Albert Romkes

_____

Dr. Peter W. Tenpas

Date Defended: _____

The Thesis Committee for Luis A. Quirós Fonseca certifies

that this is the approved Version of the following thesis:

Mathematical Models and Numerical Simulations of phase

change in Lagrangian and Eulerian descriptions Committee:

_____

Dr. Karan S. Surana, Chairperson

_____

Dr. Albert Romkes

_____

Dr. Peter W. Tenpas

Date Approved:_____

Abstract

This thesis presents development of mathematical models for liquid-solid and solid-liquid phase change phenomena in Lagrangian and Eulerian descriptions. The mathematical models are derived by assuming a smooth interface (or transition region) between the solid and liquid phases in which the specific heat, thermal conductivity, density and latent heat are continuous and differentiable functions of temperature. The width of the interface region can be as large or as small as desired by a specific application. The derivations assume the matter to be homogeneous and isotropic.

In case of Lagrangian description we assume zero velocity field i.e. no flow with free boundaries i.e. stress free medium. Under these assumptions the mathematical model reduces to the first law of thermodynamics i.e. energy equation. The derivation is based on specific total energy and the heat vector. The constitutive theory for heat vector is assumed to be Fourier heat conduction law. The specific total energy incorporates the physics of phase change in the transition region between the solid and the liquid phases. This results in a time dependent non-linear diffusion equation in temperature. The physics of initiation of the phase change as well as formation and propagation of the transition region (front) is intrinsic in the mathematical model and hence no other means of front tracking are required. For the purposes of numerical simulation, the mathematical model can also be recast as a system of first order partial differential equations.

In case of Eulerian description, the mathematical model consists of the continuity equation, momentum equations, energy equation, constitutive theories for stress tensor and heat vector in the liquid phase, solid phase and as well in the transition region. In the liquid phase we assume the matter to be Newtonian fluid, hence the details of the mathemati-

cal model are straight forward. In the solid region we assume the solid to be hypoelastic, hence the rate constitutive theory is valid for the stress tensor. We also assume Fourier heat conduction law for the solid phase. In the transition region containing a mixture of solid and liquid phases, use of mixture theory is most appropriate for conservation laws as well as the constitutive theory. Such mathematical models are beyond the scope of the work considered in this thesis. Instead, we present a simple model that is based on representative volume fractions in the transition region. Eulerian descriptions are necessitated when phase change occurs in a flowing medium.

Regardless of whether the mathematical models utilize Lagrangian or Eulerian description, the resulting mathematical models consist of a system of non-linear partial differential equation in space and time, i.e. they constitute initial value problems. Numerical solutions of these mathematical models are obtained using space-time least squares finite element process based on minimization of residual functional. This approach results in space-time variationally consistent integral forms that yield symmetric algebraic systems with positive definite coefficient matrices that ensure unconditionally stable computations during the entire evolution. The local approximations for the dependent variables in the mathematical model are considered in h,p,k framework which permits higher degree as well as higher order space-time approximations in space and time. Numerical values of the evolution are computed using a space-time strip or a space-time slab corresponding to an increment of time with time marching. Numerical studies in $\mathbb{R}^1$ and $\mathbb{R}^2$ are presented to demonstrate simulation of the initiation of the phase change as well as its subsequent propagation during evolution. These studies cannot be performed using sharp interface and phase field models.

The smooth interface approach considered in the present work has many significant

benefits: (*i*) Continuous and differentiable transition region permits desired physics and avoids singular fronts that are nonphysical. (*ii*) The mathematical model in Lagrangian description result in a single non-linear PDE from the first law of thermodynamics which provides the ability to initiate as well as locate the phase transition front during evolution without using special front tracking methods. (*iii*) In Eulerian description the Navier Stokes equations and the constitutive theories for stress tensor and heat vector result in a system of non-linear PDEs with the same features for phase change initiation and propagation as in the case of Lagrangian description. (*iv*) The mathematical models and the computational approach presented here permits initiation of the phase transition interface and its propagation without employing any special means. This is not possible in sharp interface and phase field mathematical models. (*v*) The computational methodology employed in this work ensures unconditionally stable computations in which very high accuracy of evolution is possible for each time step during evolution.

Acknowledgements

I would like to acknowledge the invaluable contribution of my home university, the "Universidad de Costa Rica". Without your support and prior education, the successful completion of this journey would not have been possible. I am especially grateful to my professor and advisor, Dr. Karan S. Surana, Deane E. Ackers Distguished Professor of Mechanical Engineering, for his guidance. Dr. Surana helped me become a more confident and knowledgeable engineer. I also thank the other committee members, Dr. Albert Romkes and Dr. Peter Tenpas.

I would like to thank my friends and colleagues for their support and care. I want to express my love and gratitude to my family; my parents, brothers, grandparents, aunt, and uncles, for their unconditional support and love. This work is dedicated to my parents and my grandparents.

Contents

List of Tables

List of Figures

Nomenclature

ρ	Density
c	Specific Heat
c_p	Specific Heat
c_s	Specific Heat in Solid Phase
c_{ps}	Specific Heat in Solid Phase
c_l	Specific Heat in Liquid Phase
c_{pl}	Specific Heat in Liquid Phase
k	Thermal Conductivity
k_s	Thermal Conductivity in Solid Phase
k_l	Thermal Conductivity in Liquid Phase
L	Latent Heat of Fusion
L_f	Latent Heat of Fusion
T	Temperature
T_s	Temperature in Solid Phase
T_l	Temperature in Liquid Phase
T_{sat}	Saturation Temperature
t	Time
$\boldsymbol{n}$	Unit Exterior Normal

v_n	Normal Velocity of Sharp Interface
Γ	Liquid-Solid Interface Boundary
Ω	Domain
Ω_x^s	Domain of Solid
Ω_x^l	Domain of Liquid
h	Enthalpy
h_s	Specific Enthalpy
S	Source Term
f	Liquid Fraction
p	Phase Field Variable
F	Free Energy Functional
ξ	Parameter that Controls Interface Length in Phase Field
ε	Interface Length in Phase Field
α	Relaxation Time
$\boldsymbol{q}$	Heat Conduction
q_x	Heat Conduction in x-direction
q_y	Heat Conduction in y-direction
e	Specific Total Energy
$\boldsymbol{v}$	Velocity
p	Pressure
$\boldsymbol{F}^b$	Body forces
$\boldsymbol{\sigma}^{(0)}$	Contravariant Cauchy stress tensor
${}_d\boldsymbol{\sigma}^{(0)}$	Deviatoric contravariant Cauchy stress tensor

$\boldsymbol{\gamma}^{(1)}$	Symmetric part of the velocity gradient tensor
$\boldsymbol{D}$	Symmetric part of the velocity gradient tensor
Re	Reynolds number
Ec	Eckret number
Br	Brinkman number
$\boldsymbol{\nabla}$	Del (Gradient) Operator
$\boldsymbol{\phi}$	Vector of Dependent Variables
$\boldsymbol{\phi}_h$	Global Approximation of $\boldsymbol{\phi}$
$\boldsymbol{\phi}_h^e$	Local Approximation of $\boldsymbol{\phi}$
n_e	Number of Equations
p-level	Degree of Local Approximation
E_i^e	Error (Residual) Equation for an Element 'e'
V_h	Approximation Space
$I(\boldsymbol{\phi}_h)$	Error Functional in Least Squares Finite Element Formulation
$\boldsymbol{g}$	Measure of how well GDE is Satisfied in Point-Wise Sense
PDEs	Partial Differential Equations
IVPS	Initial Value Problems
AHC	Apparent Heat Capacity Method
LINH	Linearization Method
GM	Galerkin Method
STGM	Space-time Galerkin Method
PGM	Petrov Galerkin Method
STPGM	Space-time Petrov Galerkin Method

WRM	Weighted Residuals Method
STWRM	Space-time Weighted Residuals Method
GM/WF	Galerkin Method with Weak Form
STGM/WF	Space-time Galerkin Method with Weak Form
STVC	Space-time Variational Consistent
STVIC	Space-time Variational Inconsistent
LSFEF	Least Squares Finite Element Formulation
STLSP	Space-time Least Squares Process

Chapter 1

Introduction, Literature Review and Scope of Work

1.1 Introduction

The phase change phenomena in which the matter transitions and transforms from one state to another is of significant academic and industrial importance. Solid-liquid or liquid-solid phase transitions and their numerical simulation has been a subject of research and investigation over a century. There are many sources of difficulties in the numerical simulation of phase change phenomena. Phase transition physics and its mathematical modeling is quite complex due to the fact that this phenomenon creates a transition region, a mixture of solid and liquid phases, in which the phase change occurs resulting in complex changes in transport properties such as density, specific heat, conductivity and the latent heat of fusion that are dependent on temperature. During evolution the phase transition region propagates in spatial directions, i.e. its location changes as the time elapses. Ideal-

ized physics of phase change, in which jumps in the transport properties is often assumed, results in singular interfaces. As a consequence the mathematical models describing such evolution result in initial value problems that contain singularities at the interfaces. When solving such non-linear initial value problems, one must assume existence of the interface. Numerical simulation of the propagation of such fronts during evolution also presents many difficulties that cannot be resolved satisfactorily. Major shortcomings of this approach are that formation of the phase transition front cannot be simulated. Secondly, singular nature of the front is obviously not possible to simulate numerically.

In the second approach of phase transition physics and its mathematical modeling, one assumes that the phase transition region is of finite width, i.e. the phase transition occurs over a finite but small temperature range in which the transport properties such as density, specific heat, conductivity and latent heat are function of temperature and vary in a continuous and differentiable matter between the two states. Thus, the phase transition region is of finite width in temperature that propagates as time elapses. This approach is more realistic and more appealing form the point of view of numerical simulations of the resulting IVPs from the mathematical models as it avoids singularities present in the first approach. The phase-field approach utilizes this concept. A major source of difficulty in this approach is the physics of the transition region often referred to as 'mushy region' that consists of liquid-solid mixture in varying volume fractions as one advances from one state to the other. Adequate mathematical modeling of the physics in the transition region requires use of mixture theory [1–3], based on thermodynamic principles of continuum mechanics. Conservation of mass, balance of momenta, first law of thermodynamics and the constitutive theories for stress tensor and heat vector based on the second law of thermodynamics must all be reformulated assuming thermodynamic equilibrium in the transition

region. This approach of mathematical modeling of the transition region has not been explored in the published literature (to our knowledge), but must be considered to account for the realistic physics.

The third and perhaps another vital issue lies in the selection of the methods of approximation that are utilized to obtain numerical solutions of the initial value problems describing evolution. It is now well established in computational mathematics that methods of approximation such as finite difference, finite volume and finite element methods based on Galerkin Method (GM), Petrov-Galerkin method (PGM), weighted residual method (WRM), and Galerkin method with weak form (GM/WF) used in context with space-time decoupled or space-time coupled methodologies are inadequate for simulating time accurate evolutions of the non-linear IVPs describing phase change processes [4–9].

Thus, in order to address numerical solutions of phase transition processes, in our view a simple strategy would be to: (i) Decide on a mathematical model with desired but limited physics. (ii) Employ a method of approximation that does not disturb the physics in (i), results in unconditionally stable computations and has inherent (built in) mechanism of the measure of error in the computed solution without the knowledge of theoretical solution as such solutions may not be obtainable for the problem of interest. The work presented in this thesis follows this approach. In the following we present literature review on mathematical modeling and methods of approximation for obtaining numerical solutions of the IVPs resulting from the mathematical models. This is followed by the scope of work undertaken in this thesis.

1.2 Literature Review

In this section we present some literature review that is pertinent in context with the approach utilized in the research work presented in this thesis. We group the literature review in two major categories: mathematical models and methods of approximation for obtaining numerical solutions of the initial value problems resulting from the mathematical models.

1.2.1 Mathematical Models: Lagrangian Description

A large majority of published work on the mathematical models for phase change processes consider Lagrangian description only with further assumptions of zero velocity field, i.e. no flow and free boundaries i.e. the medium undergoing phase change to be stress free. We first present literature review and a discussion of commonly used mathematical modeling methodologies in Lagrangian description based on the assumptions stated above. With the assumptions of no flow and stress free medium, the mathematical the mathematical model of the phase change process reduces to energy equation. In the published works there are three commonly used approaches: sharp interface models, enthalpy models and phase field models.

In the mathematical models derived using sharp interface the liquid and solid phases are assumed to be separated by a hypothetically and infinitely thin curve or surface called sharp phase. The transport properties such as density, specific heat and conductivity are assumed to experience a jump at the interface. The latent heat of fusion is assumed to be instantaneously released or absorbed at the interface. This of course results in step (sharp) change in the transport properties and latent heat of fusion at the interface, hence the name

sharp interface models. The mathematical models for liquid and solid phases are derived individually. At the interface, energy balance provides an additional relation (equation) that is used to determine the movement of the interface. The sharp interface models are also called Stefan models derived by J. Stefan [10] to study freezing of ground. The derivation of this model is presented in Chapter 2. The proof of existence and uniqueness of the classical solution of the Stefan mathematical model has been given by Rubinstein [11] in 1947. An analytical solution for temperature for one dimensional Stefan problem has been presented in reference [12]. The sharp interface models have three major shortcomings: (*i*) Assumption of sharp interface leads to mathematical model in which the initial value problem contains singularity at the interface. (*ii*) When obtaining solutions of the initial value problems based on sharp interface assumption, the location of the interface is required a priori. That is sharp interface models are unable to simulate the formation of the interface or front. (*iii*) Movement of the interface i.e. spatial location during evolution requires use of what are called front tracking methods.

The second category of mathematical models for phase change processes are called enthalpy models. In these models the energy equation is recast in terms of enthalpy and temperature with an additional equation describing enthalpy. Both enthalpy and temperature are retained as dependent variables in the mathematical model. Computations of the numerical solution of the resulting initial value problem are performed on a fixed discretization. This approach eliminates energy balance equation at the interface used in the sharp interface models. These mathematical models have been derived using different approaches [13–15]. Enthalpy model is also presented in Chapter 2. These models generally introduce a finite phase transition region (over a small temperature change) called mushy region between the liquid and the solid phases. The transport properties are assumed to

vary in some manner from one phase to the other phase. The concept of liquid or solid fraction is generally introduced to account for the fact that the mushy region is a mixture of solid and liquid phases. Due to the assumption of the mushy region separating the solid and the liquid phases, sharp interface is avoided in this approach.

The third category of mathematical models are called phase field models. These mathematical models are based on the work of Cahn and Hilliard [4]. In this approach the solid and liquid phases are also assumed to be separated by a finite width (in temperature) transition region in which the transport properties are assumed to vary with temperature between the two states. Landau-Ginzburg [5] theory of phase transition is used to derive the mathematical model. The basic foundation of the method lies in standard mean theories of critical phenomena based on free energy functional. Thus, the method relies on specification of free energy density functional which is the main driving force for the movement of the phase transition region. Details of phase field mathematical model in $\mathbb{R}^1$ are presented in Chapter 2. The method shows good agreement with the Stefan problem in $\mathbb{R}^1$. While the phase field models eliminate the sharp interfaces and their tracking, the main disadvantages of this approach are: (*i*) It requires a priori knowledge of the free energy density function for the application at hand. (*ii*)The mathematical model is incapable of simulating the initiation or formation of the solid-liquid interface, hence the liquid-solid phases and the transition region must be defined as initial conditions. This limitation is due to specific nature of the free energy function (generally a double well potential, see Chapter 2). However, if a liquid-solid interface is specified as initial condition, then the phase field models are quite effective in simulating the movement of the front during evolution. In most applications of interest, simulation of the formation of the transition region i.e. solid-liquid interface is essential as it may not be possible to know its location a priori.

These limitations have resulted in lack of wide spread use of these mathematical models in practical applications.

1.2.2 Mathematical Models: Eulerian Description

When the velocity of the medium is not zero (as in case of flow of a fluid), the mathematical models discussed in the section 1.2.1 are not applicable. In such cases Eulerian description is ideally suited. The mathematical model in this case consists of conservation of mass, balance of momenta, first law of thermodynamics and constitutive theory for stress tensor and heat vector based on the second law of thermodynamics for each of the two phases (i.e. liquid and solid) as well as the transition region.

The published works on these mathematical models is rather sketchy, the models are not based on rigorous derivation and in most cases are aimed at solving a specific problem as opposed to developing a general infrastructure that addresses totality of a large group of applications. We present some account of the published works in the following. Almost in all cases fluid is treated as Newtonian fluid. In some cases [16] the fluid is also considered inviscid. Sharp interface models generally force (set) the relative movement of the material particles to be zero in the solid phase [17, 18]. In case of enthalpy and phase field models the constitutive theory for the transition region is still unclear and published works in many instances are conflicting. There are three main ideas that are commonly found in the majority of the published works on mathematical models using Eulerian description: (*i*) In the first approach both the liquid and the solid phases are assumed to be Newtonian fluids. The viscosity in the solid phase is artificially increased to a very high value and is assumed to vary along the interface between the two states in order to approximate no

velocity condition in the solid phase [19]. (*ii*) In the second approach a varying interfacial force is employed such that it satisfies the no velocity condition in the solid phase [20]. (*iii*) The third approach assumes that the solid particles in the transition region form a porous medium through which the fluid flows. Voller and Cross [15] use Darcy model for flow in porous media in which the velocity field is assumed to be proportional to the pressure gradient in order to compare their results with variable viscosity model. Beckermann [21] assumed the average stress to be proportional to the gradient of superficial liquid viscosity in the porous media. There are other approaches [22] that utilize these three basic ideas in some manner or the other. In most cases, solid phase behavior is neglected by setting the velocity to zero. In general, our conclusion is that published phase change models in Eulerian description are crude, ad hoc and are aimed to obtain some numerical solutions for specific applications. A general theory of mathematical modeling based on thermodynamic principles and continuum mechanics is not available to our knowledge.

1.2.3 Computational Methodology

Regardless of the type of description (i.e. Lagrangian or Eulerian) the resulting mathematical models for phase change phenomena are non-linear partial differential equations in dependent variables, space coordinates and time, hence they are non-linear initial value problems. If we incorporate realistic physics of phase transition, the mathematical models become complex enough not to permit determination of theoretical solution, hence numerical solutions of these IVPs based on methods of approximation is necessary. The methods of approximation for IVPs can be classified in two broad categories [6–9] : space-time decoupled methods and space-time coupled methods. In space-time decoupled methods, for

an instant of time, the spatial discretization is performed by assuming the time derivatives to be constant. This approach reduces the original PDEs in space and time to ODEs in time which are then integrated using explicit or implicit time integration methods to obtain evolution. Almost all finite difference, finite volume and finite element methods (based on GM/WF) used currently [7] for initial value problems fall into this category. The assumption of constant time derivatives necessitates extremely small time increments during the integration of ODEs in time. The issues of stability, accuracy and lack of time accuracy of evolution are all well known in the space-time decoupled approaches. Majority of the currently used methods of approximation for phase change processes fall into this category. The non-concurrent treatment in space and time in space-time decoupled methods is contrary to the physics in which all dependent variables exhibit simultaneous dependence on space coordinates and time. In a large majority of published works on phase change processes, often the distinction between the mathematical models and the computational approaches is not clear either i.e. elements of the methods of approximation are often introduced during the development of the mathematical models. As a consequence, it is difficult to determine if the non-satisfactory numerical solutions are a consequence of the methods of approximation used or the deficiencies in the mathematical models.

The space-time coupled methods on the other hand maintain simultaneous dependence of the dependent variables on space coordinates and time [6, 8, 9]. In these methods the discretizations in space and time are concurrent as required by the IVPs. These methods are far more superior than the space-time decoupled methods in terms of mathematical rigor as well as accuracy. Whether to choose space-time finite difference, finite volume or finite element method depends upon the mathematical nature of the space-time differential operator and whether the computational strategy under consideration will yield unconditionally

stable computations, will permit error assessment, and will yield time accurate evolution upon convergence.

1.3 Scope of Work

In the present work we consider phase change processes in $\mathbb{R}^1$ and $\mathbb{R}^2$ using Lagrangian as well as Eulerian descriptions. The mathematical models in Lagrangian description are constructed with the assumption of no flow and stress free medium. Thus, the mathematical models in this case consist of the energy equation and heat flux(es), a system of first order PDEs in temperature and heat flux(es). By substituting heat flux(es) in the energy equation the mathematical model can be reduced to a single non-linear diffusion equation in temperature. In the derivation of the energy equation the specific total energy is expressed in terms of storage and latent heat of fusion. The Fourier heat conduction law is assumed to hold. In the solid and liquid phases the transport properties (ρ, c_p, k, L_f) are assumed to be constant. In the transition region the solid-liquid mixture is assumed to be isotropic and homogeneous. The transport properties are assumed to vary in a continuous and differentiable manner, third or fifth degree polynomials with continuous temperature derivatives at the boundaries between the transition region and the solid and liquid phases. With this approach the phase change process is a smooth process in which the transition region provides the smooth interface.

In the Eulerian description, necessitated in phase change processes with flowing medium, the mathematical models consist of: continuity equation, momentum equations, energy equation and the constitutive equations for deviatoric contravariant Cauchy stress tensor and heat vector. We summarize details in the following:

(*i*) In the liquid phase (assumed incompressible), we consider standard continuity equation, momentum equations, energy equation, Newton's law of viscosity for deviatoric Cauchy stress tensor and Fourier heat conduction law with constant transport properties.

(*ii*) In the solid phase, the continuity equation is replaced with pressure constraint equation. This is essential to ensure that mechanical pressure is indeed mean normal Cauchy stress. The momentum and energy equations remain the same as in the case of liquid phase except an additional term in the energy equation due to velocity field not being divergence free. The constitutive equations for deviatoric Cauchy stress tensor are rate equations based on the hypoelastic solid assumption. Fourier heat conduction law is assumed to hold.

(*iii*) In the transition region, the continuity equation is replaced with the pressure constraint equation plus continuity equation (divergence free velocity field) with volume fractions determined using relative position in the transition region defined by $[T_s, T_l]$. Momentum equations and the energy equation remain the same as in liquid or solid phases with solid volume fraction assigned to the divergence free velocity field term in the energy equation. The constitutive equations for deviatoric Cauchy stress are the sum of the weighted residuals of the constitutive equation for deviatoric Cauchy stress for liquid and solid phase. The weight factors used are the volume fractions based on the location in the transition region. Fourier heat conduction law is also assumed to hold in the transition region.

(*iv*) As in Lagrangian descriptions, the transport properties are assumed to vary in a continuous and differentiable manner in the transition region.

(*v*) The mathematical models in Eulerian description as well as Lagrangian description are derived using heat flux(es) as dependent variable(s). Heat flux(es) can be eliminated by substituting them in the energy equation but at the cost of higher order derivatives of the temperature with respect to spatial coordinates. However, in Eulerian descriptions the deviatoric Cauchy stresses must remain dependent variables, as the rate constitutive equations do not permit explicit expressions for them in terms of strain rates.

(*vi*) This mathematical model is a rather complex system of nonlinear PDEs in spatial coordinates and time in which their explicit form depends upon: whether heat flux(es) are used as dependent variables or not.

In Lagrangian as well as in Eulerian descriptions, L_f is not used as a dependent variable (as in reference [23]). It is shown that using L_f as independent variable in the mathematical model affects linear heat conduction adversely for low p-levels. Numerical solutions of IVPs described by the mathematical model are obtained using space-time finite element processes based on residual functional (STLSP) for an increment of time with time marching.

Numerical studies in Lagrangian description consist of liquid-solid and solid-liquid phase change problems in $\mathbb{R}^1$ and $\mathbb{R}^2$. The liquid and solid phases are assumed to be water and ice. Numerical studies in $\mathbb{R}^1$ are presented using a single energy equation in temperature with space-time local approximations of class C^{11}. Numerical studies in $\mathbb{R}^2$ are presented using the mathematical model consisting of first order PDEs with C^{00} space-time local approximation to demonstrate their usefulness due to smoothness of the evolution.

Numerical studies in Eulerian description are presented using flow between parallel

plates as a model problem. Additional numerical studies are also presented: (1) for mathematical model using L_f as a dependent variable, (2) using continuity equation as opposed to pressure constraint equation for solid phase, and (3) simulation of viscous dissipation in the presence of externally applied heat flux and the role of higher p-levels.

Chapter 2

Mathematical Models in Lagrangian Description

2.1 Introduction

In this chapter we present mathematical models describing phase change processes in Lagrangian description that are commonly used in the published works. These include: sharp interface, enthalpy, and phase field models. These are followed by the mathematical model used in reference [23] and the mathematical models used in the present work. The mathematical models used in published works for phase change are only presented for the one dimensional case (for the sake of brevity). All mathematical models presented in this chapter are based on the following assumptions.

(a) The mathematical models use Lagrangian description i.e. the position coordinates of the material points in the reference configuration (fixed) and time are independent variables.

(b) We assume velocity field to be zero i.e. no flow assumption.

(c) The configurations of the matter during evolution are assumed to be stress free i.e. the IVPs describing phase change evolution are posed as free boundary problems.

(d) We assume the matter to be homogeneous and isotropic and incompressible regardless of the phase.

(e) Based on assumptions (b) and (c), conservation of mass and balance of momenta are identically satisfied, hence only the energy equation needs to be considered in the development of the mathematical model in addition to the constitutive theory for the heat vector.

(f) Due to the assumption (b), the viscous effects are absent in the energy equation.

In the derivation of the energy equation the physics of phase change is incorporated in different forms depending upon the choice of modeling approach (i.e.sharp interface, enthalpy, phase field or smooth interface, etc.).

2.2 Sharp Interface Model

Under the assumption stated above (section 2.1), the energy equation reduces to heat conduction in homogeneous and isotropic medium. In this approach we assume that the solid and liquid phases are separated by an infinitely thin interface (in temperature). These mathematical models generally assume constant and same specific heat c_p, density ρ, and conductivity k in both phases. Consider case in $\mathbb{R}^1$:

Solid Phase:

$$\rho c_{ps}\frac{\partial T}{\partial t} - \boldsymbol{\nabla}\cdot(k_s\boldsymbol{\nabla}T_s) = 0 \qquad \forall\,(x,t)\ \in\ \Omega^s_{xt} = \Omega^s_x \times \Omega_t = \Omega^s_x \times (0,\tau) \tag{2.1}$$

Liquid Phase:

$$\rho c_{pl}\frac{\partial T}{\partial t} - \boldsymbol{\nabla}\cdot(k_l\boldsymbol{\nabla}T_l) = 0 \qquad \forall\,(x,t)\ \in\ \Omega^l_{xt} = \Omega^l_x \times \Omega_t = \Omega^l_x \times (0,\tau) \tag{2.2}$$

At the interface:

$$L_f\rho v_n = [(-k_s\boldsymbol{\nabla}T_s) - (-k_l\boldsymbol{\nabla}T_l)]\cdot\boldsymbol{n} \qquad \forall\,(x,t)\ \in\ \Gamma_{x,t} = \Gamma_x \times \Omega_t \tag{2.3}$$

where

$$\boldsymbol{\nabla} = \frac{\partial}{\partial x} \tag{2.4}$$

Ω^s_x and Ω^l_x are solid and liquid spatial domains. $\Gamma_x(t) = \Omega^s_x \bigcap \Omega^l_x$ is the interface between the solid and liquid phases. L_f is the latent heat of fusion, $\boldsymbol{n}$ is the unit exterior normal from the solid phase at the interface, and v_n is the normal velocity of the interface. Subscripts and superscripts s and l stand for solid and liquid phases.

When the mathematical model is posed as a system of integral equations, a complete proof of existence and uniqueness of the classical solution in $\mathbb{R}^1$ phase change was given by Rubinstein in 1947 [11]. For the one dimensional case, analytical solutions to some specific problems are derived in reference [12] for the temperature distribution $T = T(x,t)$. One example problem solves for T in the domain $x \geq 0$ with initial and boundary conditions:

$$T(x,0) = T_0 \qquad ;\quad x\ > 0 \tag{2.5}$$

$$T(0,t) = 0 \qquad ;\quad t\ \geq 0 \tag{2.6}$$

$$T(x,t) \to T_0 \qquad ;\quad \text{as } x \to \infty \tag{2.7}$$

where $T_0 > T_{sat} > 0$. Then the solution is

$$T(x,t) = \frac{T_{sat}}{\text{erf}(\lambda)}\text{erf}\left(\frac{x}{2\sqrt{\alpha t}}\right) \qquad ; \quad x \ \leq \Gamma_{xt}(t) \tag{2.8}$$

$$T(x,t) = T_0 - \frac{(T_0 - T_{sat})}{\text{erfc}(\lambda)}\text{erfc}\left(\frac{x}{2\sqrt{\alpha t}}\right) \qquad ; \quad x \ > \Gamma_{xt}(t) \tag{2.9}$$

$\alpha = \dfrac{k}{\rho c_p}$ is thermal diffusivity, and λ is obtained from solving the following equation.

$$\frac{1}{\text{erf}(\lambda)} - \frac{(T_0 - T_{sat})}{T_{sat}\text{erfc}(\lambda)} = \frac{e^{\lambda^2}\lambda L_f\sqrt{\pi}}{c_p T_{sat}} \tag{2.10}$$

The location of the interface, $\Gamma_{xt}(t)$, is defined by

$$\Gamma_{xt}(t) = 2\lambda\sqrt{\alpha t} \tag{2.11}$$

In this mathematical model the enthalpy increases or reduces by a large amount at a constant temperature. This poses serious problems in numerical simulations of the IVPs described by these models. Sharp interface, of course is a singularity that is not possible to account for properly in the numerical processes.

2.3 Enthalpy Models

Various forms of the enthalpy models are used in published works. We present two typical mathematical models in the following. The first mathematical model is due to references [13, 14].

$$\frac{\partial}{\partial t}(\rho h) - \boldsymbol{\nabla}\cdot(k\boldsymbol{\nabla}T) = S \qquad \forall\ (x,t)\ \in\ \Omega_{xt} = \Omega_x \times \Omega_t \tag{2.12}$$

$$h = h_s + fL + c(T - T_{sat}) \tag{2.13}$$

$$f = \begin{cases} 0 & ; \quad h < h_s \\ \dfrac{h - h_s}{L_f} & ; \quad h_s \leq h \leq h_s + L \\ 1 & ; \quad h > h_s + L \end{cases} \tag{2.14}$$

Let

$$H = \rho \left(h_s + fL - cT_{sat} \right) \tag{2.15}$$

Then

$$\rho h = H + \rho cT \tag{2.16}$$

Substituting (2.16) into (2.12)

$$\frac{\partial}{\partial t} \left(\rho cT \right) + \frac{\partial H}{\partial t} - \boldsymbol{\nabla} \cdot \left(k \boldsymbol{\nabla} T \right) = S \qquad \forall \ (x,t) \ \in \ \Omega_{xt} \tag{2.17}$$

and

$$H = \rho \left(h_s + fL - cT_{sat} \right) \tag{2.18}$$

f is defined by (2.14); and $\boldsymbol{\nabla} = \dfrac{\partial}{\partial x}$

h_s is the saturation enthalpy of the solid, T_{sat} is the saturation temperature, L is the latent heat, c is the specific heat, S is a source term and f is the liquid fraction that accounts for the latent heat capacity present.

Another mathematical model presented in the following is from reference [24].

$$\frac{\partial h}{\partial t} - \boldsymbol{\nabla} \cdot \left(k(T) \boldsymbol{\nabla} T \right) = 0 \quad \forall \ (x,t) \ \in \ \Omega_{xt} = \Omega_x \times \Omega_t \tag{2.19}$$

$$T = \begin{cases} \dfrac{h}{\rho c_s} & ; \quad h < \rho c_s T_f \\ u_T & ; \quad \rho c_s T_f \leq h < \rho \left(c_s T_f + L \right) \\ T_f + \left(h - \dfrac{\rho \left(c_s T_f + L \right)}{\rho c_l} \right) & ; \quad h \geq \rho \left(c_s T_f + L \right) \end{cases} \tag{2.20}$$

where T is temperature, $h(T)$ is enthalpy, $k(T)$ is thermal conductivity, c_s and c_f are the specific heat in the solid phase and liquid phases, T_f is the fusion temperature, and L is the latent heat of fusion. Generally $k(T)$, the temperature dependent thermal conductivity is taken to be k_s and k_l in the solid and liquid phases.

Most currently used enthalpy models lack comparison with sharp interface and phase field solutions. These models generally use a larger transition region.

2.4 Phase Field Models

Phase field models are based on the work of Cahn and Hilliard [4] and are derived using Landau-Ginzburg theory of critical phenomena [5]. Let p be the phase field variable. For a pure material, p is assigned a value of -1 in the solid phase and $+1$ in the liquid phase. The length of the transition region between solid and liquid phases is controlled by ξ (Figure 2.1).

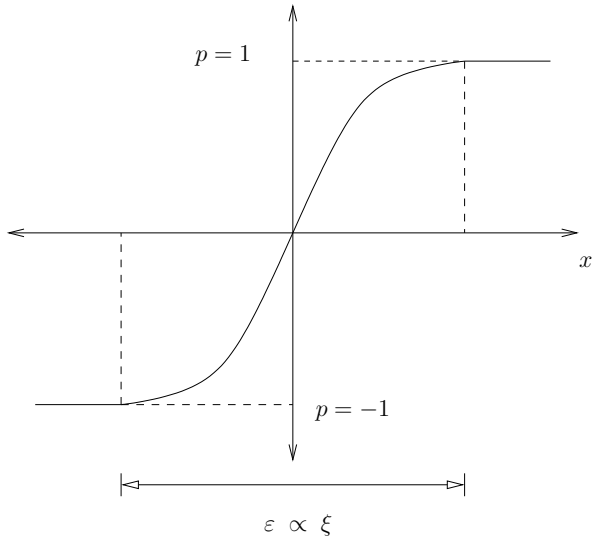

Figure 2.1: Phase field variable p width(ε)

The method is derived using standard mean theories of critical phenomena where the free energy functional is defined by:

$$F(p,T) = \int \left(\frac{1}{2}\xi^2 (\nabla p)^2 + f(p,T) \right) dV \tag{2.21}$$

where ξ is a parameter proportional to the interface thickness ε, and $f(p,T)$ is the free energy density of the system which often takes the form of a double well potential, for example:

$$f(p,T) = \frac{1}{8a}\left(p^2 - 1\right)^2 - \frac{\Delta s}{2} pT \tag{2.22}$$

Δs is the entropy change from the liquid to solid, and a is an scaling parameter (see [25, 26]). A plot of $f(p,T)$ as a function of p for $T = 0$, $T < 0$, $T > 0$ is shown in figure 2.2.

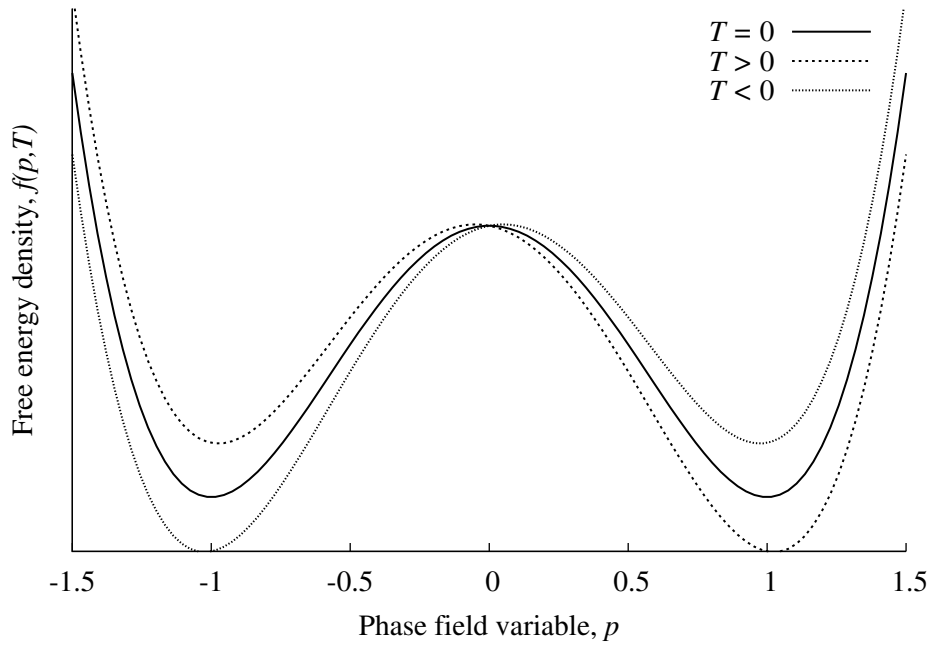

Figure 2.2: Free Energy Density of a Pure Material

The phase field model for a pure material can be defined:

$$\rho c_p \frac{\partial T}{\partial t} - \boldsymbol{\nabla} \cdot (k \, \boldsymbol{\nabla} T) + \frac{1}{2} L_f \frac{\partial p}{\partial t} = 0 \qquad \forall \ (x,t) \ \in \ \Omega_{xt} = \Omega_x \times \Omega_t \qquad (2.23)$$

$$\alpha \xi^2 \frac{\partial p}{\partial t} - \xi^2 \Delta p + \frac{\partial f}{\partial p} = 0 \qquad \forall \ (x,t) \ \in \ \Omega_{xt} = \Omega_x \times \Omega_t \qquad (2.24)$$

This model relies on the free energy density f. In many cases, f is defined as a polynomial, that is the driving force behind the movement of the phase transition front. In this mathematical model , if the phase transition interface is specified (or defined) as an initial condition, the model predicts accurate evolution (movement) of the transition region. However, when the spatial domain is either solid or liquid, the free energy density functions used presently do not allow initiation of the transition zone or front due to the presence of two distinct minima, regardless of the temperature. For example if the spatial domain is liquid and heat is removed from some boundary, the liquid will remain in the liquid state although the temperature may have fallen below the freezing temperature. This drawback of phase field models presents serious problems in simulating phase transition processes in which initiation and detection of the location of the transition zone is essential as it may not be known a priori.

2.5 Mathematical Models used in the Present Work

The mathematical models used in the present work and presented in this section are derived based on the assumptions that the transition region between the liquid and solid phases occurs over a small temperature change (width of the transition region $[T_s, T_l]$) in which specific heat, thermal conductivity, density and latent heat of fusion change in a continuous and differentiable manner. Figures 2.3 (a),(b),(c) and (d) show distributions of

ρ, c_p, k, and L_f in the transition region $[T_s, T_l]$ between the solid and liquid phases. The range $[T_s, T_l]$ i.e. the width of he transition region, can be as narrow or as wide as desired by the physics of phase change in a specific application. The transition region is assumed to be homogeneous and isotropic. This assumption is not so detrimental as is this case the constitutive theory only consists of the heat vector due to the zero velocity field assumption.

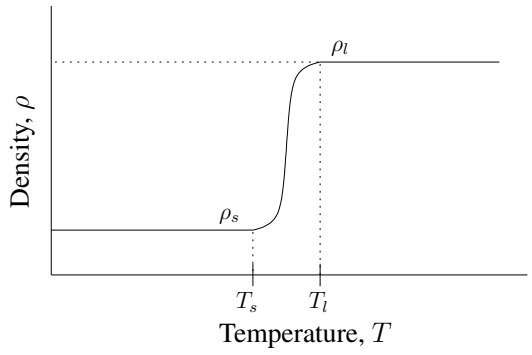

(a) Density ρ in the smooth interface

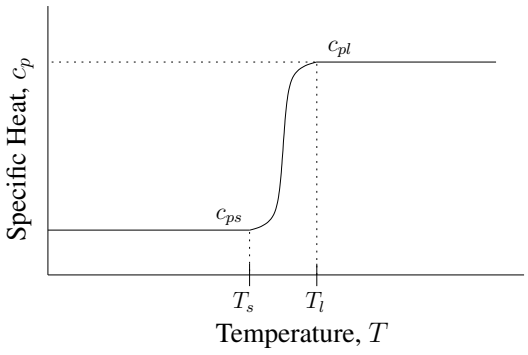

(b) Specific Heat c_p in the smooth interface

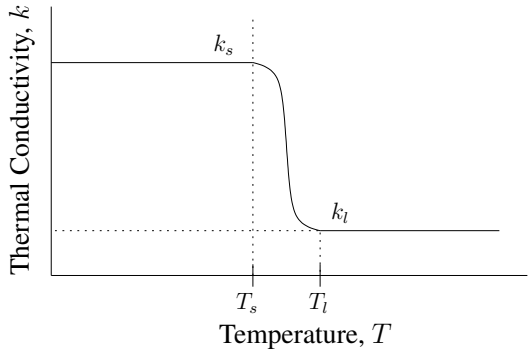

(c) Thermal Conductivity k in the smooth interface

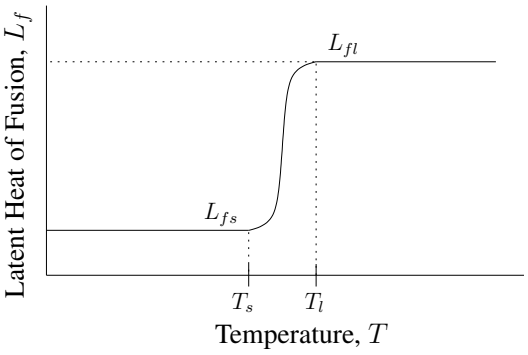

(d) Latent Heat of Fusion L_f in the smooth interface

Figure 2.3: ρ, c_p, k, L_f and in the smooth interface transition region between the solid and liquid phases as functions of Temperature T

The mathematical models derived and presented here in Lagrangian description are based on a simple statement of the first law of thermodynamics using specific total energy and the heat vector augmented by the constitutive equation for the heat vector (Fourier heat conduction law) and the statement of specif total energy incorporating the physics of phase change in the smooth interface zone between liquid and solid phases.

2.5.1 Basic Mathematical Model

The basic equations are presented in the following. These can be used to derive different forms of the mathematical model. In Lagrangian description the energy equation can be written as

$$\rho \frac{\partial e}{\partial t} + \boldsymbol{\nabla} \cdot \boldsymbol{q} = 0 \qquad \forall \ (\boldsymbol{x}, t) \ \in \ \Omega_{\boldsymbol{x}} \times \Omega_t = \Omega_{\boldsymbol{x}} \times (0, \tau) \tag{2.25}$$

Fourier heat conduction law is used as constitutive theory for the heat vector

$$\boldsymbol{q} = -k(T) \boldsymbol{\nabla} T \qquad \forall \ (\boldsymbol{x}, t) \ \in \ \Omega_{\boldsymbol{x}} \times \Omega_t = \Omega_{\boldsymbol{x}} \times (0, \tau) \tag{2.26}$$

The specific total energy e is given by (in the absence of velocity field):

$$e = \int_{T_0}^{T} c_p(T) dT + L_f(T) \tag{2.27}$$

Using (2.27), we can obtain $\dfrac{\partial e}{\partial t}$

$$\frac{\partial e}{\partial t} = \frac{\partial}{\partial T} \left(\int_{T_0}^{T} c_p(T) dT + L_f(T) \right) \frac{\partial T}{\partial t} + \frac{\partial L_f}{\partial t} = c_p(T) \frac{\partial T}{\partial t} + \frac{\partial L_f(T)}{\partial t} \tag{2.28}$$

Substituting from (2.28) into (2.25), we obtain

$$\rho(T) c_p(T) \frac{\partial T}{\partial t} + \boldsymbol{\nabla} \cdot \boldsymbol{q} + \rho(T) \frac{\partial L_f(T)}{\partial t} = 0 \tag{2.29}$$

$$\boldsymbol{q} = -k(T) \boldsymbol{\nabla} T \tag{2.30}$$

Equations (2.29) and (2.30) constitute the desired mathematical model in which $\rho = \rho(T)$, $c_p = c_p(T)$, $k = k(T)$ and $L_f = L_f(T)$ and vary accordingly to Figure 2.3. More specifically

$$\rho(T) = \begin{cases} \rho_s & ; \ T < T_s \\ \rho(T) & ; \ T_s \leq T \leq T_l \\ \rho_l & ; \ T > T_l \end{cases} \quad ; \quad c_p(T) = \begin{cases} c_{ps} & ; \ T < T_s \\ c_p(T) & ; \ T_s \leq T \leq T_l \\ c_{pl} & ; \ T > T_l \end{cases}$$

$$k(T) = \begin{cases} k_s & ; \ T < T_s \\ k(T) & ; \ T_s \leq T \leq T_l \\ k_l & ; \ T > T_l \end{cases} \quad ; \quad L_f(T) = \begin{cases} 0 & ; \ T < T_s \\ L_f(T) & ; \ T_s \leq T \leq T_l \\ L_f & ; \ T > T_l \end{cases} \tag{2.31}$$

Remarks:

(1) Using $\boldsymbol{\nabla} = \dfrac{\partial}{\partial x}$, $\boldsymbol{\nabla} = \left[\dfrac{\partial}{\partial x}, \dfrac{\partial}{\partial y}\right]^{\mathsf{T}}$ or $\boldsymbol{\nabla} = \left[\dfrac{\partial}{\partial x}, \dfrac{\partial}{\partial y}, \dfrac{\partial}{\partial z}\right]^{\mathsf{T}}$ and $\boldsymbol{q} = q_x$, $\boldsymbol{q} = [q_x, q_y]^{\mathsf{T}}$ or $\boldsymbol{q} = [q_x, q_y, q_z]^{\mathsf{T}}$ in (2.29) and (2.30) the explicit forms of the mathematical models for phase change can be derived for 1D, 2D, and 3D cases i.e. in R^k; $k = 1, 2, 3$. We note that since $L_f = L_f(T)$, $\dfrac{\partial L_f}{\partial t} = \left(\dfrac{\partial L_f}{\partial T}\right)\dfrac{\partial T}{\partial t}$ in which $\dfrac{\partial L_f}{\partial T}$ can be obtained explicitly using $L_f(T)$.

(2) When performing computations using (2.29)-(2.31), it may be more beneficial to recast (2.29)-(2.30) in different forms. We consider various alternatives in the following that are based on (2.29)-(2.31).

2.5.2 Model A: Mathematical model as a single PDE in temperature T only

Since $L_f = L_f(T)$ we can write

$$\frac{\partial L_f(T)}{\partial t} = \left(\frac{\partial L_f(T)}{\partial T}\right)\frac{\partial T}{\partial t} \tag{2.32}$$

Substituting from (2.30) and (2.32) in (2.29)

$$\rho(T)c_p(T)\frac{\partial T}{\partial t} - \boldsymbol{\nabla}\cdot\left(k(T)\boldsymbol{\nabla}T\right) + \rho(T)\left(\frac{\partial L_f(T)}{\partial T}\right)\frac{\partial T}{\partial t} = 0 \tag{2.33}$$

or

$$\rho(T)\left(c_p(T) + \frac{\partial L_f(T)}{\partial T}\right)\frac{\partial T}{\partial t} - \boldsymbol{\nabla}\cdot\left(k(T)\boldsymbol{\nabla}T\right) = 0 \qquad \forall\ (\boldsymbol{x}, t)\ \in\ \Omega_{\boldsymbol{x}t} = \Omega_{\boldsymbol{x}} \times \Omega_t \tag{2.34}$$

Equation (2.34) is the desired mathematical model in temperature (only). $\rho(T)$, $c_p(T)$, $k(T)$, and $L_f(T)$ are defined to be continuous and differentiable functions of temperature T in the transition region $[T_s, T_l]$ and have constant values (ρ_s, c_{ps}, k_s, 0) and (ρ_l, c_{pl}, k_l, L_f) in solid and liquid phases. This model contains up to second order derivatives of temperature in space coordinates but only first order time derivative of the temperature. This model contains only a single dependent variable i.e. $T = T(\boldsymbol{x}, t)$, temperature.

2.5.3 Model B: Mathematical model expressed as a system of first order PDEs

This mathematical model essentially consists of equations (2.29), (2.30) and (2.31). We rewrite these by introducing (2.32) in (2.29) and regrouping the terms.

$$\rho(T)\left(c_p(T)+\frac{\partial L_f(T)}{\partial T}\right)\frac{\partial T}{\partial t}+\boldsymbol{\nabla}\cdot\boldsymbol{q}=0 \qquad \forall\ (\boldsymbol{x},t)\ \in\ \Omega_{\boldsymbol{x}t}=\Omega_{\boldsymbol{x}}\times\Omega_t \tag{2.35}$$

$$\boldsymbol{q}=-k(T)\boldsymbol{\nabla}T \qquad \forall\ (\boldsymbol{x},t)\ \in\ \Omega_{\boldsymbol{x}t}=\Omega_{\boldsymbol{x}}\times\Omega_t \tag{2.36}$$

We treat T and $\boldsymbol{q}$ (i.e. $q_x,\ \ q_x, q_y$ or $\ \ q_x, q_y, q_z$) as dependent variables.

Equations (2.35), (2.36) and (2.31) constitute the desired mathematical model that only contains the first order derivatives of T and $\boldsymbol{q}$ in space coordinates and time (hence a system of first order PDEs). This form of the mathematical model has some benefits when used in methods of approximation such as finite element method.

2.5.4 Model C: Mathematical model using T and L_f as dependent variables

Consider the basic form of the mathematical model described by (2.29) and (2.30). If we substitute $\boldsymbol{q}$ from (2.30) in (2.29) and introduce another equation $L_f=G(T)$ in which $G(T)$ explicitly describes dependence of L_f in temperature, then we have

$$\rho(T)c_p(T)\frac{\partial T}{\partial t}-\boldsymbol{\nabla}\cdot\left(k(T)\boldsymbol{\nabla}T\right)+\rho(T)\frac{\partial L_f}{\partial t}=0 \qquad \forall\ (\boldsymbol{x},t)\ \in\ \Omega_{\boldsymbol{x}t}=\Omega_{\boldsymbol{x}}\times\Omega_t \tag{2.37}$$

$$L_f=G(T) \qquad \forall\ (\boldsymbol{x},t)\ \in\ \Omega_{\boldsymbol{x}t}=\Omega_{\boldsymbol{x}}\times\Omega_t \tag{2.38}$$

Equation (2.37) and (2.38) are assumed to constitute the mathematical model in dependent variables T and L_f.

2.5.5 Model D: Mathematical model using T, $\boldsymbol{q}$ and L_f as dependent variables

Consider the basic form of the mathematical model described by (2.29) and (2.30). If we consider (2.29) and (2.30) and introduce $L_f = G(T)$ as the third equation, then the mathematical model becomes

$$\rho(T)c_p(T)\frac{\partial T}{\partial t} + \boldsymbol{\nabla \cdot q} + \rho(T)\frac{\partial L_f}{\partial t} = 0 \qquad \forall\ (\boldsymbol{x}, t)\ \in\ \Omega_{\boldsymbol{x}t} = \Omega_{\boldsymbol{x}} \times \Omega_t \qquad (2.39)$$

$$\boldsymbol{q} = -k(T)\boldsymbol{\nabla} T \qquad \forall\ (\boldsymbol{x}, t)\ \in\ \Omega_{\boldsymbol{x}t} = \Omega_{\boldsymbol{x}} \times \Omega_t \qquad (2.40)$$

$$L_f = G(T) \qquad \forall\ (\boldsymbol{x}, t)\ \in\ \Omega_{\boldsymbol{x}t} = \Omega_{\boldsymbol{x}} \times \Omega_t \qquad (2.41)$$

Equations (2.39)-(2.41) are a system of first order PDEs in dependent variables T, $\boldsymbol{q}$, and L_f.

Remarks:

(1) The mathematical models presented in sections 2.5.1 to 2.5.5 are all time dependent nonlinear diffusion equations (convection term being absent due to zero velocity) in various forms.

(2) Which form of these equations are meritorious for which methods of approximation for obtaining their numerical solution remains to be seen (see Chapter 4).

(3) We remark that when the velocity field is zero and the deformed configurations are stress free, the Lagrangian and Eulerian descriptions are identical. In case of zero velocity field $\dfrac{D}{Dt} = \dfrac{\partial}{\partial t}$ holds i.e. the material derivative is equal to the partial derivative with respect to time. Nonetheless, we call these mathematical models in Lagrangian description to maintain distinction and clarity.

Chapter 3

Mathematical Models in Eulerian Description

3.1 Introduction

In the matter undergoing phase change has non-zero velocity field as in the case of flowing fluids, then it is essential to construct mathematical models in Eulerian description due to the fact that complex motion of fluid particles may not be possible to describe using position coordinates of the material points in the reference configuration (the configuration at the commencement of the evolution) and time.

In order to derive mathematical models of phase change processes in Eulerian description, we first describe basic notations. Let x_i; $i = 1, 2, 3$ be the position coordinates of a material point P in the reference configuration at time $t = t_0 = 0$, just before the commencement of the evolution. Let the material particle P occupy a position $\bar{x}_i$; $i = 1, 2, 3$ ($\bar{P}$) in the current configuration at time $t > t_0$. Clearly $\bar{x}_i$; $i = 1, 2, 3$ are the deformed

coordinates. If Q is a quantity of interest we wish to monitor during deformation, then

$$Q = Q\left(x_1, x_2, x_3, t\right) \tag{3.1}$$

$$\text{and} \qquad \bar{Q} = \bar{Q}\left(\bar{x}_1, \bar{x}_2, \bar{x}_3, t\right) \tag{3.2}$$

are referred to as Lagrangian and Eulerian descriptions for the quantity Q. We note that the functional relationships in Q and $\bar{Q}$ are different but their numerical values are identically the same and hold at position $\bar{P}$ i.e. $\bar{x}_i$; $i = 1, 2, 3$. In Eulerian description we express all quantities of interest using (3.2) i.e. all dependent variables are functions of $\bar{x}_i$; $i = 1, 2, 3$ and time t. We use over bar on all dependent variables to emphasize the fact that their descriptions are Eulerian.

We use the following assumptions in the derivation of the mathematical models.

(*i*) We assume liquid, solid as well as the transition region to be incompressible

(*ii*) We consider liquid and solid phases to be homogeneous and isotropic with constant transport properties.

(*iii*) The liquid phase is treated as Newtonian fluid.

(*iv*) The solid phase is treated as hypoelastic solid.

(*v*) The transition region is a mixture of solid and liquid phases with their varying volume fractions. We assume this phase to be isotropic and homogeneous for describing $\bar{\rho}(\bar{T})$, $\bar{c}_p(\bar{T})$, $\bar{k}(\bar{T})$ and $\bar{L}_f(\bar{T})$. These transport properties are assumed to be continuous and differentiable between the solid and the liquid phases (as described in case of Lagrangian descriptions).

(*vi*) For the liquid phase, solid phase as well as transition region, the mathematical model are derived in Eulerian descriptions so that the interaction of the three phases are inherent in the mathematical model.

(*vii*) The constitutive theories for the stress tensor and heat vector for the liquid phase and the solid phase are straight forward [27–29]. However in the transition region special considerations are required (see section 3.2).

(*viii*) We assume thermodynamic equilibrium during the evolution of phase change process, thus conservation laws and thermodynamic principles can be used in the derivations of the mathematical models.

3.2 Development of Mathematical Model

Since we assume the phase change evolution to be in thermodynamic equilibrium, the mathematical model for the phase change process can be derived using: conservation of mass, balance of momenta, first law of thermodynamics, the constitutive theory for the stress tensor and the heat vector based on the second law of thermodynamics or entropy inequality and other thermodynamic relations. Since, conservation of mass, balance of momenta and the first law of thermodynamics are independent of the constitution of matter, these hold for the liquid phase, solid phase as well as transition region (assuming it to be homogeneous and isotropic for $\bar{\rho}(\bar{T})$, $\bar{c}_p(\bar{T})$, $\bar{k}(\bar{T})$ and $\bar{L}_f(\bar{T})$ i.e. for transport properties). Conservation of mass, balance of momenta and the first law of thermodynamics yield continuity, momentum and energy equations. For homogeneous, isotropic and incompressible matter we easily derive these [29]. In the following we present complete mathematical

models for phase change processes. Details are presented separately for each of the three phases (liquid, solid and transition) so that we can clearly observe differences in the models for the three phases.

We consider fixed coordinate system to be the orthogonal x-frame with o-x_1, o-x_2 and o-x_3 as the axes. All quantities are measured in this frame. It is necessary to use x_1, x_2, x_3 as opposed to x, y, z so that Einstein notation can be used.

Liquid Phase

We assume the liquid phase to be homogeneous, isotropic, incompressible newtonian fluid with constant transport properties. Under these assumptions, the mathematical model consists of:

Continuity equation:
$$\bar{\rho}_l \text{ Div } \bar{\boldsymbol{v}} = \bar{\rho}_l \frac{\partial \bar{v}_i}{\partial \bar{x}_i} = 0 \tag{3.3}$$

Momentum equations:
$$\bar{\rho}_l \frac{\partial \bar{v}_i}{\partial t} + \bar{\rho}_l \bar{v}_j \frac{\partial \bar{v}_i}{\partial \bar{x}_j} + \frac{\partial \bar{p}}{\partial \bar{x}_i} - \frac{\partial_d \bar{\sigma}_{ij}^{(0)}}{\partial \bar{x}_j} - \bar{\rho}_l \bar{F}_i^b = 0 \tag{3.4}$$

Energy equation:
$$\bar{\rho}_l \bar{c}_{pl} \left(\frac{\partial \bar{T}}{\partial t} + \bar{\boldsymbol{v}} \cdot \bar{\boldsymbol{\nabla}} \bar{T} \right) + \bar{\boldsymbol{\nabla}} \cdot \bar{\boldsymbol{q}} - {}_d\bar{\sigma}_{ij}^{(0)} \frac{\partial \bar{v}_i}{\partial \bar{x}_j} = 0 \tag{3.5}$$

Constitutive equations:

$${}_d\bar{\sigma}_{ij}^{(0)} = 2\bar{\mu}\bar{\gamma}_{ij}^{(1)} = 2\bar{\mu}\bar{D}_{ij} \tag{3.6}$$

$$\bar{\boldsymbol{q}} = -\bar{k}_l \bar{\boldsymbol{\nabla}} \bar{T} \tag{3.7}$$

$$\bar{D}_{ij} = \frac{1}{2} \left(\frac{\partial \bar{v}_i}{\partial \bar{x}_j} + \frac{\partial \bar{v}_j}{\partial \bar{x}_i} \right) \tag{3.8}$$

In which $\bar{\rho}_l$ is liquid phase density (constant), $\bar{\boldsymbol{v}}$ are velocities in x_1, x_2, x_3 directions, $\bar{p}$ is mechanical pressure (positive when compressive), ${}_d\bar{\boldsymbol{\sigma}}^{(0)}$ is the deviatoric contravariant Cauchy stress tensor [29], $\bar{F}_i^b$ are body forces per unit mass in x_i; $i = 1, 2, 3$ directions, $\bar{T}$ is

temperature, $\bar{c}_{pl}$ is specific heat of liquid phase, $\bar{\boldsymbol{q}}$ is the heat vector in x_1, x_2, x_3 directions, $\bar{\mu}$ is viscosity, $\bar{k}_l$ is thermal conductivity of liquid phase, $\bar{\boldsymbol{\gamma}}^{(1)}$ and $\bar{\boldsymbol{D}}$ are the first convected time derivative of the Almansi strain tensor and symmetric part of the velocity gradient tensor.

This mathematical model contains fourteen variables $\bar{v}_i$, $\bar{p}$, ${}_d\bar{\sigma}_{ij}^{(0)}$; $i = 1, 2, 3$; $j \geq i$, $\bar{T}$ and $\bar{q}_i$; $i = 1, 2, 3$ in fourteen equations ((3.3) to (3.7)), hence the mathematical model has closure. We also note that this mathematical model is a system of first order PDEs. By substituting ${}_d\bar{\boldsymbol{\sigma}}^{(0)}$ in the momentum and energy equations and $\bar{\boldsymbol{q}}$ in the energy equation we can eliminate ${}_d\bar{\boldsymbol{\sigma}}^{(0)}$ and $\bar{\boldsymbol{q}}$ as dependent variables, but the resulting mathematical model will contain up to second order derivatives of the velocities and temperature with respect to $\bar{x}_i$; $i = 1, 2, 3$.

Solid Phase

We treat the solid phase as homogeneous, isotropic, incompressible hypoelastic solid with constant material properties. The mathematical model based on conservation laws and the constitutive theory for hypoelastic solids yields the following:

Continuity equation:
$$\bar{\rho}_s \text{ Div } \bar{\boldsymbol{v}} = \bar{\rho}_s \frac{\partial \bar{v}_i}{\partial \bar{x}_i} = 0 \tag{3.9}$$

Momentum equations:
$$\bar{\rho}_s \frac{\partial \bar{v}_i}{\partial t} + \bar{\rho}_s \bar{v}_j \frac{\partial \bar{v}_i}{\partial \bar{x}_j} + \frac{\partial \bar{p}}{\partial \bar{x}_i} - \frac{\partial_d \bar{\sigma}_{ij}^{(0)}}{\partial \bar{x}_j} - \bar{\rho}_s \bar{F}_i^b = 0 \tag{3.10}$$

Energy equation:
$$\bar{\rho}_s \bar{c}_{ps} \left(\frac{\partial \bar{T}}{\partial t} + \bar{\boldsymbol{v}} \cdot \bar{\boldsymbol{\nabla}} \bar{T} \right) + \bar{\boldsymbol{\nabla}} \cdot \bar{\boldsymbol{q}} - {}_d\bar{\sigma}_{ij}^{(0)} \frac{\partial \bar{v}_i}{\partial \bar{x}_j} + \bar{p} \frac{\partial \bar{v}_i}{\partial \bar{x}_i} = 0 \tag{3.11}$$

Rate constitutive equations [29, 30]:

$$ {}_d\bar{\sigma}_{ij}^{(1)} = \underset{\sim}{\bar{D}}_{ik}\bar{\gamma}_{kj}^{(1)} = \underset{\sim}{\bar{D}}_{ik}\bar{D}_{kj} \tag{3.12} $$

$$ \bar{\boldsymbol{q}} = -\bar{k}_s\bar{\boldsymbol{\nabla}}\bar{T} \tag{3.13} $$

in which ${}_d\bar{\boldsymbol{\sigma}}^{(1)}$ is the first convected time derivative of the contravariant deviatoric Cauchy stress tensor ${}_d\bar{\boldsymbol{\sigma}}^{(0)}$, $\underset{\sim}{\bar{D}}_{ik}$ are the components of the material tensor recast as a matrix.

Remarks:

(1) Unlike fluids, in elastic solid matter, the material points stay connected to the neighboring material points during elastic deformation. Thus an elongation in a direction is accompanied by contraction in the other two orthogonal directions. This behavior is intrinsic in the constitutive equations. Thus, for incompressible solid matter, the conservation of mass described by (3.9) is invalid for such matter. That is, the velocity field for solid elastic matter is not divergence free. Elimination of (3.9) from the mathematical model obviously results in lack of closure i.e. now we have one less equation than the number of dependent variables. This situation is corrected in remark (2).

(2) For solid elastic matter, the mechanical pressure $\bar{p}$ is mean normal stress, hence cannot be a dependent variable in the mathematical model. Thus, we have two alternatives: (*i*) either eliminate pressure $\bar{p}$ from the model by using $\bar{p}$ to be equal to mean normal stress or (*ii*) use an additional constraint equation describing $\bar{p}$ as a function of normal stresses to replace continuity. The mechanical pressure $\bar{p}$ is still no longer a dependent variable in the mathematical model but can be retained as a dependent variable due to the presence of the constraint equation. The second alternative is

easier and is necessitated due to the fact presence of $\bar{p}$ is necessary as it appears as dependent variable in the mathematical model for the liquid phase. We present details in the following (assuming positive $\bar{p}$ to be tension):

3D case:

$$ {}_d\bar{\boldsymbol{\sigma}}^{(0)} = \bar{\boldsymbol{\sigma}}^{(0)} - \bar{p}\,[\,\mathrm{I}\,] \tag{3.14} $$

but for elastic solid matter

$$ \bar{p} = \frac{1}{3}\mathrm{tr}\left(\bar{\boldsymbol{\sigma}}^{(0)}\right) \tag{3.15} $$

substituting from (3.15) into (3.14)

$$ {}_d\bar{\boldsymbol{\sigma}}^{(0)} = \bar{\boldsymbol{\sigma}}^{(0)} - \frac{1}{3}\mathrm{tr}\left(\bar{\boldsymbol{\sigma}}^{(0)}\right)[\,\mathrm{I}\,] \tag{3.16} $$

Taking the trace of (3.16)

$$ \mathrm{tr}\left({}_d\bar{\boldsymbol{\sigma}}^{(0)}\right) = \mathrm{tr}\left(\bar{\boldsymbol{\sigma}}^{(0)}\right) - \frac{1}{3}\mathrm{tr}\left(\bar{\boldsymbol{\sigma}}^{(0)}\right)\mathrm{tr}\left([\,\mathrm{I}\,]\right) = 0 \tag{3.17} $$

Hence, we have

$$ \mathrm{tr}\left({}_d\bar{\boldsymbol{\sigma}}^{(0)}\right) = 0 \tag{3.18} $$

Hence for the 3D case, i.e. $\mathbb{R}^3$, the continuity equation (3.9) must be replaced with (3.18) while still maintaining $\bar{p}$ as dependent variable in the mathematical model.

2D case:

We begin with (3.14) i.e.

$$ {}_d\bar{\boldsymbol{\sigma}}^{(0)} = \bar{\boldsymbol{\sigma}}^{(0)} - \bar{p}\,[\,\mathrm{I}\,] $$

in which $\bar{p} = \frac{1}{3}\mathrm{tr}\left(\bar{\boldsymbol{\sigma}}^{(0)}\right)$

$$ \therefore\ {}_d\bar{\boldsymbol{\sigma}}^{(0)} = \bar{\boldsymbol{\sigma}}^{(0)} - \frac{1}{3}\mathrm{tr}\left(\bar{\boldsymbol{\sigma}}^{(0)}\right)[\,\mathrm{I}\,] \tag{3.19} $$

Taking the trace of (3.19)

$$\begin{aligned}\text{tr}\left({}_d\bar{\boldsymbol{\sigma}}^{(0)}\right) &= \text{tr}\left(\bar{\boldsymbol{\sigma}}^{(0)}\right) - \frac{1}{3}\text{tr}\left(\bar{\boldsymbol{\sigma}}^{(0)}\right)\text{tr}\left([\,\text{I}\,]\right) \\ &= \text{tr}\left(\bar{\boldsymbol{\sigma}}^{(0)}\right) - \frac{2}{3}\text{tr}\left(\bar{\boldsymbol{\sigma}}^{(0)}\right) = \frac{1}{3}\text{tr}\left(\bar{\boldsymbol{\sigma}}^{(0)}\right) = \bar{p}\end{aligned}$$

therefore $\quad \text{tr}\left({}_d\bar{\boldsymbol{\sigma}}^{(0)}\right) - \bar{p} = 0.$

If we assume compressive pressure to be positive, then

$$\text{tr}\left({}_d\bar{\boldsymbol{\sigma}}^{(0)}\right) + \bar{p} = 0 \tag{3.20}$$

We can write (3.20) for the 2D case as follows:

$${}_d\bar{\sigma}^{(0)}_{x1x1} + {}_d\bar{\sigma}^{(0)}_{x2x2} + \bar{p} = 0 \tag{3.21}$$

Thus, for the 2D case, i.e. $\mathbb{R}^2$, the continuity equation (3.9) must be replaced with (3.21) while still maintaining $\bar{p}$ as a dependent variable.

1D case:

Again

$${}_d\bar{\boldsymbol{\sigma}}^{(0)} = \bar{\boldsymbol{\sigma}}^{(0)} - \bar{p}\,[\,\text{I}\,]$$

$$\bar{p} = \frac{1}{3}\text{tr}\left(\bar{\boldsymbol{\sigma}}^{(0)}\right) \tag{3.22}$$

$$\therefore\ {}_d\bar{\boldsymbol{\sigma}}^{(0)} = \bar{\boldsymbol{\sigma}}^{(0)} - \frac{1}{3}\text{tr}\left(\bar{\boldsymbol{\sigma}}^{(0)}\right)[\,\text{I}\,] \tag{3.23}$$

taking the trace on both sides

$$\text{tr}\left({}_d\bar{\boldsymbol{\sigma}}^{(0)}\right) = \text{tr}\left(\bar{\boldsymbol{\sigma}}^{(0)}\right) - \frac{1}{3}\text{tr}\left(\bar{\boldsymbol{\sigma}}^{(0)}\right)\text{tr}\left([\,\text{I}\,]\right) \tag{3.24}$$

$$\text{tr}\left({}_d\bar{\boldsymbol{\sigma}}^{(0)}\right) = \text{tr}\left(\bar{\boldsymbol{\sigma}}^{(0)}\right) - \frac{1}{3}\text{tr}\left(\bar{\boldsymbol{\sigma}}^{(0)}\right) = \frac{2}{3}\text{tr}\left(\bar{\boldsymbol{\sigma}}^{(0)}\right) \tag{3.25}$$

Using (3.22), (3.25) becomes

$$\text{tr}\left({}_d\bar{\boldsymbol{\sigma}}^{(0)}\right) - 2\bar{p} = 0 \tag{3.26}$$

or

$$ {}_d\bar{\sigma}^{(0)}_{x1x1} - 2\bar{p} = 0 $$

If we assume compressive $\bar{p}$ to be positive, then

$$ {}_d\bar{\sigma}^{(0)}_{x1x1} + 2\bar{p} = 0 \tag{3.27} $$

Thus, for the 1D case, i.e. $\mathbb{R}^1$, (3.27) replaces the continuity equation (3.9).

(3) In view of the remark (2), the term $\bar{p}\dfrac{\partial \bar{v}_i}{\partial \bar{x}_i}$ in the energy equation (3.11) is not zero (as it is for newtonian fluids in which the velocity field is divergence free) and hence must be retained for the solid phase.

Transition Region

The transition region is a mixture of solid and liquid phases. Their concentrations vary depending upon the location in the transition region . If we assume that this mixture is saturated and that the volume fraction of solid ($\bar{f}_s$) varies from zero to one when traversing from pure liquid to pure solid region and the volume fraction of liquid ($\bar{f}_l = 1 - \bar{f}_s$, for the saturated mixture) likewise varies from one to zero in the transition zone when traversing from the liquid to the solid region, then it is possible to derive a mathematical model based on conservation of mass, balance of momenta and the first law of thermodynamics using mixture theory [1–3]. The second law of thermodynamics provides a mechanism for the constitutive theory for the stress tensor and the heat vector [1–3]. This approach is mathematically rigorous and is based on principles of continuum mechanics and thermodynamics, but is beyond the scope of work undertaken in this thesis. Instead, we consider a more simplistic approach based on volume fractions assigned as weight factors to the

corresponding residuals resulting from the constitutive equation for liquid and solid phases and the sum of the weighted residuals is assumed to be the residual resulting from the constitutive equation for the transition region.

Continuity equation:

$$\bar{f}_s\,(\textit{pressure constraint equation for solid region}) + \bar{f}_l\left(\bar{\rho}_l\frac{\partial \bar{v}_i}{\partial \bar{x}_i}\right) = 0$$

Momentum equations:

$$\bar{\rho}\frac{\partial \bar{v}_i}{\partial t} + \bar{\rho}\bar{v}_j\frac{\partial \bar{v}_i}{\partial \bar{x}_j} + \frac{\partial \bar{p}}{\partial \bar{x}_i} - \frac{\partial_d \bar{\sigma}_{ij}^{(0)}}{\partial \bar{x}_j} - \bar{\rho}\bar{F}_i^b = 0 \tag{3.28}$$

Energy equation: [29]

$$\bar{\rho}\left(\bar{c}_p + \frac{\partial \bar{L}_f}{\partial \bar{T}}\right)\left(\frac{\partial \bar{T}}{\partial t} + \bar{\boldsymbol{v}}\cdot\bar{\boldsymbol{\nabla}}\bar{T}\right) + \bar{\boldsymbol{\nabla}}\cdot\bar{\boldsymbol{q}} - {}_d\bar{\sigma}_{ij}^{(0)}\frac{\partial \bar{v}_i}{\partial \bar{x}_j} + \bar{f}_s\bar{p}\frac{\partial \bar{v}_i}{\partial \bar{x}_i} = 0$$

Constitutive equations:

$$\bar{f}_l\left({}_d\bar{\sigma}_{ij}^{(0)} - 2\bar{\mu}\bar{D}_{ij}\right) + \bar{f}_s\left({}_d\bar{\sigma}_{ij}^{(1)} - \underset{\sim}{\bar{D}}_{ik}\bar{D}_{kj}\right) = 0$$

$$\bar{\boldsymbol{q}} = -\bar{k}\bar{\boldsymbol{\nabla}}\bar{T}$$

Remarks:

(1) The volume fraction $\bar{f}_l$ (or $\bar{f}_s$) is determined based on the temperature in the transition region. If $\bar{T}_l$ and $\bar{T}_s$ are the temperatures at the two ends of the transition region, then

$$\bar{f}_s = \frac{\bar{T}_l - \bar{T}}{\bar{T}_l - \bar{T}_s} \qquad \text{and} \qquad \bar{f}_l = 1 - \bar{f}_s = \frac{\bar{T} - \bar{T}_s}{\bar{T}_l - \bar{T}_s} \tag{3.29}$$

Thus when $\bar{T} = \bar{T}_l$ (i.e. pure liquid) $\bar{f}_s = 0$ and $\bar{f}_l = 1$

(2) $\bar{\rho}$, $\bar{k}$, $\bar{c}_p$, $\bar{L}_f$ are fifth degree polynomials in temperature (of class $C^2(T)$) in the transition region as shown in Figures 2.3.

Chapter 4

Methods of Approximation for IVPs describing Phase Change Phenomena

4.1 Introduction

The mathematical models describing the phase change phenomena consist of a system of non-linear PDEs in spatial coordinates and time i.e. non-linear IVPs in which the space-time differential operator is non-linear. The computational methodology for obtaining numerical solutions of the IVPs i.e. evolution must be such that accurate numerical solutions are possible upon convergence. In the following, we list some features that are essential in choosing a computational methodology for obtaining numerical solutions of the non-linear IVPs describing phase change phenomena.

(1) Must be applicable to non-linear space-time differential operators regardless of the nature of the non-linearity without any ad-hoc adjustments or treatments that are dependent on the nature of the non-linearity (such as SUPG, DC, LS and other up-

winding methods and linearizing methods [7]).

(2) The dependent variables must exhibit simultaneous dependence on space coordinates and time as necessitated by the physics. Hence the computational methodology must only entertain a space-time coupled approach.

(3) Must yield a computational infrastructure in which the computations remain unconditionally stable regardless of the choices of computational or physical parameters. This feature essentially requires that the algebraic systems resulting from the methods of approximation must contain positive definite coefficient matrices.

(4) The approximation must be of higher degree (polynomial of order p) as well as of higher order in space and in time. These features allow simulation of complex evolution over larger sub-domains. The higher order feature of the approximation permits us to incorporate the desired global differentiability of approximations in space and time.

(5) The computational infrastructure must be time marching so that the evolution can be computed for an increment of time and then time marched to obtain the entire evolution. This feature is essential for efficiency of computations when evolution may be needed for a large value of time with relatively small time increments.

(6) The computational method must have means of measuring (i.e. computing) the error or residuals without the knowledge of theoretical or reference solution and must also have mechanism to reduce them to the desired level. This feature is also essential for adaptivity.

Based on the material presented in Chapter 1 and the requirements (1) - (6), we rule out finite difference and finite volume methods as viable computational methodologies. This leaves us with space-time coupled finite element methods as a possible approach for obtaining numerical solutions of the IVPs in phase change phenomena.

4.2 Space-Time Finite Element Method

In space-time finite element methods we construct an integral form using the GDEs in the mathematical model over the space-time domain of the IVP. This can be done in two ways: (i) using fundamental lemma of the calculus of variations [31–35] or (ii) based on the minimization of the residual functional. The use of fundamental lemma results in space-time Galerkin Method (STGM), space-time Petrov-Galerkin method (STPGM) and space-time weighted residuals method (STWRM). The choice of the test function determines the type of method. If we begin with STGM and perform integration by parts, we obtain the weak form i.e. we have space-time Galerkin Method with weak form (STGM/WF). The second category of methods based on minimization of the residual functional results in space-time least squares processes (STLSP). When these space-time integral forms are recast over the space-time discretization of the space time domain, we have space-time finite element processes based on the chosen strategy of constructing the integral form. We note that these methods only provide the space-time integral form from which numerical solution is computed, thus we only have necessary condition. Existence and sufficient conditions must also be addressed on problem by problem basis. Surana et. al. [8, 9, 36] have shown that:

(i) All space-time differential operators can be classified over the entire space-time do-

main or over a space-time strip or slab corresponding to an increment of time into two mathematical categories: non-self adjoint and non-linear.

(ii) By establishing a correspondence between the integral forms and the elements of calculus of variations and by introducing the definition of space-time variationally consistent integral forms (STVC) and space-time variationally inconsistent integral forms (STVIC), it is possible to determine which space-time integral forms are STVC or STVIC for the two categories of differential operators [9].

(iii) The STVC integral forms yield computational processes that are unconditionally stable. The coefficient matrices in the algebraic systems are symmetric and positive definite. In case of STVIC integral forms, unconditional stability of computations is not always ensured, the coefficient matrices in the algebraic system are not symmetric, and hence their positive definiteness is not always ensured.

(iv) The STGM, STPGM, STWRM, and STGM/WF yield space-time variationally inconsistent integral forms. STLSP yield STVC integral forms when the space-time differential operator is non-self adjoint. When the space-time differential operator is non-linear, the space-time integral form in STLSP can be made variationally consistent if (a) the non-linear algebraic equations are solved using Newton's linear method (Newton-Raphson method) and (b) if the second variation of the residuals is neglected in the second variation of the residual functional.

Based on these works described above, only STLSP are a viable computational strategy for obtaining numerical solutions of the IVPs describing the evolution for phase change phenomena. This approach also has all of the desired features (1) - (6) listed in section 4.1.

In the following, we consider STLSP for IVPs in which the space-time differential operator is non-linear. We present details of the STLSP based on space-time residuals. In specific applications, once E_i, residuals and δE_i are defined, the rest of the details are transparent.

4.2.1 Space-time Least Squares Finite Element Processes for Non-linear Space-time Differential Operators [8, 9, 36]

Let

$$\boldsymbol{A\phi} - \boldsymbol{f} = 0 \qquad \forall\ (\boldsymbol{x}, t)\ \in\ \Omega_{xt} = \Omega_x \times \Omega_t = \Omega_x \times (0, \tau) \tag{4.1}$$

be a system of n_e partial differential equations defined over the space-time domain Ω_{xt}. $\boldsymbol{A}$ is a $n_e \times n_e$ matrix containing n_e differential operators and $\boldsymbol{\phi}$ is a $(n_e \times 1)$ vector of dependent variables. Consider an increment of time $\Delta t = [t_n, t_{n+1}]$ i.e. $\Omega_t^n = (t_n, t_{n+1})$ and the n^{th} space-time strip or slab $\Omega_{xt}^n = \Omega_x \times \Omega_t^n = \Omega_x \times (t_n, t_{n+1})$ corresponding to the increment of time Δt. Let $\left(\Omega_{xt}^n\right)^T$ be a discretization of Ω_{xt}^n, the n^{th} space-time strip or slab such that

$$\left(\bar{\Omega}_{xt}^n\right)^T = \bigcup_{e=1}^{m} \bar{\Omega}_{xt}^e \tag{4.2}$$

in which $\bar{\Omega}_{xt}^n = \Omega_{xt}^n \bigcup \Gamma^n$ where Γ^n is the closed boundary of the n^{th} space-time strip or slab. $\bar{\Omega}_{xt}^e = \Omega_{xt}^e \bigcup \Gamma^e$ is a typical space-time element 'e' of the discretization $\left(\bar{\Omega}_{xt}^n\right)^T$. Γ^e is the closed boundary of element 'e'. Let $\boldsymbol{\phi}_h$ be approximation of $\boldsymbol{\phi}$ over $\left(\bar{\Omega}_{xt}^n\right)^T$ and $\boldsymbol{\phi}_h^e$ be local approximation of $\boldsymbol{\phi}$ over an element 'e' with space-time domain $\bar{\Omega}_{xt}^e$ such that

$$\boldsymbol{\phi}_h = \bigcup_{e=1}^{m} \boldsymbol{\phi}_h^e \tag{4.3}$$

If we substitute $\boldsymbol{\phi}_h$ in (4.1) then we obtain 'n_e' residual equations i.e.

$$\boldsymbol{A\phi}_h - \boldsymbol{f} = \boldsymbol{E} \tag{4.4}$$

The vector $\boldsymbol{E}$ consists of E_i ; $i = 1, ..., n_e$ residual equations.

1. Existence of the residual functional $I(\boldsymbol{\phi}_h)$ (by construction):

$$I(\boldsymbol{\phi}_h) = \sum_{i=1}^{n_e} (E_i, E_i)_{\left(\bar{\Omega}_{xt}^n\right)^T} = \sum_{e=1}^{m} \left(\sum_{i=1}^{n_e} (E_i^e, E_i^e)_{\bar{\Omega}_{xt}^e} \right) \tag{4.5}$$

in which E_i^e are components of the vector $\boldsymbol{E}^e$ in

$$\boldsymbol{A}\boldsymbol{\phi}_h^e - \boldsymbol{f} = \boldsymbol{E}^e \tag{4.6}$$

We note $I(\boldsymbol{\phi}_h)$ is always greater than zero and is equal to zero iff $\boldsymbol{\phi}_h = \boldsymbol{\phi}$, the theoretical solution of (4.1).

2. Necessary Condition: If $I(\boldsymbol{\phi}_h)$ is differentiable in $\boldsymbol{\phi}_h$, then the necessary condition for an extremum of (4.5) is given by [31–35].

$$\delta I(\boldsymbol{\phi}_h) = 2\sum_{e=1}^{m} \left(\sum_{i=1}^{n_e} (E_i^e, \delta E_i^e)_{\bar{\Omega}_{xt}^e} \right) = 2\sum_{e=1}^{m} \{g^e\} = 2\{g\} = 0 \tag{4.7}$$

We note that $\{g^e\}$ is a non-linear function of $\boldsymbol{\phi}_h^e$ and likewise $\{g\}$ is a non-linear function of $\boldsymbol{\phi}_h$.

3. Sufficient condition or extremum principle:

$$\delta^2 I(\boldsymbol{\phi}_h) = 2\sum_{e=1}^{m} \left(\sum_{i=1}^{n_e} (\delta E_i^e, \delta E_i^e)_{\bar{\Omega}_{xt}^e} \right) + 2\sum_{e=1}^{m} \left(\sum_{i=1}^{n_e} \left(E_i^e, \delta^2 E_i^e\right)_{\bar{\Omega}_{xt}^e} \right) \tag{4.8}$$

A unique extremum principle requires

$$\delta^2 I \begin{cases} > 0 \quad ; \quad \text{minimum of } I \\ = 0 \quad ; \quad \text{saddle point of } I \qquad \forall \text{ admissible } \boldsymbol{\phi}_h \\ < 0 \quad ; \quad \text{maximum of } I \end{cases} \tag{4.9}$$

When the differential operator is linear (non-self adjoint), $\delta^2 E_i^e = 0$, $i = 1, 2, ..., n_e$. Hence $\delta^2 I(\boldsymbol{\phi}_h) > 0$ holds in (4.8). Thus, in this case, we have a unique extremum principle

and based on (4.9), hence a $\boldsymbol{\phi}_h$ obtained using (4.7) minimizes $I(\boldsymbol{\phi}_h)$ in (4.5). When the differential operator is non-linear $\delta^2 E_i^e$ are not zero, hence (4.7) in its present form does not satisfy any of the three conditions in (4.9), thus we do not have an extremum principle. This situation can be corrected by a simple modification. We note that $\delta I(\boldsymbol{\phi}_h) = 0$ yields $\big($from (4.7)$\big)$

$$\{g\} = \{g(\boldsymbol{\phi}_h)\} = 0 = \sum_{e=1}^{m} \left(\sum_{i=1}^{n_e} (E_i^e, \delta E_i^e)_{\bar{\Omega}_{xt}^e} \right) \tag{4.10}$$

Consider local approximations for the dependent variables $\boldsymbol{\phi}$ i.e. $\boldsymbol{\phi}_h^e$. Each dependent variable in $\boldsymbol{\phi}$ has its own local approximation. Collectively they constitute $\boldsymbol{\phi}_h^e$. Let all of the degrees of freedom in the local approximation $\boldsymbol{\phi}_h^e$ be $\{\delta^e\}$ and let

$$\{\delta\} = \bigcup_{e=1}^{m} \{\delta^e\} \tag{4.11}$$

be the degrees of freedom for the discretization $\left(\bar{\Omega}_{xt}^n\right)^T$, then $\{g\}$ in (4.10) is a non-linear function of $\{\delta\}$ i.e. we must find $\{\delta\}$ that satisfies

$$\{g(\{\delta\})\} = 0 \tag{4.12}$$

iteratively. We choose Newton's linear method (Newton-Raphson method). Let $\{\delta^0\}$ be an assumed solution or guess of $\{\delta\}$ in (4.12). Then

$$\{g\left(\{\delta^0\}\right)\} \neq 0 \tag{4.13}$$

Let $\{\Delta\delta\}$ be a change in $\{\delta^0\}$ such that

$$\{g\left(\{\delta^0\} + \{\Delta\delta\}\right)\} = 0 \tag{4.14}$$

Expanding $\{g(\{\delta^0\} + \{\Delta\delta\})\}$ in Taylor series about $\{\delta^0\}$ and retaining only up to linear terms in $\{\Delta\delta\}$ yields

$$\{g\left(\{\delta^0\} + \{\Delta\delta\}\right)\} \approx \{g\left(\{\delta^0\}\right)\} + \left.\frac{\partial\{g\}}{\partial\{\delta\}}\right|_{\{\delta^0\}} \{\Delta\delta\} = 0 \tag{4.15}$$

From (4.15), we can solve for $\{\Delta\delta\}$.

$$\{\Delta\delta\} = -\left[\frac{\partial\{g\}}{\partial\{\delta\}}\right]^{-1}_{\{\delta^0\}} \{g\left(\{\delta^0\}\right)\} \tag{4.16}$$

We note that

$$\frac{\partial\{g\}}{\partial\{\delta\}} = \delta\{g\} = \sum_{e=1}^{m}\left(\sum_{i=1}^{n_e}\left(\delta E_i^e, \delta E_i^e\right)_{\bar{\Omega}_{xt}^e}\right) + \sum_{e=1}^{m}\left(\sum_{i=1}^{n_e}\left(E_i^e, \delta^2 E_i^e\right)_{\bar{\Omega}_{xt}^e}\right) = \frac{1}{2}\delta^2 I\left(\boldsymbol{\phi}_h\right) \tag{4.17}$$

If $\left[\frac{\partial\{g\}}{\partial\{\delta\}}\right]$ is positive definite in (4.16), then we can ensure a unique solution $\{\Delta\delta\}$ from (4.16). Based on (4.17) this is possible if we approximate $\delta^2 I\left(\phi_h\right)$ by [6, 8, 9, 36–40]

$$\delta^2 I\left(\boldsymbol{\phi}_h\right) \approx 2\sum_{e=1}^{m}\left(\sum_{i=1}^{n_e}\left(\delta E_i^e, \delta E_i^e\right)_{\bar{\Omega}_{xt}^e}\right) > 0 \text{ , a unique extremum principle.} \tag{4.18}$$

Rationale for the approximation in (4.18) has been discussed by Surana et. al. [6, 8, 9, 36–40]. Thus, with (4.18) STLSP is STVC.

Once we find a $\{\Delta\delta\}$ using (4.16) and (4.18), it is helpful to consider the following for obtaining an updated solution $\{\delta\}$

$$\{\delta\} = \{\delta^0\} + \alpha\{\Delta\delta\} \tag{4.19}$$

in which α is a scalar generally between 0 and 2 and assumes the largest value between 0 and 2 for which $I\left(\{\delta\}\right) \leq I\left(\{\delta^0\}\right)$ holds. This is referred to as line search. The entire process of solving for $\{\Delta\delta\}$ and to update $\{\delta^0\}$ using (4.19) to obtain $\boldsymbol{\phi}_h$ that satisfies $\{g\left(\{\delta\}\right)\} = 0$ is called Newton's method with line search.

In (4.18), we note that

$$[K^e] = \sum_{i=1}^{n_e}\left(\delta E_i^e, \delta E_i^e\right)_{\bar{\Omega}_{xt}^e} \tag{4.20}$$

is in fact the element coefficient matrix and

$$\sum_{e=1}^{m}\left(\sum_{i=1}^{n_e}\left(\delta E_i^e, \delta E_i^e\right)_{\bar{\Omega}_{xt}^e}\right) = \sum_{e=1}^{m}[K^e] = [K] \tag{4.21}$$

is the assembly of the element matrices. The same holds true for $\{g\}$ and $\{g^e\}$ in (4.7). We note that the computation of $\{g^e\}$ and $[K^e]$ needed in (4.16) requires E_i^e; $i = 1, 2, ..., n_e$ and δE_i^e; $i = 1, 2, ..., n_e$. Once we have $[K^e]$ and $\{g^e\}$, we assemble them and solve for $\{\Delta\delta\}$ using (4.16) followed by an updated $\{\delta\}$ using (4.19). Using a new $\{\delta\}$ we check if $|g_i(\{\delta\})|_{max} \leq \Delta$ holds, in which Δ is a preset tolerance, a threshold value of numerically computed zero. If not, we repeat the process by replacing $\{\delta^0\}$ with $\{\delta\}$.

4.2.2 Summary of Computational Steps and Time-Marching Procedure

In the following we list important computational steps in the STLSP and the time marching procedure for computing the complete evolution.

1. Consider PDEs in the mathematical model (either a higher order system or a system of first order PDEs) and identify dependent variables. The mathematical model obviously must have closure.

2. Consider the first space-time strip or slab for an increment of time and its spatial discretization into space-time finite elements, generally nine-node p-version elements (in x, t) or 27-node p-version elements (in x, y, and t) with higher order continuity local approximations in space and time.

3. Consider local approximations for each dependent variable. p-level and the order of space $k = (k_1, k_2)$ (in space and time) can be different for each dependent variable. Minimally conforming choice of k is dependent on the highest orders of the derivatives in space and time for each dependent variable and whether the integrals are in

Riemann or Lebesgue sense.

4. Arrange nodal degrees of freedom for each variable as a vector and then arrange these individual vectors in a single vector $\{\delta^e\}$ representing all degrees of freedom for all of the dependent variables for an element 'e'. Thus we have $\{\delta^e\}$ as nodal degrees of freedom for each element and

$$\{\delta\} = \bigcup_{e=1}^{m} \{\delta^e\} \tag{4.22}$$

where $\{\delta\}$ are the total degrees of freedom for the entire discretization for the first space-time strip or slab.

5. Assume a starting solution $\{\delta^0\}$ for $\{\delta\}$.

6. Using local approximation for each dependent variable and $\{\delta\} = \{\delta^0\}$ we compute

$$\{g^e\} = \sum_{i=1}^{n_e} (E_i^e, \delta E_i^e)_{\bar{\Omega}_{xt}^e} \quad ; \quad e = 1, 2, ..., m \tag{4.23}$$

$$[K^e] = \sum_{i=1}^{n_e} (\delta E_i^e, \delta E_i^e)_{\bar{\Omega}_{xt}^e} \quad ; \quad e = 1, 2, ..., m \tag{4.24}$$

$$[I^e] = \sum_{i=1}^{n_e} (E_i^e, E_i^e)_{\bar{\Omega}_{xt}^e} \quad ; \quad e = 1, 2, ..., m \tag{4.25}$$

7. Assemble $\{g^e\}$ and $[K^e]$ to obtain $\{g\}$ and $[K]$ i.e

$$\{g\} = \sum_{e=1}^{m} \{g^e\} \tag{4.26}$$

$$[K] = \sum_{e=1}^{m} [K^e] \tag{4.27}$$

$$I = \sum_{e=1}^{m} I^e \tag{4.28}$$

8. Use

$$\{\Delta\delta\} = -[K]^{-1} \{g\} \tag{4.29}$$

to calculate $\{\Delta\delta\}$ after imposing boundary conditions (BCs) and initial conditions (ICs) on $\{\delta\}$.

9. Find new updated solution using,

$$\{\delta\} = \{\delta^0\} + \alpha\{\Delta\delta\} \qquad ; \quad 0 < \alpha \leq 2 \text{ such that } I\left(\{\delta\}\right) \leq I\left(\{\delta^0\}\right) \tag{4.30}$$

10. Recalculate $\{g^e\}$ using (4.25) and updated $\{\delta\}$. Assemble $\{g^e\}$ to obtain $\{g\}$ as in (4.26). Check if the absolute value of each component of $\{g\}$ is less than or equal to Δ, a preset threshold value for numerically computed zero (generally 10^{-6} or lower suffices).

    If this condition is satisfied then we have a solution of the non-linear algebraic system defined by $\{g\} = 0$ and we say that Newton's linear method is converged. If not, then reset $\{\delta^0\}$ to $\{\delta\}$ and repeat steps 6 through 10 until convergence of the Newton's linear method is achieved.

The steps described here provide a solution for the first space-time strip or slab between $t = 0$ and $t = \Delta t$. Next, consider the second space-time strip between $t = \Delta t$ and $t = 2\Delta t$. Initial conditions for this space-time strip or slab are obtained from the solution for the first space-time strip or slab at $t = \Delta t$. Repeat the same procedure as used for the first space-time strip or slab. This procedure known as 'time marching procedure' can be continued until the desired time is reached.

We remark that E_i^e, I^e, and I are scalars, δE_i^e are vectors and hence $\{g^e\}$ are also vectors but $(\delta E_i^e, \delta E_i^e)_{\bar{\Omega}_{xt}^e}$ is a matrix. Thus, care must be taken in various scalar products encountered in the space-time least squares finite element process.

4.3 Dimensionless forms of the mathematical models

In using methods of approximation for obtaining numerical solutions of the IVPs describing phase change processes, we must non-dimensionalize the PDEs to ensure that the wide range of magnitudes of the dependent variables does not lead to ill conditioned coefficients matrices in the resulting algebraic systems. In order to do so, we choose reference quantities to obtain dimensionless dependent variables and other quantities. The quantities with hat ($\hat{}$) are with their usual dimensions, quantities with zero subscript are reference quantities and the quantities without hat ($\hat{}$) are dimensionless quantities. We define

$$x_i = \hat{x}_i/L_0 \ , \ v_i = \hat{v}_i/v_0 \ , \ \mu = \hat{\mu}/\mu_0 \ , \ p = \hat{p}/p_0 \ , \ {}_d\sigma_{ij}^{(0)} = {}_d\hat{\sigma}_{ij}^{(0)}/\tau_0 \ , \ L_f = \hat{L}_f/L_{f0}$$
$$k = \hat{k}/k_0 \ , \ c_p = \hat{c}_p/c_{p0} \ , \ \rho = \hat{\rho}/\rho_0 \ , \ T = (\hat{T} - T_0)/T_0 \ , \ t = \hat{t}/t_0 \ , \ \boldsymbol{q} = \hat{\boldsymbol{q}}/q_0 \tag{4.31}$$

In the case of Eulerian descriptions, the quantities will contain an over bar ($\bar{}$) as well.

4.3.1 Lagrangian description

Recall the mathematical model presented in Chapter 2 (equations (2.29) and (2.30)).

$$\hat{\rho}\hat{c}_p\frac{\partial\hat{T}}{\partial\hat{t}} + \hat{\boldsymbol{\nabla}}\cdot\hat{\boldsymbol{q}} + \hat{\rho}\frac{\partial\hat{L}_f}{\partial\hat{t}} = 0 \qquad \forall\ (\boldsymbol{x},t)\ \in\ \Omega_{\boldsymbol{x}t} \tag{4.32}$$

$$\hat{\boldsymbol{q}} = -\hat{k}\hat{\boldsymbol{\nabla}}\hat{T} \qquad \forall\ (\boldsymbol{x},t)\ \in\ \Omega_{\boldsymbol{x}t} \tag{4.33}$$

Using (4.31) in (4.32) and (4.33), we obtain

$$\rho c_p\frac{\partial T}{\partial t} + \left(\frac{q_0 t_0}{L_0\rho_0 c_{p0}T_0}\right)\boldsymbol{\nabla}\cdot\boldsymbol{q} + \left(\frac{L_{f0}}{c_{p0}T_0}\right)\rho\frac{\partial L_f}{\partial t} = 0 \tag{4.34}$$

$$\boldsymbol{q} = -\left(\frac{1}{q_0}\right)\left(\frac{k_0T_0}{L_0}\right)k\boldsymbol{\nabla}T \tag{4.35}$$

If we choose

$$q_0 = \frac{k_0 T_0}{L_0} \tag{4.36}$$

Then, (4.34) and (4.35) can be written as

$$\rho c_p \frac{\partial T}{\partial t} + \left(\frac{t_0 k_0}{L_0^2 \rho_0 c_{p0}} \right) \boldsymbol{\nabla} \cdot \boldsymbol{q} + \left(\frac{L_{f0}}{c_{p0} T_0} \right) \rho \frac{\partial L_f}{\partial t} = 0 \tag{4.37}$$

$$\boldsymbol{q} = -k \boldsymbol{\nabla} T \tag{4.38}$$

Since the velocity field is assumed zero, t_0 cannot be defined using L_0 and v_0. We can choose the following:

$$\begin{aligned} t_0 &= \frac{L_0^2 \rho_0 c_{p0}}{k_0} \\ L_{f0} &= c_{p0} T_0 \end{aligned} \tag{4.39}$$

Using (4.39), the mathematical model (4.37) and (4.38) reduces to

$$\rho c_p \frac{\partial T}{\partial t} + \boldsymbol{\nabla} \cdot \boldsymbol{q} + \rho \left(\frac{\partial L_f}{\partial T} \right) \frac{\partial T}{\partial t} = 0 \tag{4.40}$$

$$\boldsymbol{q} = -k \boldsymbol{\nabla} T \tag{4.41}$$

Equations (4.40) and (4.41) are a system of first order PDEs in T and $\boldsymbol{q}$ in which reference time t_0 and reference latent heat of fusion L_{f0} are defined by (4.39). Alternatively, if we substitute $\boldsymbol{q}$ from (4.41) into (4.40), then we obtain a single PDE in temperature T.

$$\rho c_p \frac{\partial T}{\partial t} - \boldsymbol{\nabla} \cdot (k \boldsymbol{\nabla} T) + \rho \left(\frac{\partial L_f}{\partial T} \right) \frac{\partial T}{\partial t} = 0 \tag{4.42}$$

Equation (4.42) contains up to second order derivatives of temperature T in space coordinates. The mathematical models (4.40) and (4.41) as well as (4.42) can be used in numerical studies, but the choice of local approximations for minimally conforming approximation spaces differ in the two. Since $L_f = L_f(T)$; $\dfrac{\partial L_f}{\partial T}$ is strictly deterministic. Other mathematical models (Model C and Model D) presented in Chapter 2 have similar dimensionless forms.

4.3.2 Eulerian description

In this section we derive dimensionless form of the mathematical models for liquid, solid and transition phases.

Liquid Phase:

Recall equations (3.3)-(3.7) from Chapter 3 in the absence of body forces.

$$
\begin{aligned}
&\hat{\bar{\rho}}_l \frac{\partial \hat{\bar{v}}_i}{\partial \hat{\bar{x}}_i} = 0 \\
&\hat{\bar{\rho}}_l \frac{\partial \hat{\bar{v}}_i}{\partial \hat{t}} + \hat{\bar{\rho}}_l \hat{\bar{v}}_j \frac{\partial \hat{\bar{v}}_i}{\partial \hat{\bar{x}}_j} + \frac{\partial \hat{\bar{p}}}{\partial \hat{\bar{x}}_i} - \frac{\partial_d \hat{\bar{\sigma}}^{(0)}_{ij}}{\partial \hat{\bar{x}}_j} = 0 \\
&\hat{\bar{\rho}}_l \hat{\bar{c}}_{pl} \left(\frac{\partial \hat{\bar{T}}}{\partial \hat{t}} + \hat{\bar{\boldsymbol{v}}} \cdot \hat{\bar{\boldsymbol{\nabla}}} \hat{\bar{T}} \right) + \hat{\bar{\boldsymbol{\nabla}}} \cdot \hat{\bar{\boldsymbol{q}}} - {}_d\hat{\bar{\sigma}}^{(0)}_{ij} \frac{\partial \hat{\bar{v}}_i}{\partial \hat{\bar{x}}_j} = 0 \\
&{}_d\hat{\bar{\sigma}}^{(0)}_{ij} = 2\hat{\bar{\mu}} \hat{\bar{D}}_{ij} \\
&\hat{\bar{\boldsymbol{q}}} = -\hat{\bar{k}}_l \hat{\bar{\boldsymbol{\nabla}}} \hat{\bar{T}}
\end{aligned}
\tag{4.43}
$$

Using (4.31) (quantities with "$\hat{}$" are replaced with "$\bar{}$"), (4.43) can be written in the following dimensionless form:

$$
\begin{aligned}
&\bar{\rho}_l \frac{\partial \bar{v}_i}{\partial \bar{x}_i} = 0 \\
&\bar{\rho}_l \frac{\partial \bar{v}_i}{\partial t} + \bar{\rho}_l \bar{v}_j \frac{\partial \bar{v}_i}{\partial \bar{x}_j} + \left(\frac{p_0}{\rho_0 v_0^2} \right) \frac{\partial \bar{p}}{\partial \bar{x}_i} - \left(\frac{\tau_0}{\rho_0 v_0^2} \right) \frac{\partial_d \bar{\sigma}^{(0)}_{ij}}{\partial \bar{x}_j} = 0 \\
&\frac{\bar{\rho}_l \bar{c}_{pl}}{Ec} \left(\frac{\partial \bar{T}}{\partial t} + \bar{\boldsymbol{v}} \cdot \bar{\boldsymbol{\nabla}} \bar{T} \right) + \frac{1}{Re\, Br} \left(\bar{\boldsymbol{\nabla}} \cdot \bar{\boldsymbol{q}} \right) - \left(\frac{\tau_0}{\rho_0 v_0^2} \right) {}_d\bar{\sigma}^{(0)}_{ij} \frac{\partial \bar{v}_i}{\partial \bar{x}_j} = 0 \\
&{}_d\bar{\sigma}^{(0)}_{ij} = \left(\frac{\mu_0 v_0}{L_0 \tau_0} \right) 2\bar{\mu} \bar{D}_{ij} \\
&\bar{\boldsymbol{q}} = -\bar{k}_l \bar{\boldsymbol{\nabla}} \bar{T}
\end{aligned}
\tag{4.44}
$$

where Reynolds number Re, Brinkman number Br and Eckret number Ec are defined as

$$
Re = \frac{\rho_0 v_0 L_0}{\mu_0} \quad ; \quad Br = \frac{\mu_0 v_0^2}{k_0 T_0} \quad ; \quad Ec = \frac{v_0^2}{c_{p0} T_0} \tag{4.45}
$$

Solid Phase:

Recall equations (3.9) to (3.13) from Chapter 3 in the absence of body forces and the pressure constraint equation.

Pressure constraint equation (in place of continuity):

$$\begin{aligned}
&\text{tr}\left({}_d\hat{\hat{\boldsymbol{\sigma}}}^{(0)}\right) = 0 && ;\ \text{in } \mathbb{R}^3 \\
&{}_d\hat{\hat{\sigma}}^{(0)}_{x1x1} + {}_d\hat{\hat{\sigma}}^{(0)}_{x1x1} + \hat{\hat{p}} = 0 && ;\ \text{in } \mathbb{R}^2 \\
&{}_d\hat{\hat{\sigma}}^{(0)}_{x1x1} + 2\hat{\hat{p}} = 0 && ;\ \text{in } \mathbb{R}^1
\end{aligned}$$

Momentum and energy equations:

$$\begin{aligned}
&\hat{\hat{\rho}}_s \frac{\partial \hat{\hat{v}}_i}{\partial \hat{t}} + \hat{\hat{\rho}}_s \hat{\hat{v}}_j \frac{\partial \hat{\hat{v}}_i}{\partial \hat{\hat{x}}_j} + \frac{\partial \hat{\hat{p}}}{\partial \hat{\hat{x}}_i} - \frac{\partial {}_d\hat{\hat{\sigma}}^{(0)}_{ij}}{\partial \hat{\hat{x}}_j} = 0 \\
&\hat{\hat{\rho}}_s \hat{\hat{c}}_{ps} \left(\frac{\partial \hat{\hat{T}}}{\partial \hat{t}} + \hat{\hat{\boldsymbol{v}}} \cdot \hat{\hat{\boldsymbol{\nabla}}} \hat{\hat{T}} \right) + \hat{\hat{\boldsymbol{\nabla}}} \cdot \hat{\hat{\boldsymbol{q}}} - {}_d\hat{\hat{\sigma}}^{(0)}_{ij} \frac{\partial \hat{\hat{v}}_i}{\partial \hat{\hat{x}}_j} + \hat{\hat{p}} \frac{\partial \hat{\hat{v}}_i}{\partial \hat{\hat{x}}_i} = 0
\end{aligned} \tag{4.46}$$

Constitutive equations:

$$\begin{aligned}
&{}_d\hat{\hat{\sigma}}^{(1)}_{ij} = \underset{\sim}{\hat{\hat{D}}}_{ik} \hat{\hat{D}}_{kj} \\
&\hat{\hat{\boldsymbol{q}}} = -\hat{\hat{k}}_s \hat{\hat{\boldsymbol{\nabla}}} \hat{\hat{T}}
\end{aligned}$$

Using (4.31) (quantities with "$\hat{\ }$" are replaced with "$^-$"), (4.46) can be written in the following dimensionless form:

Pressure constraint equation:

$$\begin{aligned}
&\text{tr}\left({}_d\bar{\boldsymbol{\sigma}}^{(0)}\right) = 0 && ;\ \text{in } \mathbb{R}^3 \\
&{}_d\bar{\sigma}^{(0)}_{x1x1} + {}_d\bar{\sigma}^{(0)}_{x1x1} + \left(\frac{p_0}{\tau_0}\right)\bar{p} = 0 && ;\ \text{in } \mathbb{R}^2 \\
&{}_d\bar{\sigma}^{(0)}_{x1x1} + 2\left(\frac{p_0}{\tau_0}\right)\bar{p} = 0 && ;\ \text{in } \mathbb{R}^1
\end{aligned}$$

Momentum and energy equations:

$$\begin{aligned}
&\bar{\rho}_s\frac{\partial\bar{v}_i}{\partial t} + \bar{\rho}_s\bar{v}_j\frac{\partial\bar{v}_i}{\partial\bar{x}_j} + \left(\frac{p_0}{\rho_0 v_0^2}\right)\frac{\partial\bar{p}}{\partial\bar{x}_i} - \left(\frac{\tau_0}{\rho_0 v_0^2}\right)\frac{\partial_d\bar{\sigma}^{(0)}_{ij}}{\partial\bar{x}_j} = 0 \\
&\frac{\bar{\rho}_s\bar{c}_{ps}}{Ec}\left(\frac{\partial\bar{T}}{\partial t} + \bar{\boldsymbol{v}}\cdot\bar{\boldsymbol{\nabla}}\bar{T}\right) + \frac{1}{Re\,Br}\bar{\boldsymbol{\nabla}}\cdot\bar{\boldsymbol{q}} - \left(\frac{\tau_0}{\rho_0 v_0^2}\right){}_d\bar{\sigma}^{(0)}_{ij}\frac{\partial\bar{v}_i}{\partial\bar{x}_j} \\
&\qquad\qquad + \left(\frac{p_0}{\rho_0 v_0^2}\right)\bar{p}\frac{\partial\bar{v}_i}{\partial\bar{x}_i} = 0
\end{aligned} \tag{4.47}$$

Constitutive equations:

$${}_d\bar{\sigma}^{(1)}_{ij} = \left(\frac{E_0}{\tau_0}\right)\underset{\sim}{\bar{D}}_{ik}\bar{D}_{kj}$$

$$\bar{\boldsymbol{q}} = -\bar{k}_s\bar{\boldsymbol{\nabla}}\bar{T}$$

Transition Region:

Recall GDEs (3.28) from Chapter 3 (in the absence of body forces).

Continuity:

$$\begin{aligned}
&\bar{f}_s\left(\text{tr}\left({}_d\hat{\hat{\boldsymbol{\sigma}}}^{(0)}\right)\right)+\bar{f}_l\left(\hat{\hat{\rho}}\frac{\partial\hat{\hat{v}}_i}{\partial\hat{\hat{x}}_i}\right)=0 \qquad ;\ \text{in } \mathbb{R}^3\\
&\bar{f}_s\left({}_d\hat{\hat{\sigma}}^{(0)}_{x1x1}+{}_d\hat{\hat{\sigma}}^{(0)}_{x1x1}+\hat{\hat{p}}\right)+\bar{f}_l\left(\hat{\hat{\rho}}\frac{\partial\hat{\hat{v}}_i}{\partial\hat{\hat{x}}_i}\right)=0 \qquad ;\ \text{in } \mathbb{R}^2\\
&\bar{f}_s\left({}_d\hat{\hat{\sigma}}^{(0)}_{x1x1}+2\hat{\hat{p}}\right)+\bar{f}_l\left(\hat{\hat{\rho}}\frac{\partial\hat{\hat{v}}_i}{\partial\hat{\hat{x}}_i}\right)=0 \qquad ;\ \text{in } \mathbb{R}^1
\end{aligned}$$

Momentum and energy equations:

$$\begin{aligned}
&\hat{\hat{\rho}}\frac{\partial\hat{\hat{v}}_i}{\partial\hat{t}}+\hat{\hat{\rho}}\hat{\hat{v}}_j\frac{\partial\hat{\hat{v}}_i}{\partial\hat{\hat{x}}_j}+\frac{\partial\hat{\hat{p}}}{\partial\hat{\hat{x}}_i}-\frac{\partial_d\hat{\hat{\sigma}}^{(0)}_{ij}}{\partial\hat{\hat{x}}_j}=0\\
&\hat{\hat{\rho}}\left(\hat{\hat{c}}_p+\frac{\partial\hat{\hat{L}}_f}{\partial\hat{\hat{T}}}\right)\left(\frac{\partial\hat{\hat{T}}}{\partial\hat{t}}+\hat{\hat{\boldsymbol{v}}}\cdot\hat{\hat{\boldsymbol{\nabla}}}\hat{\hat{T}}\right)+\hat{\hat{\boldsymbol{\nabla}}}\cdot\hat{\hat{\boldsymbol{q}}}-{}_d\hat{\hat{\sigma}}^{(0)}_{ij}\frac{\partial\hat{\hat{v}}_i}{\partial\hat{\hat{x}}_j}+\bar{f}_s\hat{\hat{p}}\frac{\partial\hat{\hat{v}}_i}{\partial\hat{\hat{x}}_i}=0
\end{aligned} \tag{4.48}$$

Constitutive equations:

$$\begin{aligned}
&\bar{f}_l\left({}_d\hat{\hat{\sigma}}^{(0)}_{ij}-2\hat{\hat{\mu}}\hat{\hat{D}}_{ij}\right)+\bar{f}_s\left({}_d\hat{\hat{\sigma}}^{(1)}_{ij}-\underset{\sim}{\hat{\hat{D}}}_{ik}\hat{\hat{D}}_{kj}\right)=0\\
&\hat{\hat{\boldsymbol{q}}}=-\hat{\hat{k}}\hat{\hat{\boldsymbol{\nabla}}}\hat{\hat{T}}
\end{aligned}$$

Using (4.31) (quantities with "$\hat{\ }$" are replaced with "$^-$"), (4.48) can be written in the dimensionless form given in the following:

Continuity:

$$\bar{f}_s \left(\text{tr} \left({}_d\bar{\boldsymbol{\sigma}}^{(0)} \right) \right) + \bar{f}_l \left(\bar{\rho} \frac{\partial \bar{v}_i}{\partial \bar{x}_i} \right) = 0 \qquad ; \text{ in } \mathbb{R}^3$$

$$\bar{f}_s \left({}_d\bar{\sigma}^{(0)}_{x1x1} + {}_d\bar{\sigma}^{(0)}_{x1x1} + \left(\frac{p_0}{\tau_0} \right) \bar{p} \right) + \bar{f}_l \left(\bar{\rho} \frac{\partial \bar{v}_i}{\partial \bar{x}_i} \right) = 0 \qquad ; \text{ in } \mathbb{R}^2$$

$$\bar{f}_s \left({}_d\bar{\sigma}^{(0)}_{x1x1} + 2 \left(\frac{p_0}{\tau_0} \right) \bar{p} \right) + \bar{f}_l \left(\bar{\rho} \frac{\partial \bar{v}_i}{\partial \bar{x}_i} \right) = 0 \qquad ; \text{ in } \mathbb{R}^1$$

Momentum and energy equations:

$$\bar{\rho} \frac{\partial \bar{v}_i}{\partial t} + \bar{\rho} \bar{v}_j \frac{\partial \bar{v}_i}{\partial \bar{x}_j} + \left(\frac{p_0}{\rho_0 v_0^2} \right) \frac{\partial \bar{p}}{\partial \bar{x}_i} - \left(\frac{\tau_0}{\rho_0 v_0^2} \right) \frac{\partial {}_d\bar{\sigma}^{(0)}_{ij}}{\partial \bar{x}_j} = 0 \tag{4.49}$$

$$\bar{\rho} \left(\frac{1}{Ec} \bar{c}_p + \frac{L_{f0}}{v_0^2} \frac{\partial \bar{L}_f}{\partial \bar{T}} \right) \left(\frac{\partial \bar{T}}{\partial t} + \bar{\boldsymbol{v}} \cdot \bar{\boldsymbol{\nabla}} \bar{T} \right) + \frac{1}{Re\, Br} \bar{\boldsymbol{\nabla}} \cdot \bar{\boldsymbol{q}} - \left(\frac{\tau_0}{\rho_0 v_0^2} \right) {}_d\bar{\sigma}^{(0)}_{ij} \frac{\partial \bar{v}_i}{\partial \bar{x}_j} + \left(\frac{p_0}{\rho_0 v_0^2} \right) \bar{f}_s \bar{p} \frac{\partial \bar{v}_i}{\partial \bar{x}_i} = 0$$

Constitutive equations:

$$\bar{f}_l \left({}_d\bar{\sigma}^{(0)}_{ij} - \left(\frac{\mu_0 v_0}{L_0 \tau_0} \right) 2 \bar{\mu} \bar{D}_{ij} \right) + \bar{f}_s \left({}_d\bar{\sigma}^{(1)}_{ij} - \left(\frac{E_0}{\tau_0} \right) \underset{\sim}{\bar{D}}_{ik} \bar{D}_{kj} \right) = 0$$

$$\bar{\boldsymbol{q}} = -\bar{k} \bar{\boldsymbol{\nabla}} \bar{T}$$

Remark:

Once the mathematical model and the local approximations of the dependent variables are chosen, the specific details of LSP based on the residual equations E_i ; $i = 1, 2, ..., n_e$ and their variations δE_i ; $i = 1, 2, ..., n_e$ are straight forward, hence are omitted.

Chapter 5

Numerical Studies using mathematical models in Lagrangian description

5.1 Introduction

In this chapter we consider phase change model problems in $\mathbb{R}^1$ and $\mathbb{R}^2$. The purpose of these numerical studies is multi-fold. From the material presented in Chapters 1 and 2 it is clear that the sharp interface method and the phase field method of describing liquid-solid phase phenomena lead to mathematical models that have their own limitations and merits. A significant shortcoming of these methods is that they require a priori existence of a liquid-solid interface at the commencement of the evolution. Secondly, a theoretical solution using the sharp interface model in $\mathbb{R}^1$ is only possible when ρ, c_p and k are constant. In the phase field approach, a priori knowledge of the free energy density function and the existence of the interface at the commencement of the solution are essential. The selection of the model problems in $\mathbb{R}^1$ in reference [23] was done in such a way that the computed evolutions

could be compared with sharp interface and phase field methods. Additional phase change problems in $\mathbb{R}^1$ were also chosen in reference [23] and were simulated to demonstrate the capability of the method proposed in reference [23] in simulating initiation and propagation of phase change front during evolution with changing c_p, k and L_f between the two phases. Model problems in $\mathbb{R}^2$ were used to demonstrate the same features as in the case of $\mathbb{R}^1$ i.e. initiation of a front, variable c_p, k and L_f between the two phases and accurate propagation of the front in $\mathbb{R}^2$ in which the interface zone separating the two phases can be complex. In reference [23], (1) L_f was used as a dependent variable, this can cause problems at lower p-levels, (2) only C^0 solutions where considered. the studies presented here eliminate L_f as a variable. This is necessary for the computed solution to be correct. Secondly, solutions of higher classes are also considered. The comparison of the evolution from smooth interface approach using L_f as a variable [23] with phase field and sharp interface methods were shown in reference [23] and are not repeated here. The numerical studies considered in this work are summarized in the following:

(1) Mathematical models in $\mathbb{R}^1$ without using L_f as a dependent variable and a comparison with the model using L_f as a variable ([23]).

(2) Model problems in $\mathbb{R}^1$ in which the capability of the smooth interface method proposed here to simulate the initiation of the liquid-solid or solid-liquid interface and its subsequent propagation during evolution is demonstrated. The density ρ, specific heat c_p, thermal conductivity k and latent heat of fusion L_f vary in a continuous and differentiable manner from liquid to solid phases and vice-versa (as described in Chapter 2). One model problem considers the initial phase to be liquid whereas in the other model problem the initial phase is considered to be solid to demonstrate

the effectiveness of the smooth interface approach in simulating the initiation of the front and its properties in either freezing or melting. These model problems can not be simulated using sharp interface or phase field methods due to the fact that: (a) they require capability to initiate a front (b) and secondly due to variations in ρ, c_p, k and L_f in the transition zone both of which are lacking in these two methods.

(3) In the next group of numerical studies we consider two model problems in $\mathbb{R}^2$ with square spatial domains.

   (a) The first model problem considers the initial phase to be liquid with uniform heat flux (cooling) on all four boundaries. This model demonstrate the initiation of complex liquid-solid front in a freezing process in $\mathbb{R}^2$ and its propagation during the evolution.

   (b) The second model problem considers the initial phase to be solid with uniform heat flux (heating) on all four boundaries. This model problem demonstrates initiation of a rather complex liquid-solid front that propagates inward from the edges of the square during evolution.

All numerical studies are performed using space-time least squares finite element processes for a space-time strip (in $\mathbb{R}^1$) or a space-time slab (in $\mathbb{R}^2$) the with time marching. The mathematical model utilized in the computational studies for $\mathbb{R}^1$ is a single PDE in T and for $\mathbb{R}^2$ is a system of first order PDEs in temperature and heat fluxes. In case of $\mathbb{R}^1$, the space-time domain of a space-time strip for an increment of time is discretized using nine-node p-version space-time elements. In the case of $\mathbb{R}^2$, the space-time slab is discretized using 27-node p-version space-time elements. The local approximations in $\mathbb{R}^1$ and $\mathbb{R}^2$ consist of class C^1 and C^0 respectively.

For an increment of time i.e. for a space-time strip or a slab, solution of the non-linear algebraic systems is obtained using Newton's linear method with line search. Newton's linear method is considered converged when the absolute value of each component of $\delta I = \{g\}$ is below a preset threshold Δ, numerically computed zero. $\Delta \leq 10^{-6}$ has been used in all numerical studies. Discretization and p-levels (considered to be uniform in space and time) are chosen such that the least squares functional I resulting from the residuals for the entire space-time strip or slab is always of order of $O(10^{-6})$ or lower and hence good accuracy of the evolution is always ensured for all space-time steps and slabs.

5.2 Transport Properties

In all numerical studies we consider the liquid phase to be water and the solid phase to be ice with the following properties.

Water: $\hat{\rho}_l = 62.38\ lbm/ft^3\ ;\ \hat{c}_{pl} = 1.006\ Btu/lbm\ R\ ;\ \hat{k}_l = 9.01 \times 10^{-5}\ Btu/s\ ft\ R$

$\hat{L}_{fl} = 143.6\ Btu/lbm\ ;\ \hat{\mu} = 0.12 \times 10^{-2}\ lbm/ft\ s$

Ice: $\hat{\rho}_s = 57.16\ lbm/ft^3\ ;\ \hat{c}_{ps} = 0.4896\ Btu/lbm\ R\ ;\ \hat{k}_s = 3.57 \times 10^{-4}\ Btu/s\ ft\ R$

$\hat{L}_{fs} = 0.000\ Btu/lbm\ ;\ \hat{E} = 6.05 \times 10^6\ lbm/ft\ s^2\ ;\ \nu = 0.33$

Transition region:

In the transition region $\rho(T)$, $c_p(T)$, $k(T)$ and $L_f(T)$ are assumed to vary in a continuous and differentiable manner between the temperatures T_s and T_l defining the transition region between solid and liquid phases. If $Q(T)$ represents a transport property then we

use the following:

$$Q(T) = c_0 + \sum_{i=1}^{n} c_i T^i \qquad ; T_s \leq T \leq T_l \tag{5.1}$$

when $n = 3$, $Q(T)$ is a cubic polynomial in T

The coefficients c_0 and c_i, $i = 1, 2, 3$ in (5.1) are calculated using the conditions:

$$\begin{aligned} &\text{at} \quad T = T_s \ : \qquad Q(T_s) = Q_s \quad , \qquad \left.\frac{\partial Q}{\partial T}\right|_{T=T_s} = 0 \\ &\text{at} \quad T = T_l \ : \qquad Q(T_l) = Q_s \quad , \qquad \left.\frac{\partial Q}{\partial T}\right|_{T=T_l} = 0 \end{aligned} \tag{5.2}$$

when $n = 5$, $Q(T)$ is a 5^{th} degree polynomial in T

The coefficients c_0 and c_i, $i = 1, ..., 5$ in (5.1) are calculated using the conditions:

$$\begin{aligned} &\text{at} \quad T = T_s \ : \qquad Q(T_s) = Q_s \quad , \qquad \left.\frac{\partial Q}{\partial T}\right|_{T=T_s} = \left.\frac{\partial^2 Q}{\partial T^2}\right|_{T=T_s} = 0 \\ &\text{at} \quad T = T_l \ : \qquad Q(T_l) = Q_s \quad , \qquad \left.\frac{\partial Q}{\partial T}\right|_{T=T_l} = \left.\frac{\partial^2 Q}{\partial T^2}\right|_{T=T_l} = 0 \end{aligned} \tag{5.3}$$

Remarks:

(1) By letting Q to be ρ, c_p, k and L_f, dependence of these properties on temperature can be easily established.

(2) In case of L_f we note that $L_f(T_s) = 0$ and $L_f(T_l) = L_f$ (value of latent heat of fusion).

(3) Thus all transport properties including latent heat of fusion are explicitly defined as functions of temperature T in the transition region.

Reference quantities:

For the dimensionless forms of all the mathematical models in Lagrangian description, the

following reference quantities are used.

$$\rho_0 = \hat{\rho}_s \qquad k_0 = \hat{k}_s \qquad c_{p0} = \hat{c}_{ps}$$

$$T_0 = (32^\circ F + 459.67) = 491.67\ R \qquad L_0 = 0.25 ft$$

$$L_{f0} = c_{p0} T_0 = 240.72\ Btu/lbm \qquad t_0 = \frac{L_0^2 \rho_0 c_{p0}}{k_0} = 4.899 \times 10^3\ s = 81.65 min$$

5.3 Numerical Studies in $\mathbb{R}^1$

In this section we present numerical studies in $\mathbb{R}^1$ i.e. for one dimensional phase change.

5.3.1 Choice of Mathematical Model

In Chapter 2 four alternate mathematical models were presented in Lagrangian description in $\mathbb{R}^1$. Their dimensionless forms were given in Chapter 4 (also listed in the following). Using $\boldsymbol{\nabla} = \dfrac{\partial}{\partial x}$, we have.

Model A: A single PDE in temperature

$$\rho(T)\left(c_p(T) + \frac{\partial L_f(T)}{\partial T}\right)\frac{\partial T}{\partial t} - \boldsymbol{\nabla}\cdot\left(k(T)\boldsymbol{\nabla} T\right) = 0 \tag{5.4}$$

Model B: A system of first order PDEs in T and q

$$\begin{aligned} &\rho(T)\left(c_p(T) + \frac{\partial L_f(T)}{\partial T}\right)\frac{\partial T}{\partial t} + \boldsymbol{\nabla}\cdot\boldsymbol{q} = 0 \\ &\boldsymbol{q} = -k(T)\boldsymbol{\nabla} T \end{aligned} \tag{5.5}$$

Model C: Using T and L_f as dependent variables

$$\begin{aligned} &\rho(T)c_p(T)\frac{\partial T}{\partial t} - \boldsymbol{\nabla}\cdot\left(k(T)\boldsymbol{\nabla} T\right) + \rho(T)\frac{\partial L_f}{\partial t} = 0 \\ &L_f = G(T) \end{aligned} \tag{5.6}$$

Model D: Using T, q and L_f as dependent variables

$$\begin{aligned} &\rho(T)c_p(T)\frac{\partial T}{\partial t} + \boldsymbol{\nabla \cdot q} + \rho(T)\frac{\partial L_f}{\partial t} = 0 \\ &\boldsymbol{q} = -k(T)\boldsymbol{\nabla} T \\ &L_f = G(T) \end{aligned} \tag{5.7}$$

Remarks:

(1) Model D was used in reference [23] in which numerical studies using this model were compared with phase field model and sharp interface model with good agreement of results during the evolution that consisted of propagation of an existing phase front specified as initial condition.

(2) We make a closer examination of the model using L_f as a dependent variable in the present work.

   (a) Since L_f is constant outside the transition region, $\frac{\partial L_f}{\partial T} = 0$, and in the transition region $L_f(T)$ is a continuous and differentiable function of temperature, this suggests that models A and B account for this behavior precisely.

   (b) Model A is preferred over model B for obvious reasons [41]. In this model inconsistencies in the local approximation due to auxiliary variables are eliminated [41] and computationally this model is more efficient as it has only one dependent variable compared to model B.

   (c) Equation $L_f = G(T)$ with L_f as a dependent variable is redundant. Additionally, when using this equation as in model C and D [23], we show that linear heat conduction is affected when p-levels are low (3-5). This is due to the fact

that δL_f adds to the element coefficient matrix in liquid and solid phases which should not be the case.

(d) In models A and B, we have

$$\delta\left(\frac{\partial L_f(T)}{\partial T}\frac{\partial T}{\partial t}\right) = \frac{\partial^2 L_f(T)}{\partial T^2}\left\{N^T\right\}\frac{\partial T}{\partial t} + \frac{\partial L_f(T)}{\partial T}\left\{\frac{\partial N^T}{\partial t}\right\} \tag{5.8}$$

In liquid and solid phases $\dfrac{\partial^2 L_f(T)}{\partial T^2}$ and $\dfrac{\partial L_f(T)}{\partial T}$ both are zero, hence (5.8) is zero therefore $\left(\dfrac{\partial L_f(T)}{\partial T}\dfrac{\partial T}{\partial t}\right)$ plays no role in the mathematical model in liquid and the solid phases. This is consistent with the physics. In (5.8), $\left\{N^T\right\}$ are local approximation functions for temperature.

(3) In all numerical studies presented in this section in $\mathbb{R}^1$ we use model A, a single PDE in temperature.

(4) STLSP for all the models is straight forward. All we need is E_i^e and δE_i^e. These are straight forward to derive once local approximations are chosen [6, 8, 9, 36–39].

5.3.2 Comparison of models B and D: linear heat conduction

Since in reference [23] model D was used for phase change studies in $\mathbb{R}^1$, we use this model and present a comparison of numerical solutions obtained using model B. Both models have T and q as dependent variables. Model D has L_f as additional dependent variable.

Figure 5.1 and 5.2 show schematics in the physical and dimensionless domains for a single space-time strip and the reference quantities used. The initial configuration consists of solid medium (ice). Uniform mesh of 50 space-time elements is used to discretize the dimensionless space-time domain (only one element in time t).

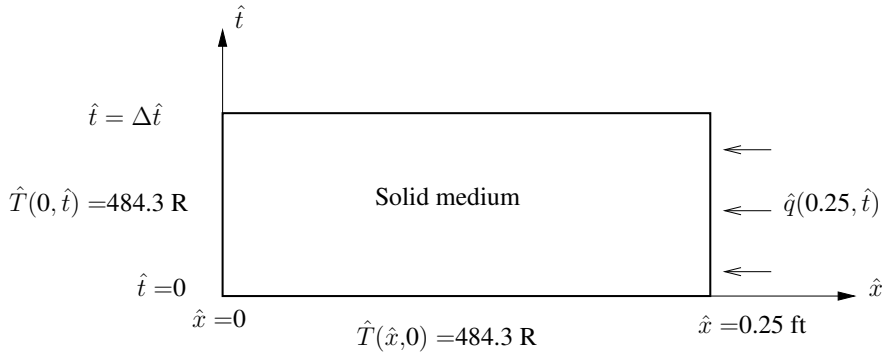

Figure 5.1: Space-time domain

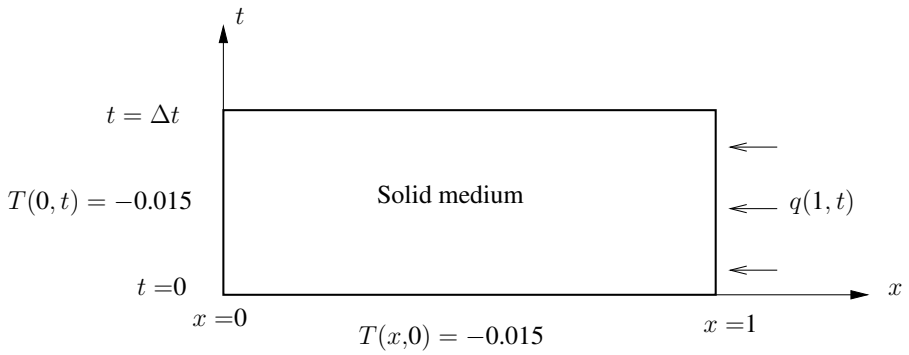

Reference quantities:

$\rho_0 = \hat{\rho}_s$, $k_0 = \hat{k}_s$, $c_{p0} = \hat{c}_{ps}$, $L_0 = 0.25ft$, $T_0 = (32°F + 459.67) = 491.67\ R$, $L_{f0} = c_{p0}T_0 = 240.72Btu/lbm$, $t_0 = L_0^2\rho_0 c_{p0}/k_0 = 4.899 \times 10^3\ s$, $q_0 = 1.42Btu/ft^2\,s$, $\Delta t = 0.005$, $\Delta\hat{t} = 24.5s$

Figure 5.2: Dimensionless space-time domain

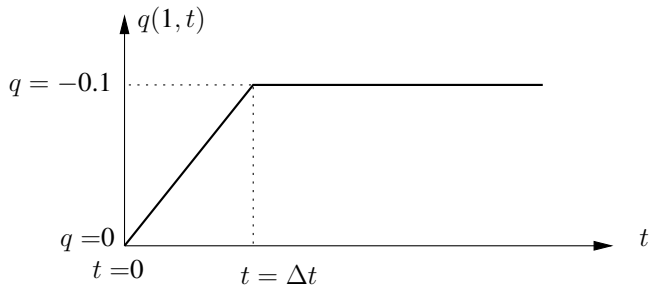

Figure 5.3: Boundary condition $q(1,t)$

Evolution of the temperature for the first five time increments with models B and D are shown in figures (5.4)-(5.6). We note that:

(*i*) When using model B, results remain unaffected due to p-level change.

(*ii*) In case of model D, lower p-levels (3-5) produce temperature evolutions that do not agree with model B. The differences are more pronounced at lower p-levels during initial stages of evolution (first and second time increments). Beyond the third increment of time, both models produce almost the same evolution of temperature.

(*iii*) We also note that the model D has twice as many dofs compared to model B, yet the evolution is in error during initial stages.

(*iv*) This numerical experiment is rather simple, but in more complex situations the consequences of using L_f as a dependent variable may be more serious than what we have observed here.

(*v*) In the work presented here, we do not use L_f as a dependent variable in any of the mathematical models.

5.3.3 Liquid-solid phase change in $\mathbb{R}^1$: Using model A

In this section we present liquid-solid phase change studies using model A. The space-time least squares formulation for a time strip (corresponding to an increment of time) with time marching is used to compute the evolution. Figure 5.7 shows a schematic of the space-time strip corresponding to the first increment of time, BCs, and ICs. Figure 5.8 shows dimensionless space-time domain, reference quantities and the dimensionless quantities.

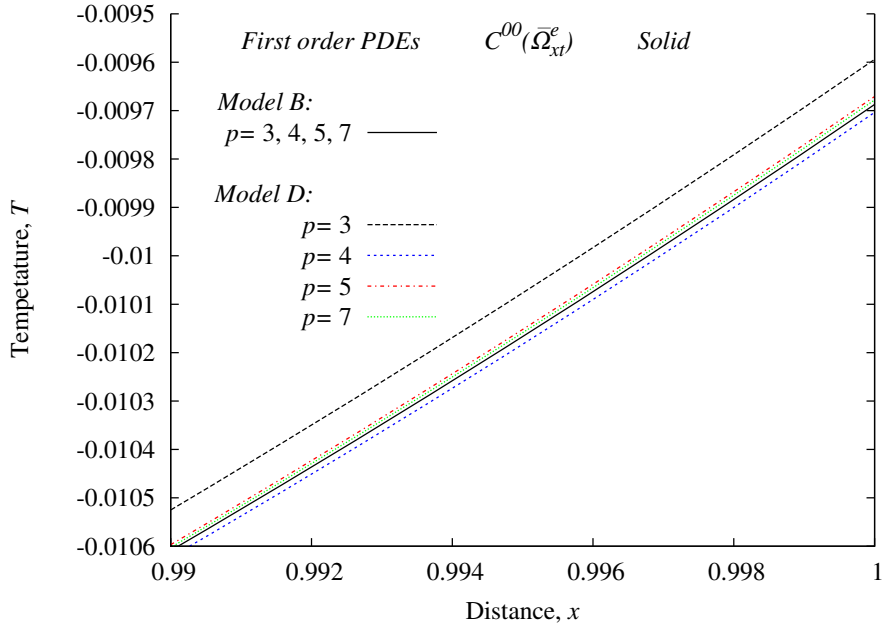

(a) Temperature at the end of the first time step ($t = 0.005$)

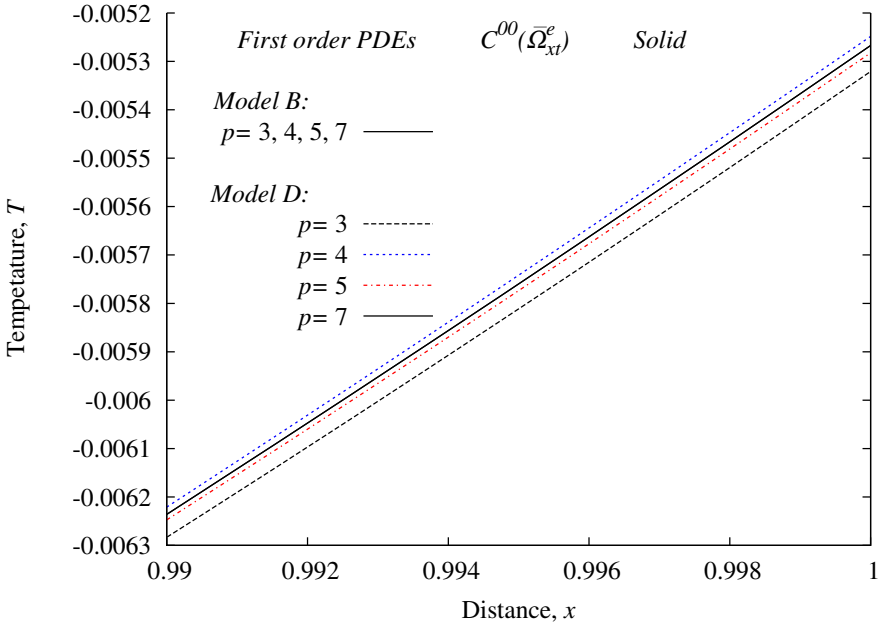

(b) Temperature at the end of the second time step ($t = 0.010$)

Figure 5.4: Temperature evolution for models B and D, ($t = 0.005$, $t = 0.010$) at the end of the first two time increments

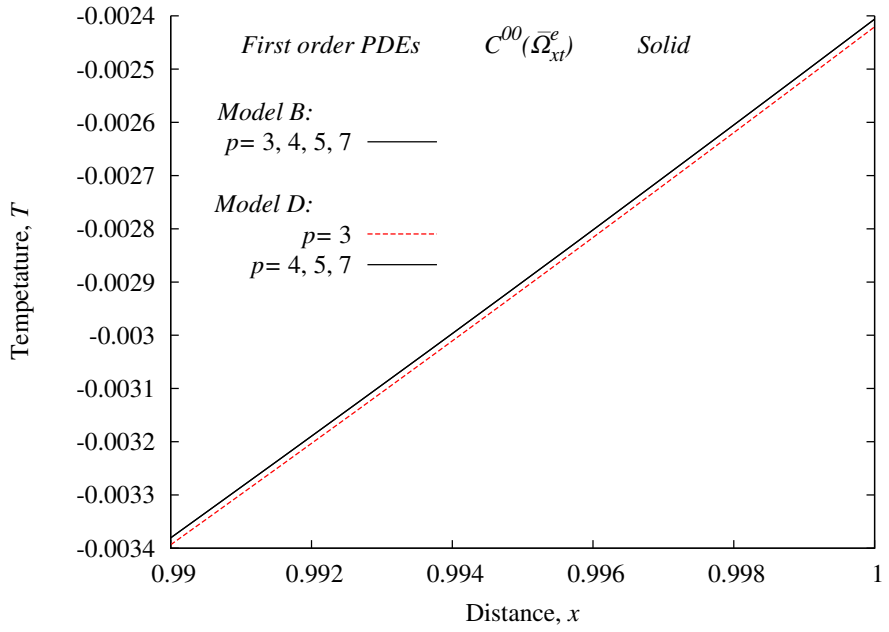

(a) Temperature at the end of the third time step ($t = 0.015$)

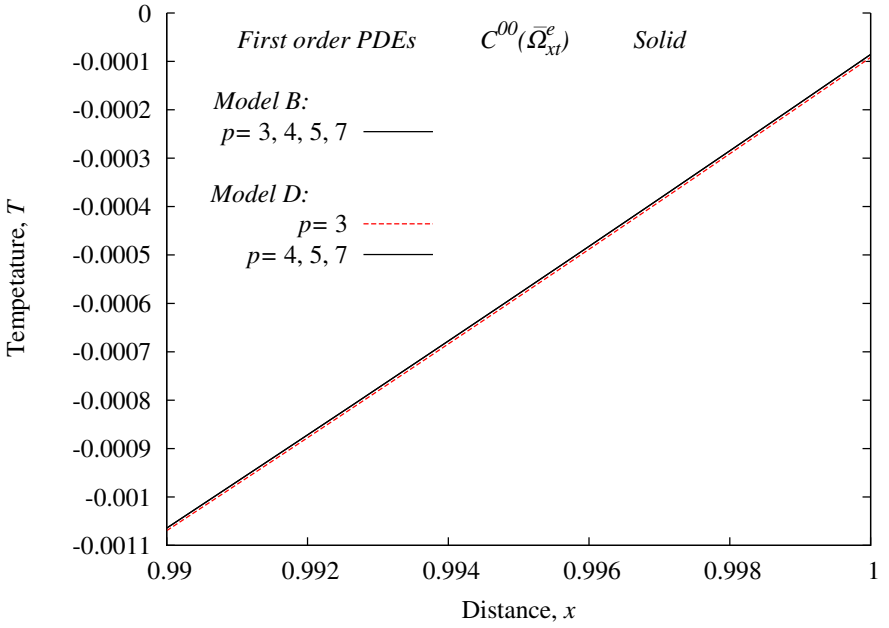

(b) Temperature at the end of the fourth time step ($t = 0.020$)

Figure 5.5: Temperature evolution for models B and D, ($t = 0.015$, $t = 0.020$) at the end of the 3^{rd} and 4^{th} time increments

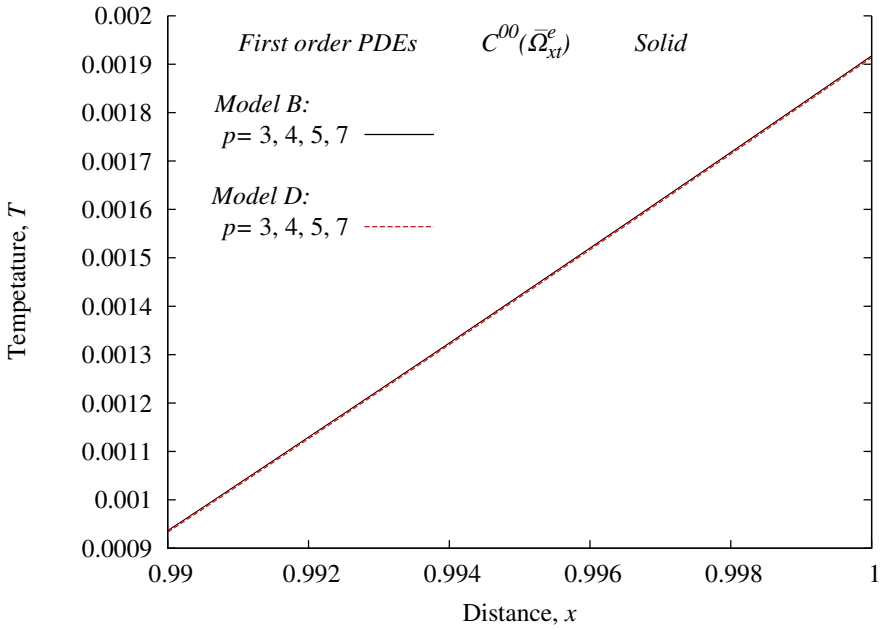

Figure 5.6: Temperature evolution for models B and D, ($t = 0.025$) at the end of the 5^{th} time increment

We note that the mathematical model described by (5.4) contains up to second order derivatives of temperature T with respect to coordinate x but only up to first order derivative of T with respect to time. Thus, in this case for the local approximation T_h^e of T, the following must hold.

$$T_h^e \in V_h \subset H^{k,p}(\bar{\Omega}_{xt}^e) \quad ; \quad k = (k_1, k_2) \ , \ k_1 \geq 2p_1 - 1 \ , \ k_2 \geq 2p_2 - 1$$

with $k_1 \geq 3$, $k_2 \geq 2$ for the integrals in the STLSP to be Riemann. Thus, $k_1 = 3$ and $k_2 = 2$ are the choices for minimally conforming approximation space $V_h \subset H^{k,p}(\bar{\Omega}_{xt}^e)$. For this choice of k_1 and k_2, T_h^e is of class $C^2(\bar{\Omega}_{xt}^e)$ in space x but only of class $C^1(\bar{\Omega}_{xt}^e)$ in time.

If we choose $k_1 = 2$ and $k_2 = 2$ i.e. T_h^e of class $C^{11}(\bar{\Omega}_{xt}^e)$, then the integrals in the STLSP are Lebesgue in x but Riemann in t. Due to the smoothness of the evolution we consider this choice in the numerical studies presented in the following. The space-time strip ($\Delta t = 0.04$) is discretized using 50 nine node space-time $C^{11}(\bar{\Omega}_{xt}^e)$ finite elements. Numerical studies were considered to determine adequate p-level for this discretization by starting with p-level of 3 (both in space and time) and incrementing it by two. At p-level of nine, the residual functional I of the order of 10^{-6} or lower and $|(g_i)|_{max} \leq 10^{-6}$ were achieved. These ensure good convergence of Newton's linear method with line search as well as very low residual values in the entire space-time domain. Computed evolution results are presented in figures (5.10) to (5.16) for $[T_s, T_l] = [-0.001, 0.001]$.

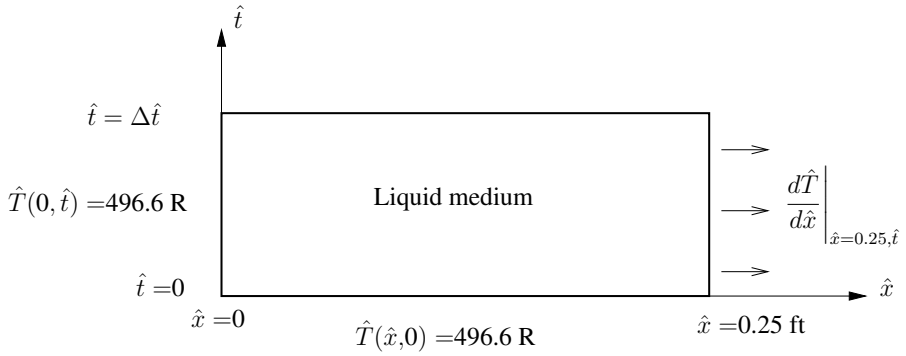

Figure 5.7: Space-time domain

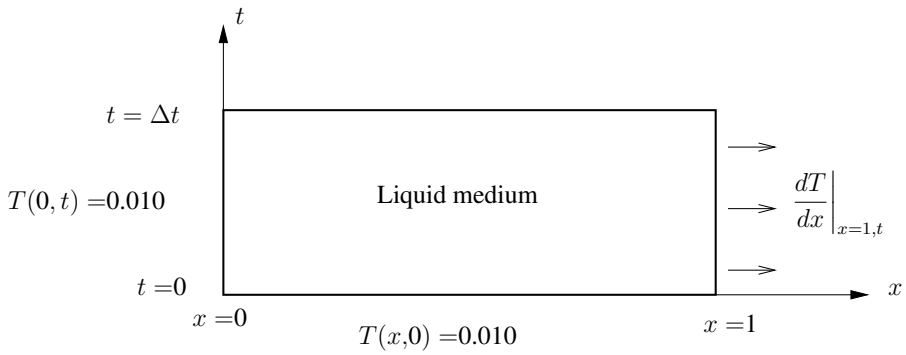

Reference quantities:

$\rho_0 = \hat{\rho}_s$, $k_0 = \hat{k}_s$, $c_{p0} = \hat{c}_{ps}$, $L_0 = 0.25ft$, $T_0 = (32°F + 459.67) = 491.67\ R$, $L_{f0} = c_{p0}T_0 = 240.72Btu/lbm$, $t_0 = L_0^2\rho_0 c_{p0}/k_0 = 4.899 \times 10^3\ s$, $q_0 = 1.42Btu/ft^2\,s$, $\Delta t = 0.04$, $\Delta\hat{t} = 196.0s$

Figure 5.8: Dimensionless space-time domain

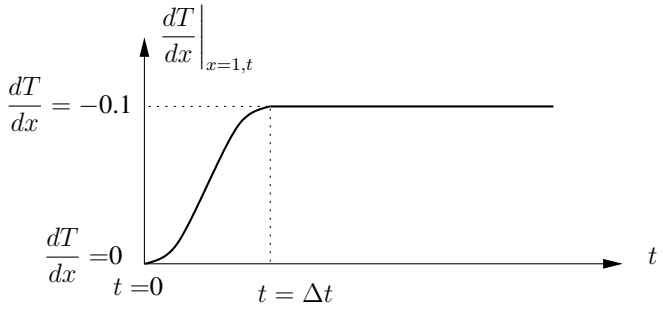

Figure 5.9: Boundary condition dT/dx at $x = 1$

Discussion of results:

Figures 5.10(a) - 5.14(a) show plots of T, L_f, c_p, k and ρ versus x during initial stages of the evolution ($0 \leq t \leq 0.24$). Continuous extraction of heat from the right boundary progressively lowers the temperature at the boundary and in the neighborhood of the boundary which eventually results in the initiation of phase change. Variations in $L_f(T)$, $c_p(T)$, $k(T)$ and $\rho(T)$ follow changes in temperature during evolution.

Figures 5.10(b) - 5.14(b) show fully formed phase change transition region (liquid to solid) beginning with $t = 0.8$ and its propagation during evolution ($0.8 \leq t \leq 4.8$). For each space-time strip during time marching using $\Delta t = 0.04$, $I < O(10^{-6})$ and $|(g_i)|_{max} \leq 10^{-6}$ ensure accurate evolution that satisfies GDE quite well over the entire space-time domain of each space-time strip. Evolutions of all quantities are smooth and free of oscillations.

If we define the center of the transition zone as the location x of the phase front, then for the results in figures 5.10 - 5.14 we can plot a graph of location x versus time t marking the location of the phase change front in time. Figure 5.15 shows such a plot for the results presented in figures 5.10 - 5.14. The transition region width for these numerical studies consist of $[T_s, T_l] = [-0.001, 0.001]$.

Similar studies were repeated for $[T_s, T_l] = [-0.002, 0.002]$ i.e. double the width of the transition zone. Figure 5.16 shows evolutions of L_f for $t = 1.6$, 3.2 and 4.8 when $[T_s, T_l] = [-0.001, 0.001]$ and $[-0.002, 0.002]$. In both cases the location of the center of the transition region matches very well (figures 5.15 and 5.16).

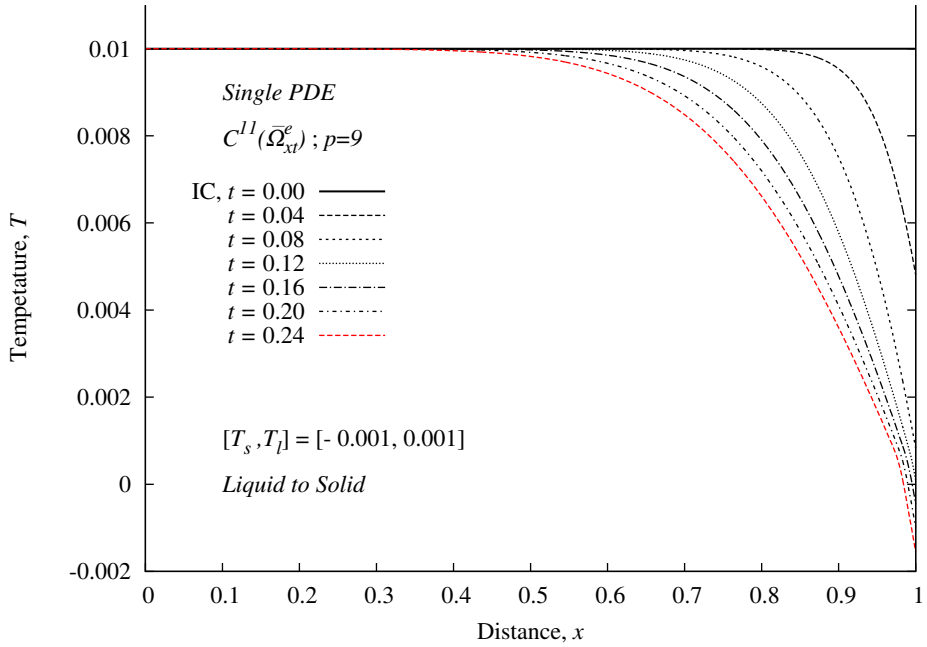

(a) Evolution of temperature, $0.0 \leq t \leq 0.24$, $\Delta t = 0.04$

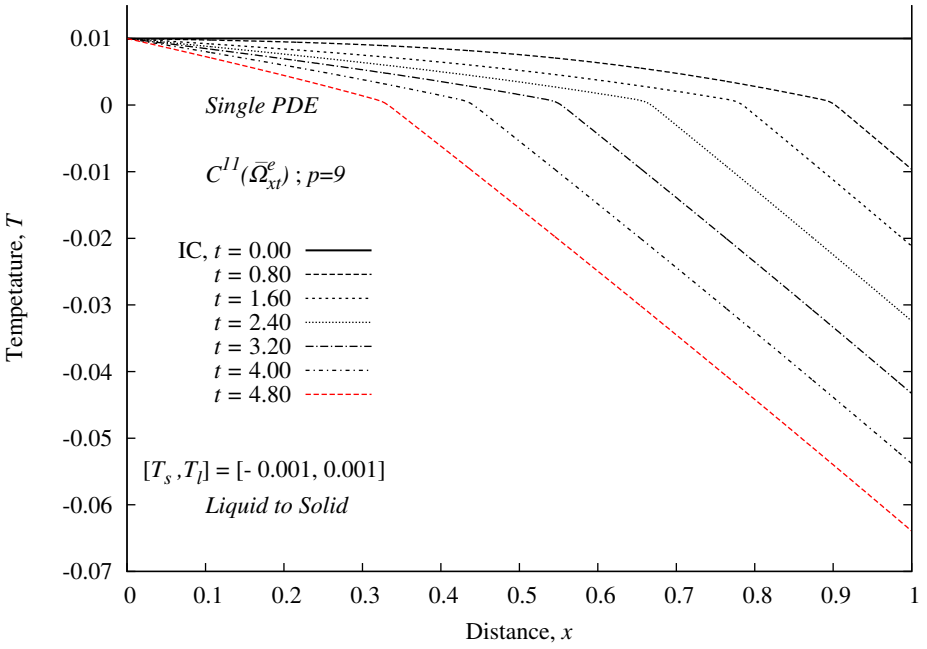

(b) Evolution of temperature, $0.0 \leq t \leq 4.8$, $\Delta t = 0.04$

Figure 5.10: Evolution of Temperature for liquid to solid phase change in $\mathbb{R}^1$

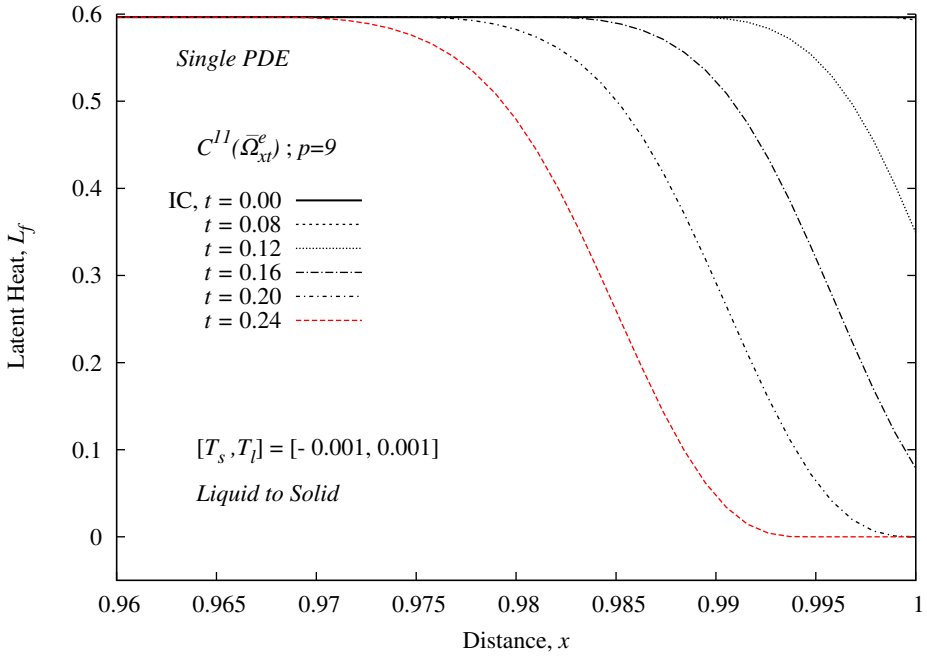

(a) Evolution of Latent heat, $0.0 \leq t \leq 0.24$, $\Delta t = 0.04$

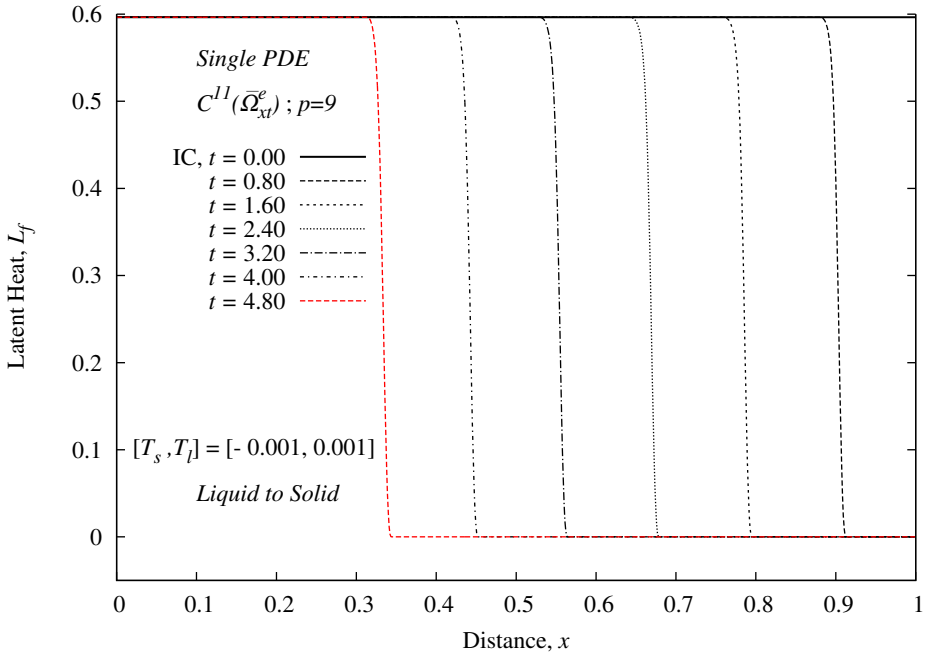

(b) Evolution of Latent heat, $0.0 \leq t \leq 4.8$, $\Delta t = 0.04$

Figure 5.11: Evolution of Latent Heat for liquid to solid phase change in $\mathbb{R}^1$

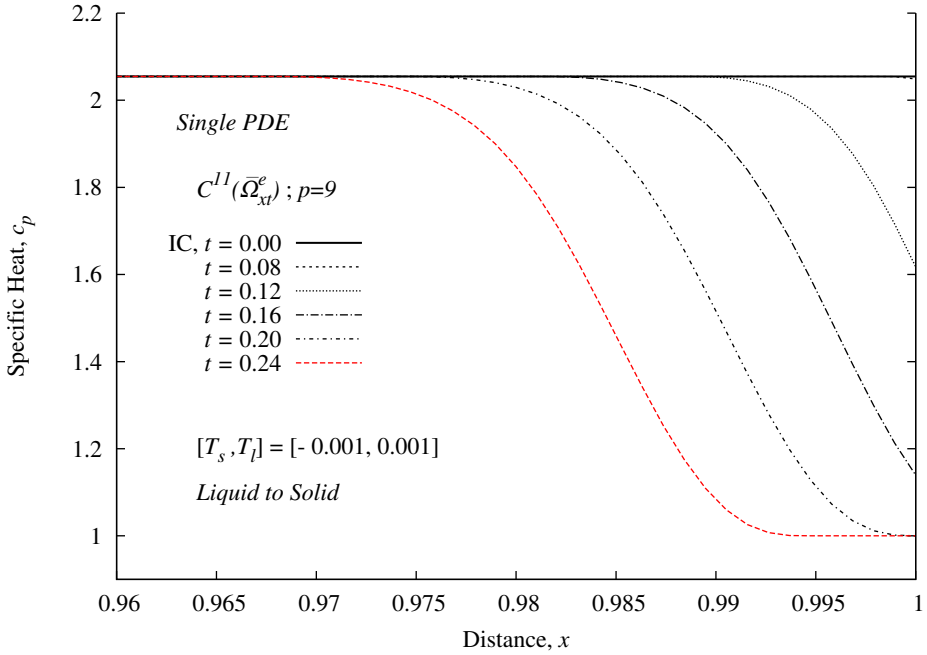

(a) Evolution of Specific heat, $0.0 \leq t \leq 0.24$, $\Delta t = 0.04$

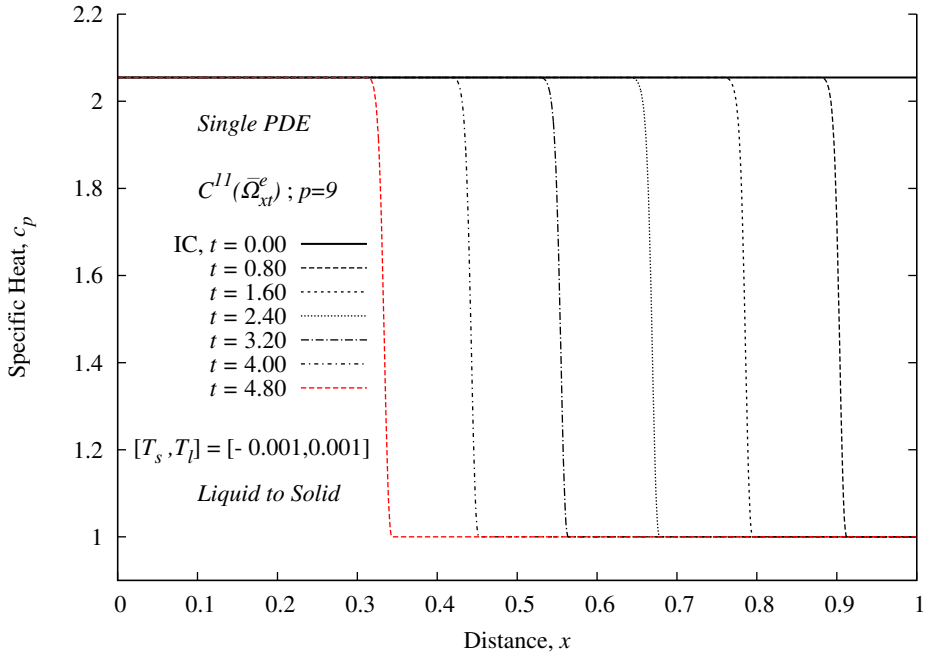

(b) Evolution of Specific heat, $0.0 \leq t \leq 4.8$, $\Delta t = 0.04$

Figure 5.12: Evolution of Specific Heat for liquid to solid phase change in $\mathbb{R}^1$

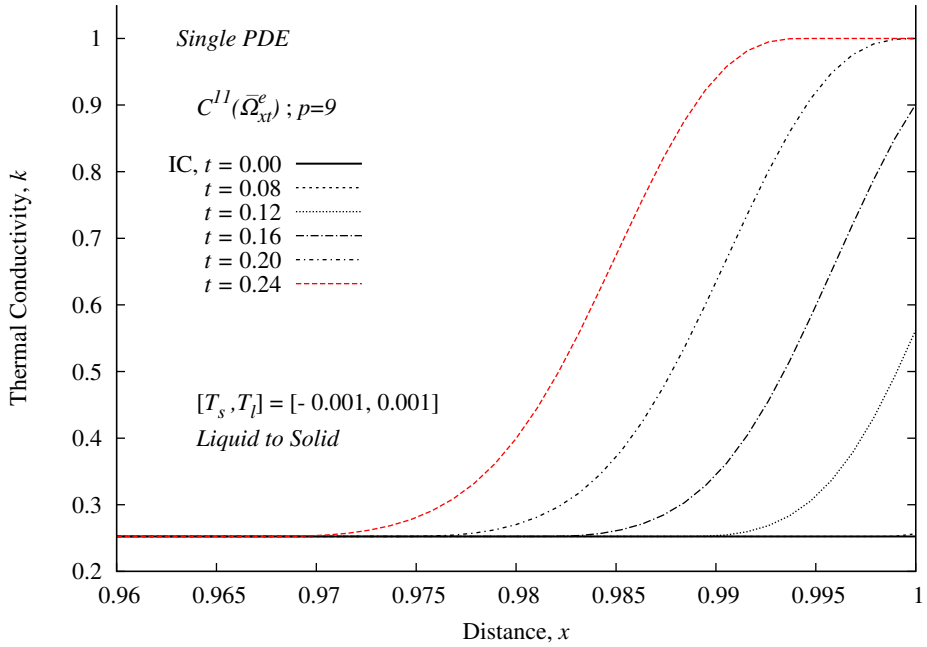

(a) Evolution of Thermal Conductivity, $0.0 \leq t \leq 0.24$, $\Delta t = 0.04$

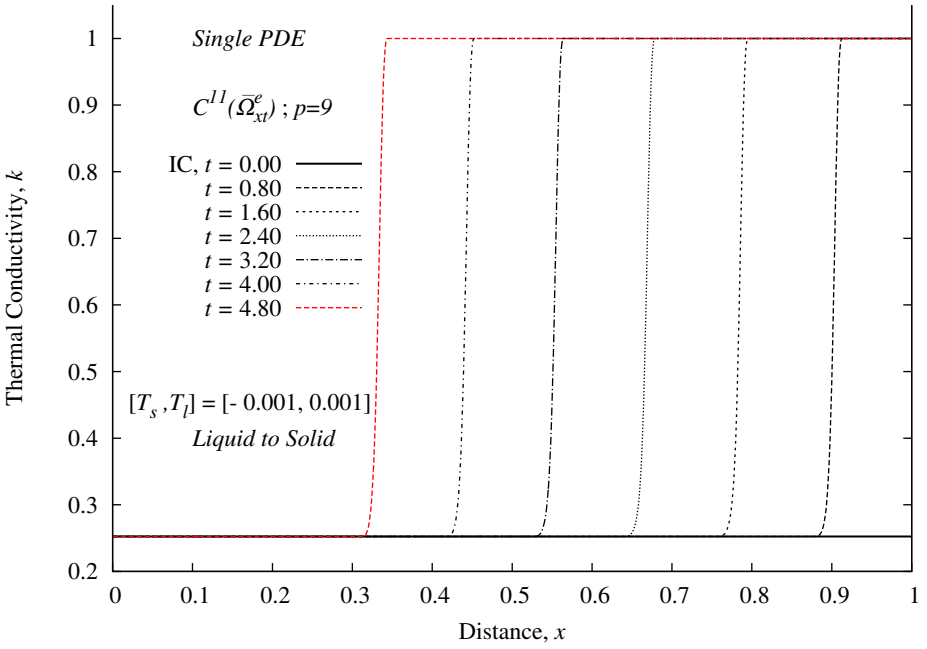

(b) Evolution of Thermal conductivity, $0.0 \leq t \leq 4.8$, $\Delta t = 0.04$

Figure 5.13: Evolution of Thermal Conductivity for liquid to solid phase change in $\mathbb{R}^1$

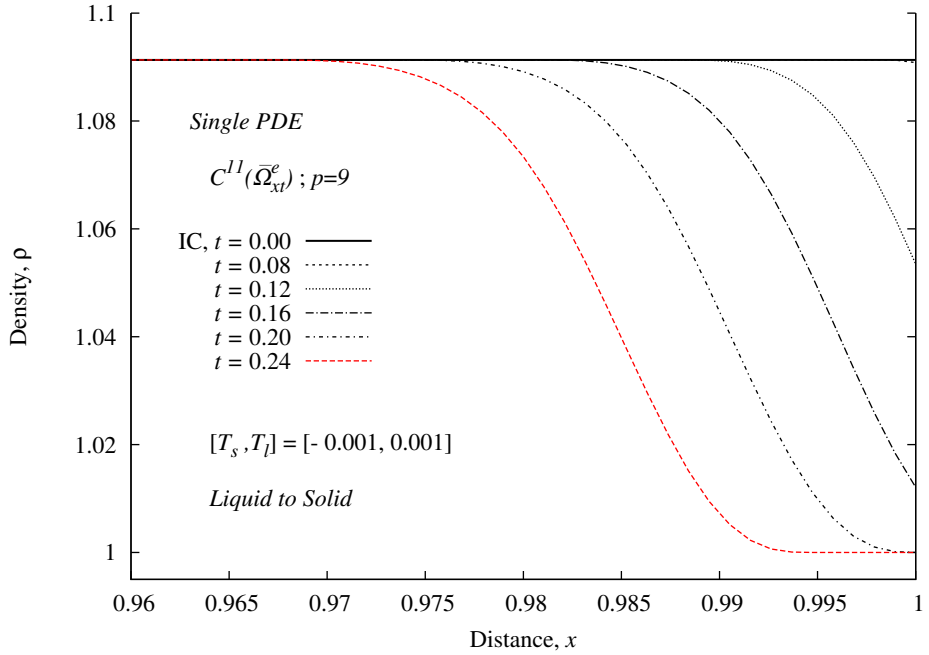

(a) Evolution of Density, $0.0 \leq t \leq 0.24$, $\Delta t = 0.04$

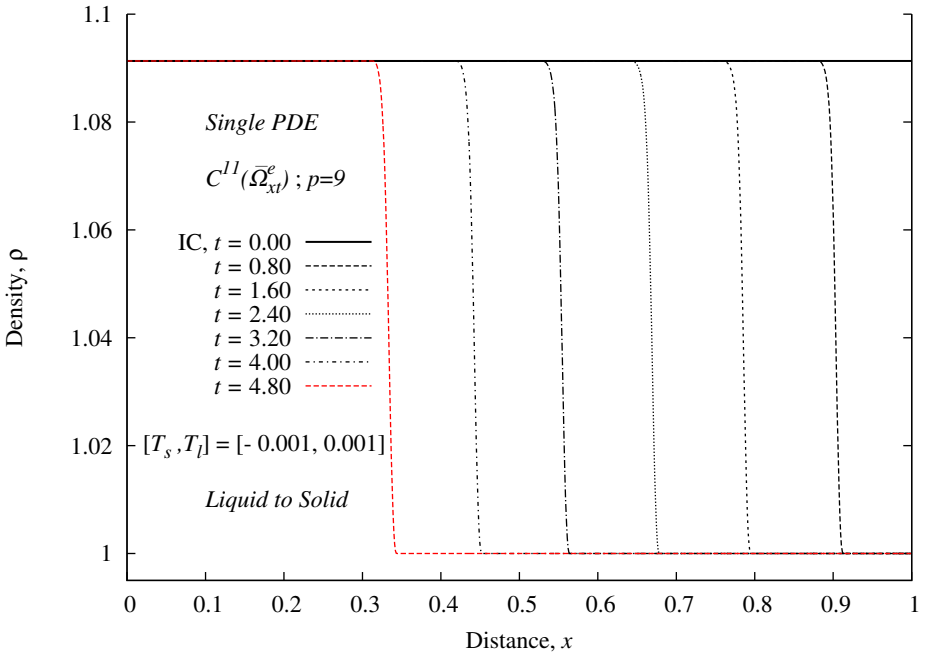

(b) Evolution of Density, $0.0 \leq t \leq 4.8$, $\Delta t = 0.04$

Figure 5.14: Evolution of Density for liquid to solid phase change in $\mathbb{R}^1$

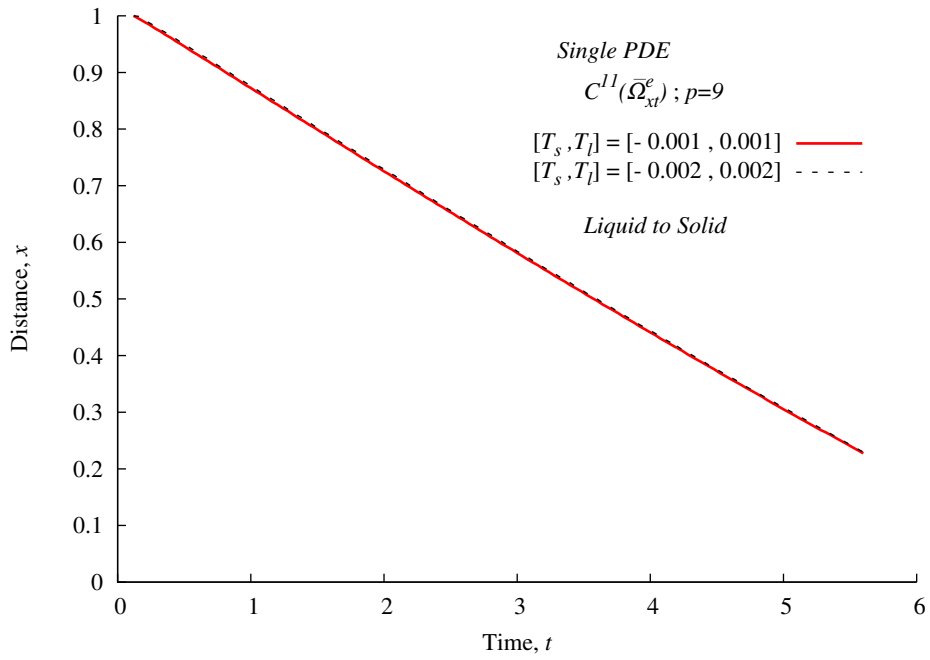

Figure 5.15: Comparison of interface location for different width of transition region: liquid to solid

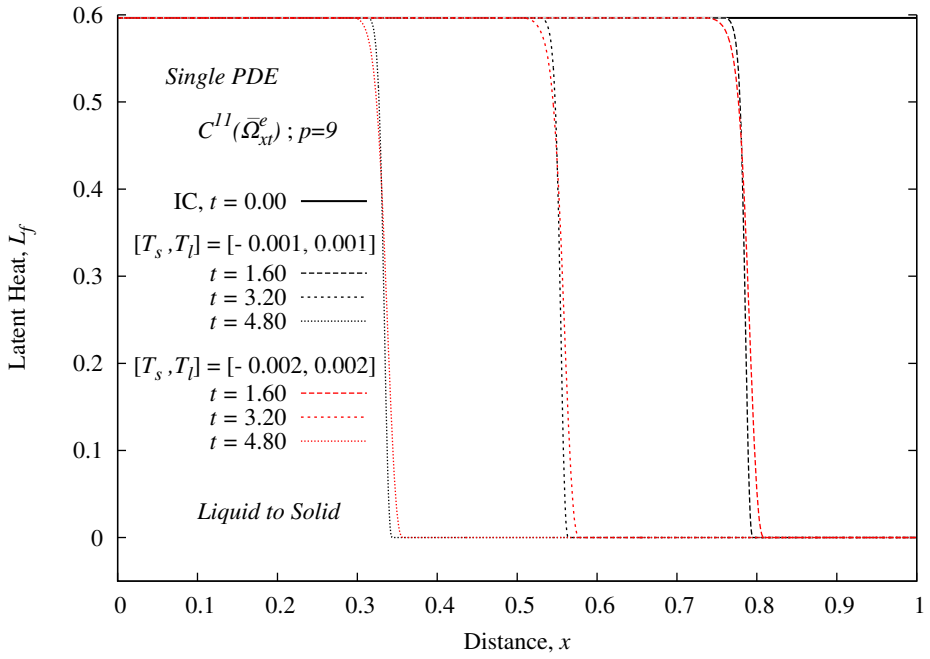

Figure 5.16: Evolution of Latent Heat for different width of transition region: liquid to solid

5.3.4 Solid-liquid phase change in $\mathbb{R}^1$: Using model A

In this section we present solid-liquid phase change studies using model A, in a similar manner as presented in section 5.3.3 for liquid-solid phase change. The space-time least squares formulation for a time strip (corresponding to an increment of time) with time marching is used to compute the evolution. Figure 5.17 shows a schematic of the space-time strip corresponding to the first increment of time, BCs, and ICs. Figure 5.18 shows dimensionless space-time domain, reference quantities and the dimensionless quantities.

Minimally conforming spaces are the same as described in section 5.3.3. Due to smoothness of the evolution, we choose $k_1 = 2$ and $k_2 = 2$ i.e. T_h^e of class $C^{11}(\bar{\Omega}_{xt}^e)$, therefore the integrals in the STLSP are Lebesgue in x but Riemann in t. The space-time strip ($\Delta t = 0.005$ for the first 10 time strips and 0.1 for the remaining) is discretized using 100 nine node space-time $C^{11}(\bar{\Omega}_{xt}^e)$ finite elements. Numerical studies were considered for the first space-time strip with phase change to determine adequate p-level for this discretization by starting with p-level of 3 (both in space and time) and incrementing it by two. At p-level of nine, I is of the order of 10^{-6} or lower and $|(g_i)|_{max} \leq 10^{-6}$ were achieved for all time steps. These ensures converged Newton's linear method with line search as well as accurate evolution in the entire space-time domain. The numerical solutions computed using these vales of *h*, *p* and *k* for $[T_s, T_l] = [-0.001, 0.001]$ are shown in figures 5.20 -5.24.

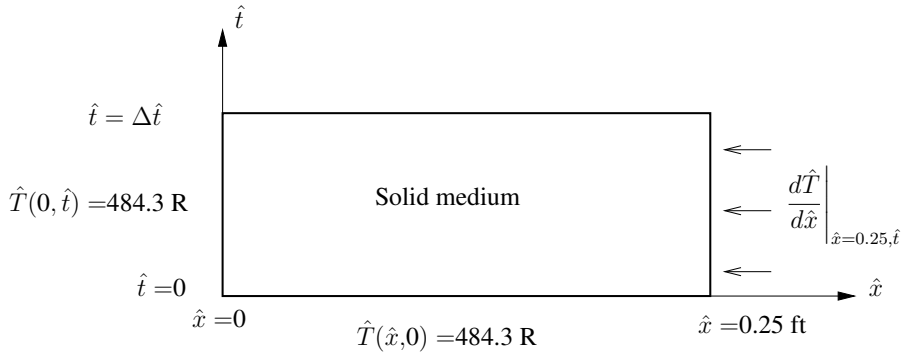

Figure 5.17: Space-time domain

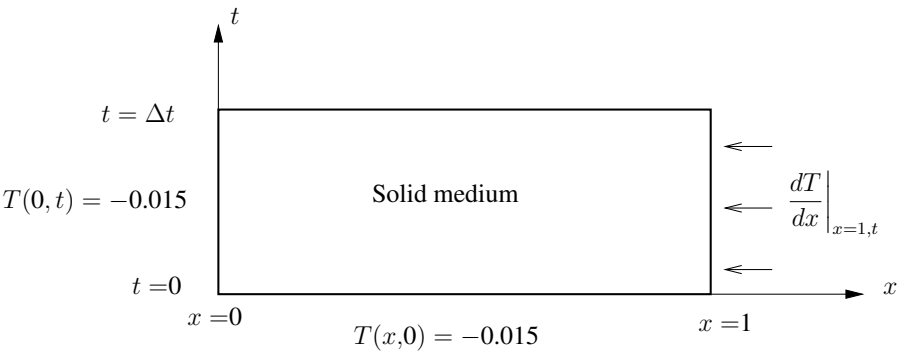

Reference quantities:

$\rho_0 = \hat{\rho}_s$, $k_0 = \hat{k}_s$, $c_{p0} = \hat{c}_{ps}$, $L_0 = 0.25ft$, $T_0 = (32^\circ F + 459.67) = 491.67\ R$, $L_{f0} = c_{p0}T_0 = 240.72Btu/lbm$, $t_0 = L_0^2\rho_0 c_{p0}/k_0 = 4.899 \times 10^3\ s$, $q_0 = 1.42Btu/ft^2\,s$, $\Delta t = 0.005, 0.1$; $\Delta\hat{t} = 24.5s, 490.0s$

Figure 5.18: Dimensionless space-time domain

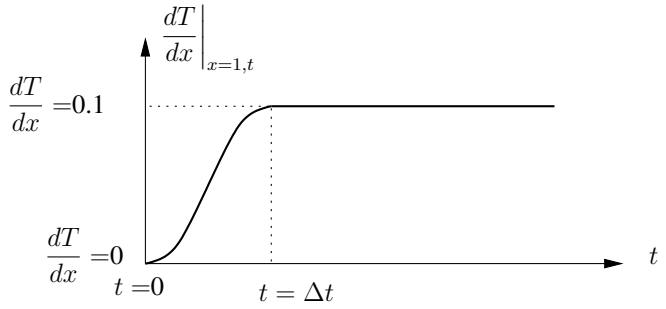

Figure 5.19: Boundary condition $q(1,t)$

Discussion of results:

Figures 5.20(a) - 5.24(a) show plots of T, L_f, c_p, k and ρ versus x during the initial stages of the evolution ($0 \leq t \leq 0.95$). Continuous addition of heat from the right boundary progressively raises the temperature at the boundary and in the neighborhood of the boundary which eventually results in the initiation of phase change. Variations in $L_f(T)$, $c_p(T)$, $k(T)$ and $\rho(T)$ follow changes in temperature during evolution.

Figures 5.20(b) - 5.24(b) show fully formed phase change transition region (solid to liquid) beginning with $t = 4.05$ and its propagation during evolution ($4.05 \leq t \leq 59.05$). For each space-time strip during time marching using $\Delta t = 0.005$ for $0 \leq t \leq 0.05$ and $\Delta t = 0.1$ for $t \geq 0.05$; $I < O(10^{-6})$ and $|(g_i)|_{max} \leq 10^{-6}$ ensure accurate evolution that satisfies GDE quite well over the entire space-time domain of each space-time strip. All evolutions are smooth and free of oscillations.

5.4 Numerical studies in $\mathbb{R}^2$

In this section we present numerical studies for phase change in $\mathbb{R}^2$ for liquid-solid and solid-liquid phase change. Unlike section 5.3, here we choose mathematical model B, a system of first order PDEs. The dimensionless form of model B is given in the following.

$$\begin{aligned} &\rho\left(c_p(T) + \frac{\partial L_f(T)}{\partial T}\right)\frac{\partial T}{\partial t} + \boldsymbol{\nabla}\cdot\boldsymbol{q} = 0 \\ &\boldsymbol{q} = -k(T)\boldsymbol{\nabla}T \qquad ; \qquad \boldsymbol{\nabla} = \left[\frac{\partial}{\partial x}, \frac{\partial}{\partial y}\right]^{\mathsf{T}} \end{aligned} \tag{5.9}$$

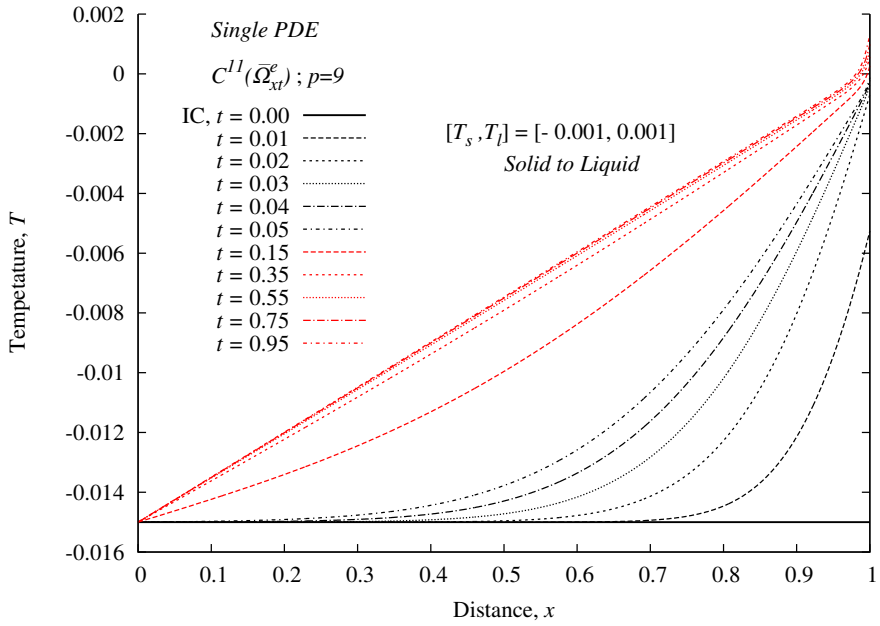

(a) Evolution of temperature, $0.0 \leq t \leq 0.95$, $\Delta t = 0.005$ for $0 \leq t \leq 0.05$ and $\Delta t = 0.1$ for $t \geq 0.05$

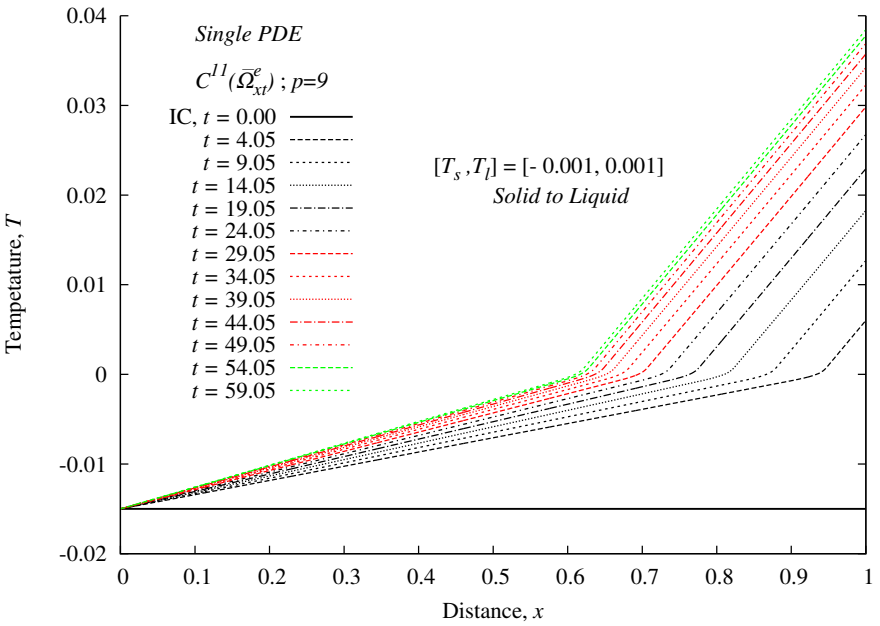

(b) Evolution of temperature, $0.0 \leq t \leq 59.05$, $\Delta t = 0.005$ for $0 \leq t \leq 0.05$ and $\Delta t = 0.1$ for $t \geq 0.05$

Figure 5.20: Evolution of Temperature for solid to liquid phase change in $\mathbb{R}^1$

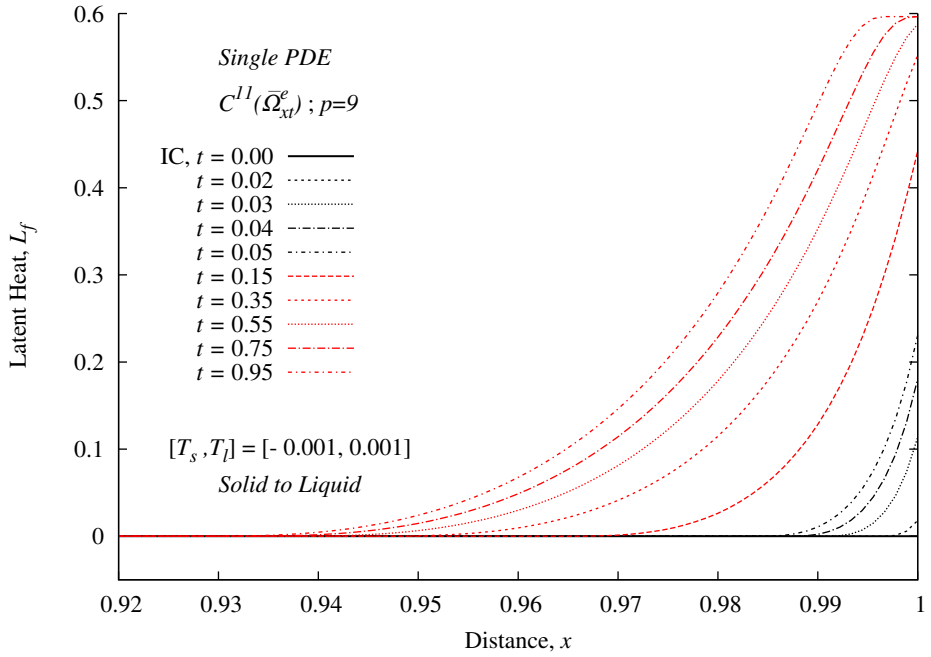

(a) Evolution of Latent heat, $0.0 \leq t \leq 0.95$, $\Delta t = 0.005$ for $0 \leq t \leq 0.05$ and $\Delta t = 0.1$ for $t \geq 0.05$

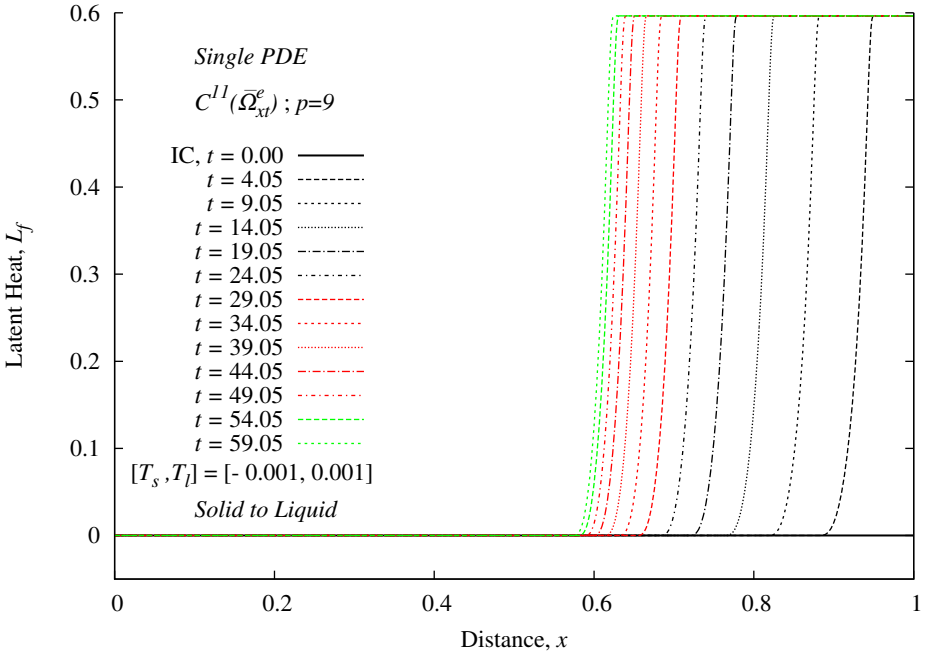

(b) Evolution of Latent heat, $0.0 \leq t \leq 59.05$, $\Delta t = 0.005$ for $0 \leq t \leq 0.05$ and $\Delta t = 0.1$ for $t \geq 0.05$

Figure 5.21: Evolution of Latent Heat for solid to liquid phase change in $\mathbb{R}^1$

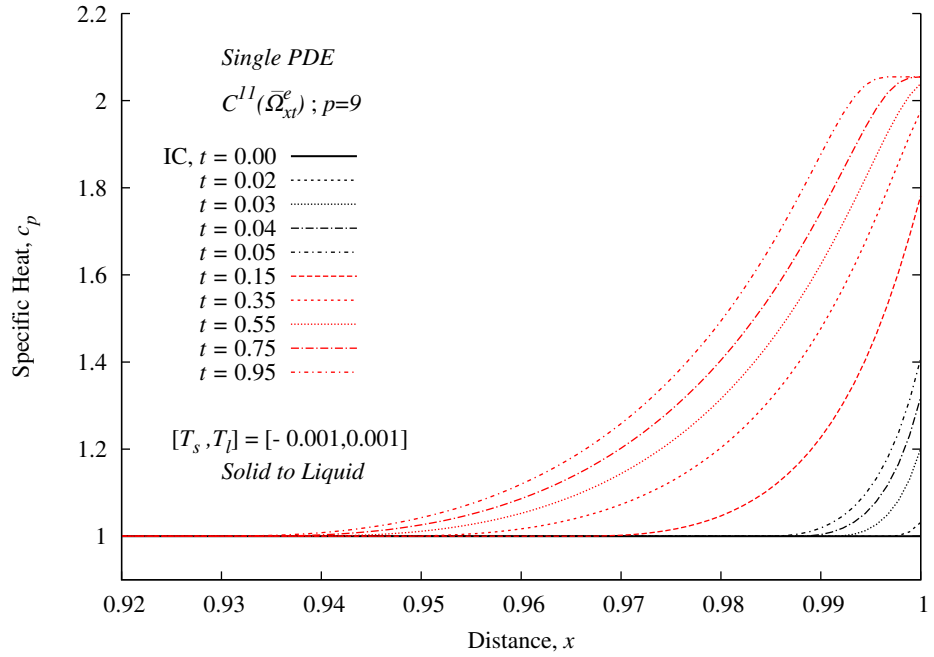

(a) Evolution of Specific heat, $0.0 \leq t \leq 0.95$, $\Delta t = 0.005$ for $0 \leq t \leq 0.05$ and $\Delta t = 0.1$ for $t \geq 0.05$

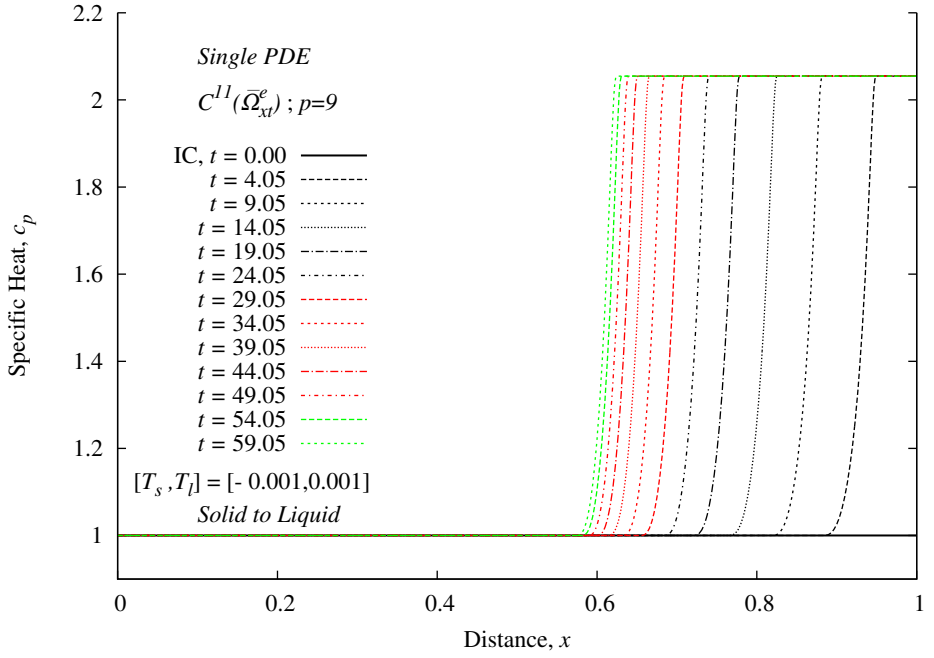

(b) Evolution of Specific heat, $0.0 \leq t \leq 59.05$, $\Delta t = 0.005$ for $0 \leq t \leq 0.05$ and $\Delta t = 0.1$ for $t \geq 0.05$

Figure 5.22: Evolution of Specific Heat for solid to liquid phase change in $\mathbb{R}^1$

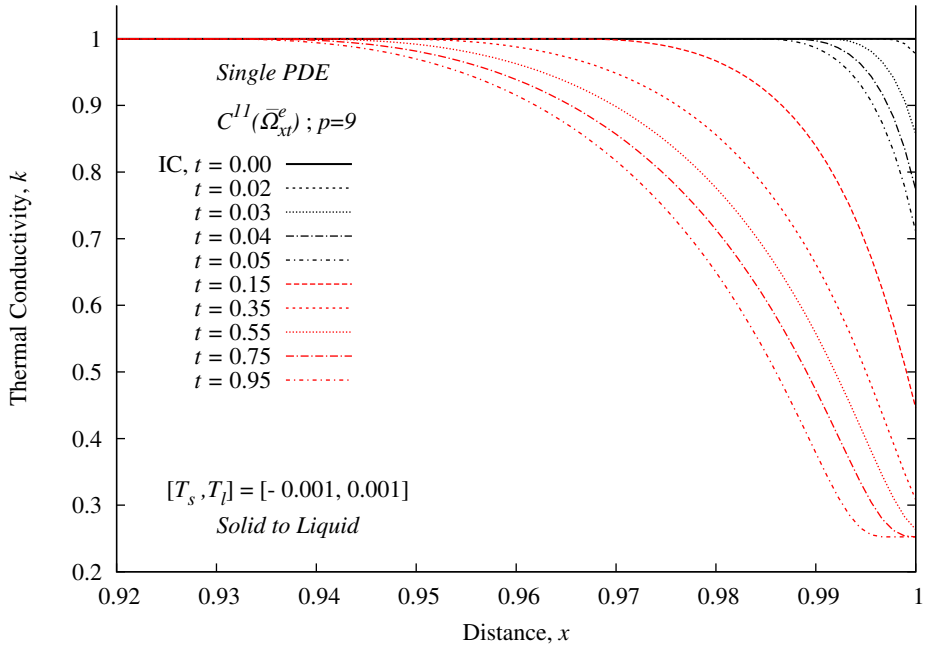

(a) Evolution of Thermal Conductivity, $0.0 \leq t \leq 0.95$, $\Delta t = 0.005$ for $0 \leq t \leq 0.05$ and $\Delta t = 0.1$ for $t \geq 0.05$

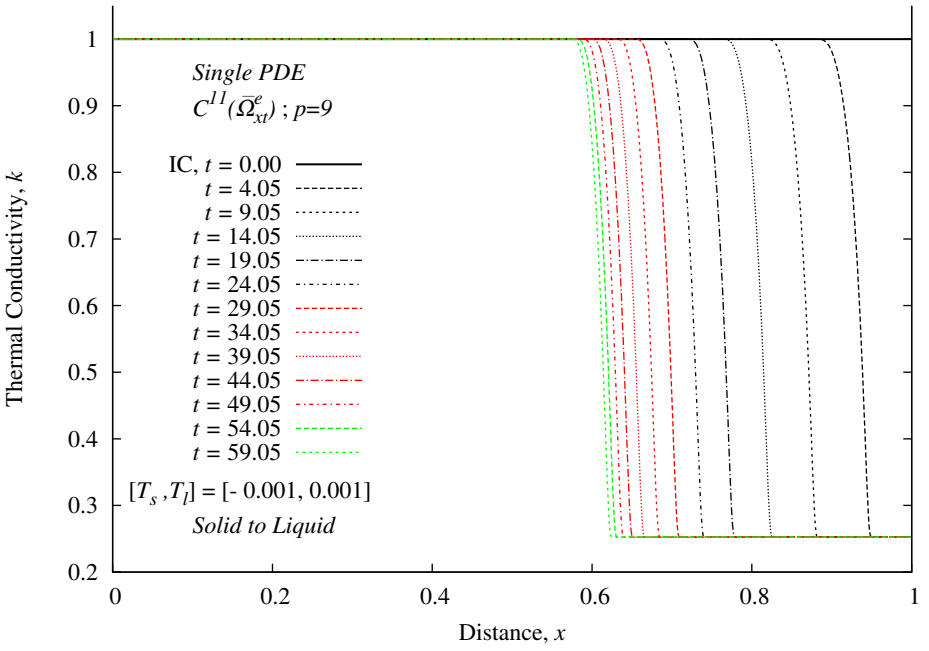

(b) Evolution of Thermal conductivity, $0.0 \leq t \leq 59.05$, $\Delta t = 0.005$ for $0 \leq t \leq 0.05$ and $\Delta t = 0.1$ for $t \geq 0.05$

Figure 5.23: Evolution of Thermal Conductivity for solid to liquid phase change in $\mathbb{R}^1$

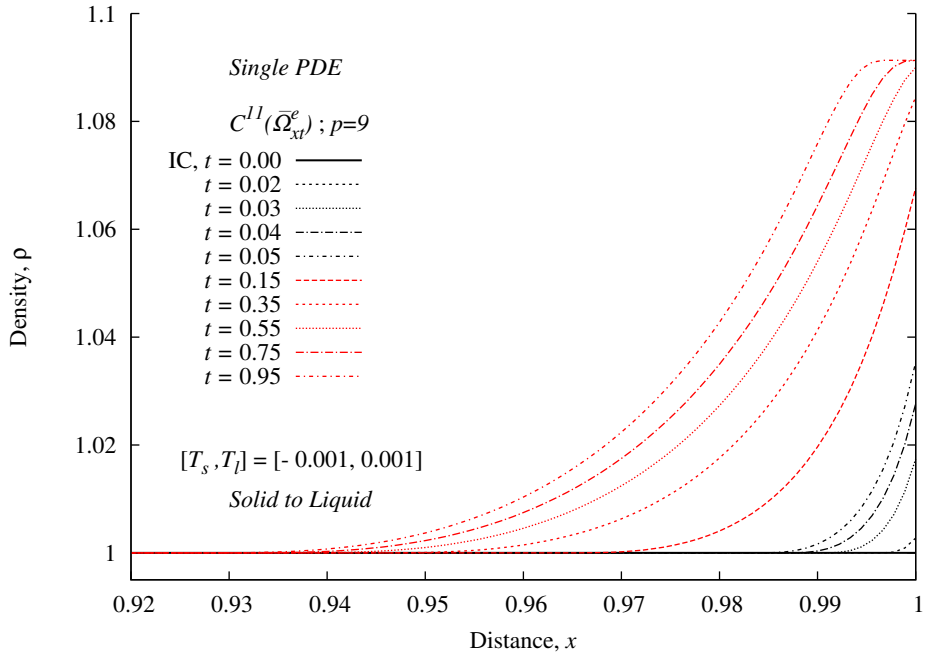

(a) Evolution of Density, $0.0 \leq t \leq 0.95$, $\Delta t = 0.005$ for $0 \leq t \leq 0.05$ and $\Delta t = 0.1$ for $t \geq 0.05$

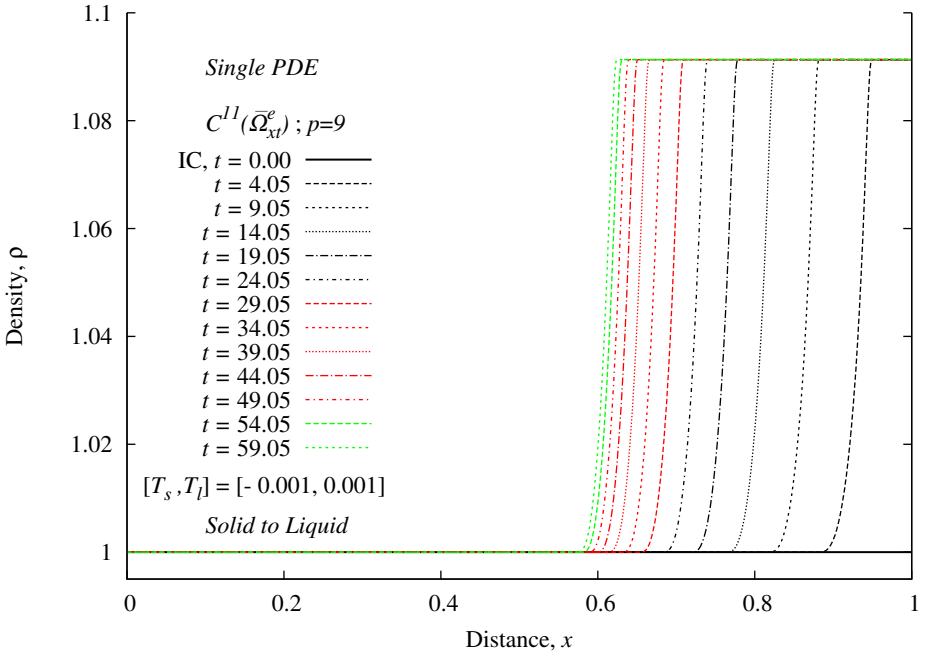

(b) Evolution of Density, $0.0 \leq t \leq 59.05$, $\Delta t = 0.005$ for $0 \leq t \leq 0.05$ and $\Delta t = 0.1$ for $t \geq 0.05$

Figure 5.24: Evolution of Density for solid to liquid phase change in $\mathbb{R}^1$

Since the phase change initiation and propagation is smooth, we expect this mathematical model to behave well as well. Contrary to reference [23], we do not use L_f as a dependent variable to avoid inconsistencies and problems associated with its use in linear heat conduction (for low p-levels).

Mathematical model (5.9) is a system of three first order PDEs in T and components of $\boldsymbol{q}$. We can choose the following for the local approximations for T, q_x and q_y.

$$
\begin{aligned}
T_h^e, q_{xh}^e, q_{yh}^e \in V_h \subset H^{k,p}(\bar{\Omega}_{\boldsymbol{x}t}^e) \quad ; \quad & k = (k_1, k_2) \\
& k_1 \geq 2p_1 - 1 \quad ; \quad \text{space } (x, y) \\
& k_2 \geq 2p_2 - 1 \quad ; \quad \text{time } (t)
\end{aligned}
$$

With $k_1 \geq 2$, $k_2 \geq 2$, the integrals in the STLSP are Riemann. Since the evolution of phase change process is smooth, we can also choose $k_1 = 1$, $k_2 = 1$, but for this choice the integrals in the STLSP in space are in Lebesgue sense. In the numerical studies presented in the following we choose $k_1 = k_2 = 1$, i.e. T_h, q_{xh} and q_{yh} of class $C^{00}(\bar{\Omega}_{\boldsymbol{x}t}^e)$.

5.4.1 Liquid-Solid phase change in $\mathbb{R}^2$

We consider a two dimensional domain in $\mathbb{R}^2$ consisting of a one unit square. A schematic of the domain, boundary conditions, initial conditions and reference quantities are shown in figure 5.25. A constant heat flux is applied to each boundary (heat removal), except for the first time step in which heat flux changes continuously from zero at $t = 0$ to the constant value at $t = \Delta t$.

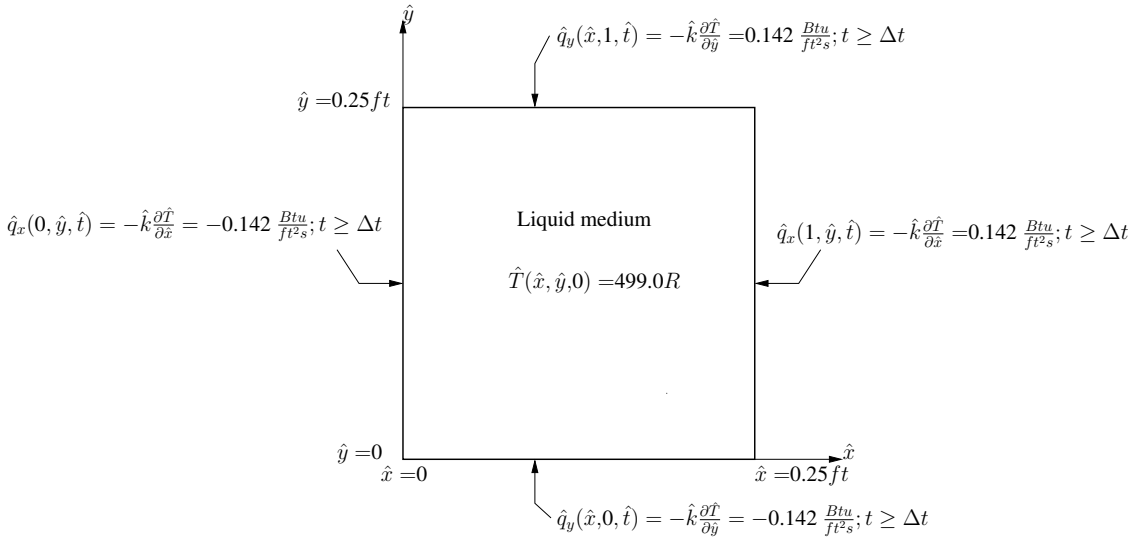

(a) Physical spatial domain

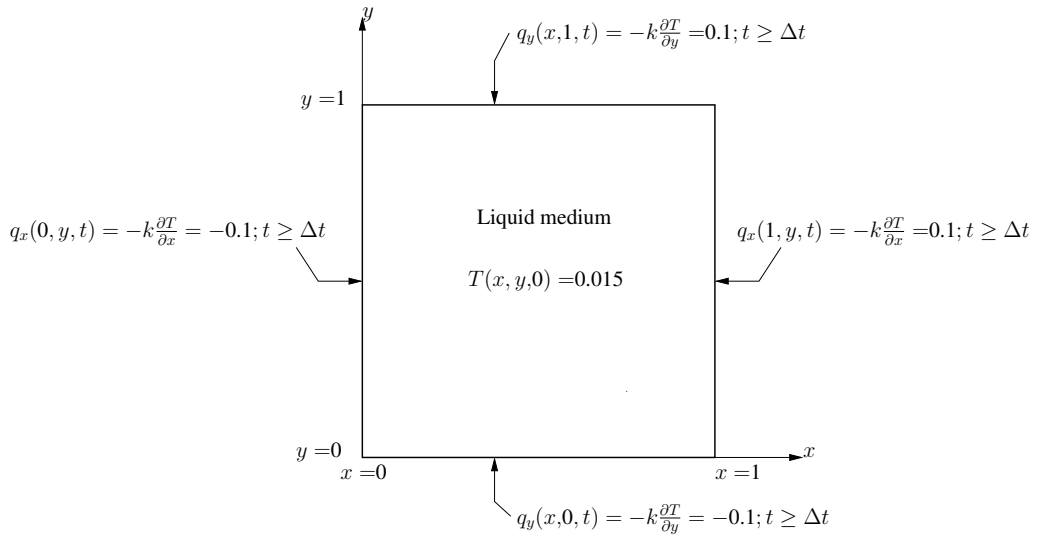

(b) Dimensionless spatial domain

Reference quantities: $\rho_0 = \hat{\rho}_s$, $k_0 = \hat{k}_s$, $c_{p0} = \hat{c}_{ps}$, $L_0 = 0.25ft$

$T_0 = (32^\circ F + 459.67) = 491.67\ R$, $L_{f0} = c_{p0}T_0 = 240.72Btu/lbm$, $q_0 = 1.42Btu/ft^2\, s$

, $t_0 = L_0^2 \rho_0 c_{p0}/k_0 = 4.899 \times 10^3\ s$, $\Delta t = 0.0025$, 0.01 ; $\Delta \hat{t} = 12.2s$, $49.0s$

Figure 5.25: Schematics and reference quantities for liquid-solid phase change in $\mathbb{R}^2$

A graded spatial discretization of the $[1 \times 1]$ spatial domain shown in figure 5.26 is constructed. Table 5.1 provides discretization details of regions A, B, C and D. All four boundaries contain uniform heat flux $q = -0.1$ (cooling) for $t \geq \Delta t$. Evolution is computed (56 time steps) using p-level of 3 in space and time with $\Delta t = 0.0025$ for the first 8 time steps and $\Delta t = 0.01$ for the remaining time steps. For this discretization, the C^{00} local approximation with p=3 yield I of $O(10^{-6})$ or lower, confirming good accuracy of the solution. $|g_i|_{max} \leq 10^{-6}$ is used for convergence check in the Newton's linear method. For most time increments Newton's linear method with line search converges in 5-10 iterations.

The evolution of the temperature for $0 \leq t \leq 0.05$ and $0.10 \leq t \leq 0.5$ are shown in figures 5.27 and 5.28. Initiation of the liquid solid front shown in figures 5.29 and 5.30 using L_f carpet plots show smooth evolution of front and its propagation without oscillations. The study demonstrates the strength of the work in simulating moving fronts in $\mathbb{R}^2$ without front tracking techniques. The transition region width for these numerical studies consist of $[T_s, T_l] = [-0.004, 0.004]$. This model problem also can not be simulated using phase field and sharp interface models due to the same reason as in the case of model problems in $\mathbb{R}^1$. Quarter symmetry of the evolution is quite obvious from the evolutions in figures 5.27 - 5.30.

Table 5.1: Spatial discretization for model problems in $\mathbb{R}^2$

Region	Number of x elements	Number of y elements	Element length in x, h_{ex}	Element length in y, h_{ey}	Number of Total Elements
A	12	12	0.0167	0.0167	144
B	6	12	0.1000	0.0167	72
C	12	6	0.0167	0.1000	72
D	6	6	0.1000	0.1000	36

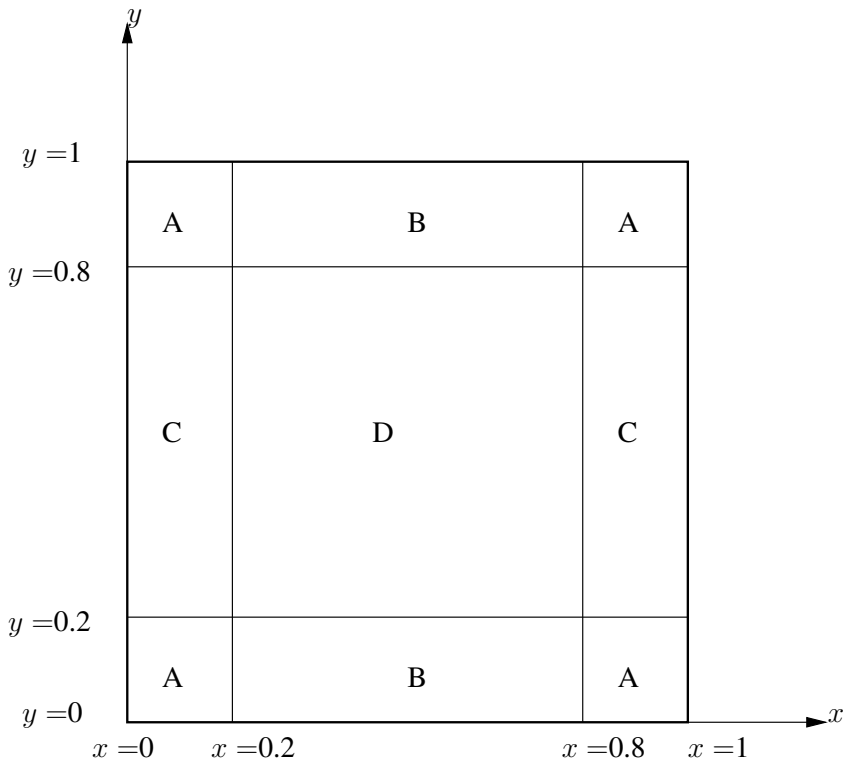

Figure 5.26: Spatial discretization for model problems in $\mathbb{R}^2$

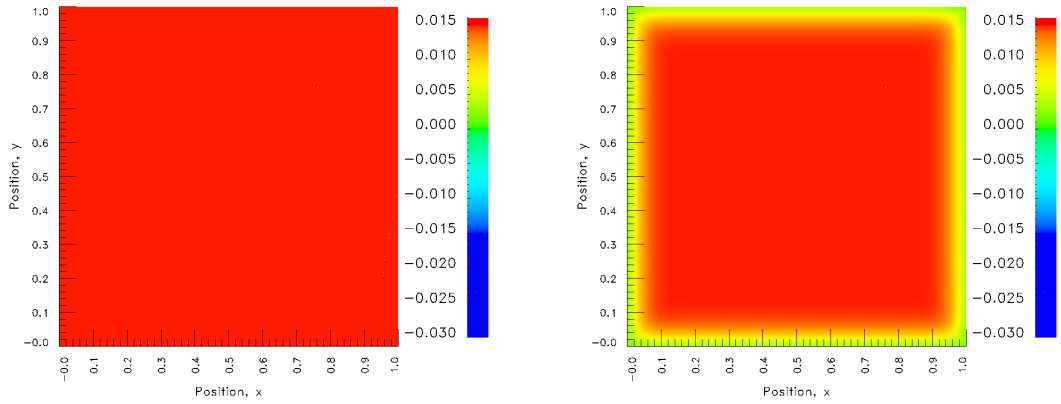

(a) Initial Condition

(b) $t = 0.01$

(c) $t = 0.02$

(d) $t = 0.03$

(e) $t = 0.04$

(f) $t = 0.05$

Figure 5.27: Evolution of Temperature for liquid to solid phase change in $\mathbb{R}^2$: $\Delta t = 0.0025$, for $0 \leq t \leq 0.02$ and $\Delta t = 0.01$ for $t \geq 0.02$

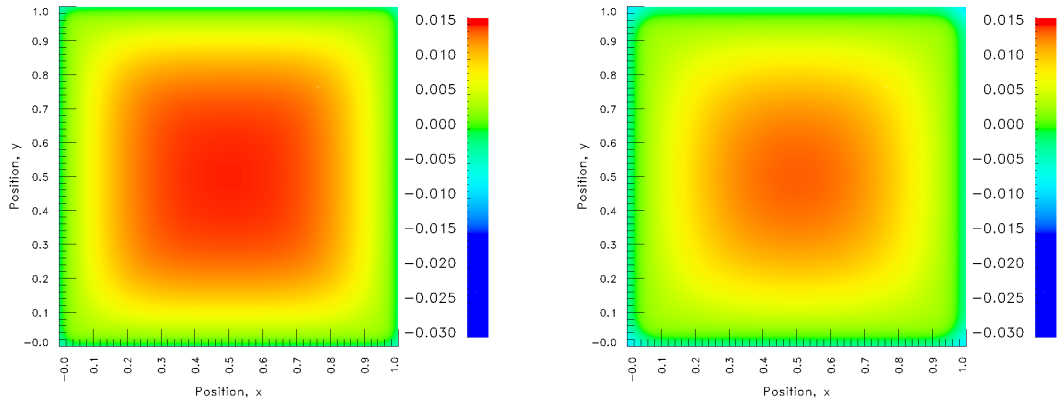

(a) $t = 0.10$ (b) $t = 0.20$

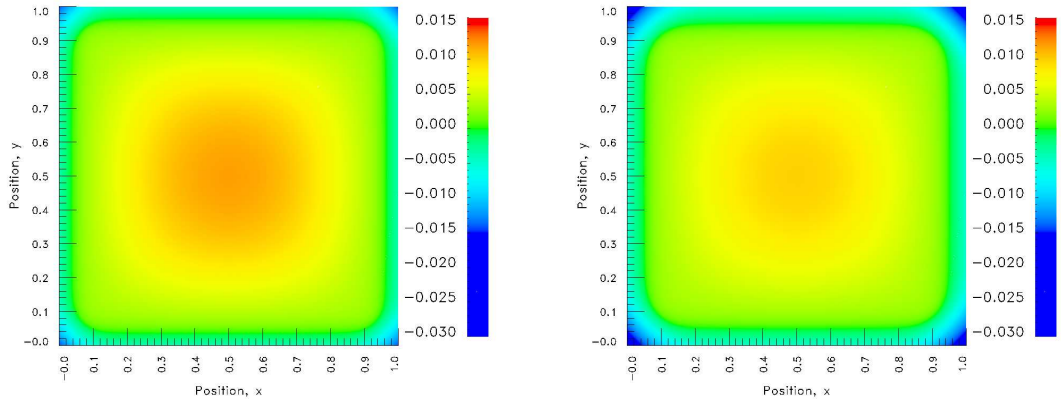

(c) $t = 0.30$ (d) $t = 0.40$

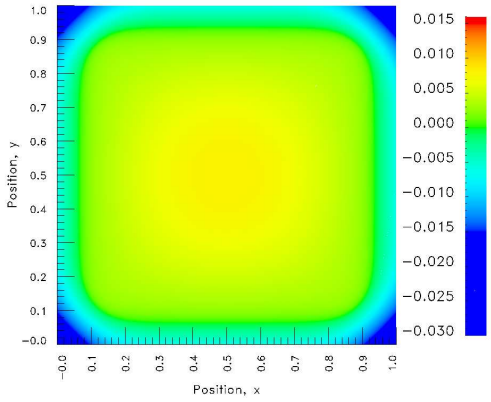

(e) $t = 0.50$

Figure 5.28: Further evolution of Temperature for liquid to solid phase change in $\mathbb{R}^2$: $\Delta t = 0.0025$, for $0 \leq t \leq 0.02$ and $\Delta t = 0.01$ for $t \geq 0.02$

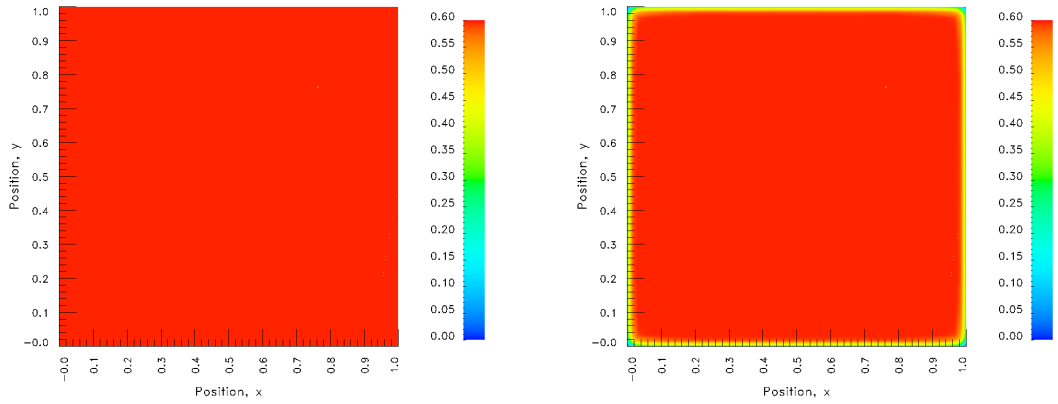

(a) Initial Condition

(b) $t = 0.05$

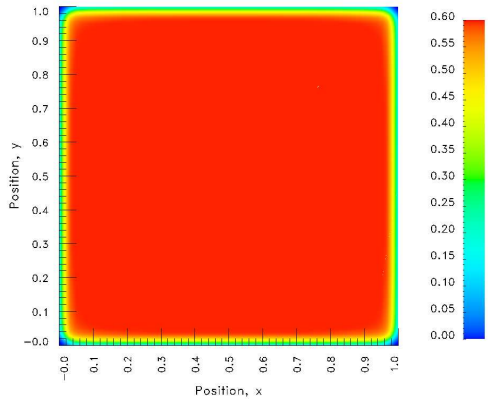

(c) $t = 0.10$

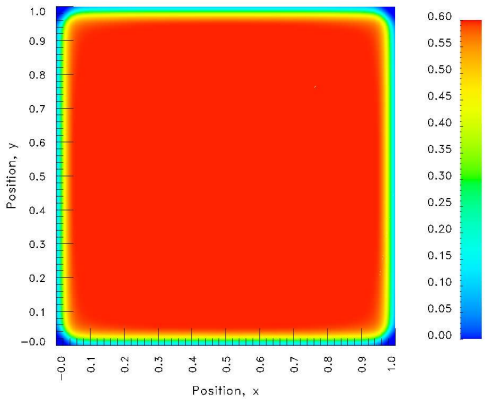

(d) $t = 0.15$

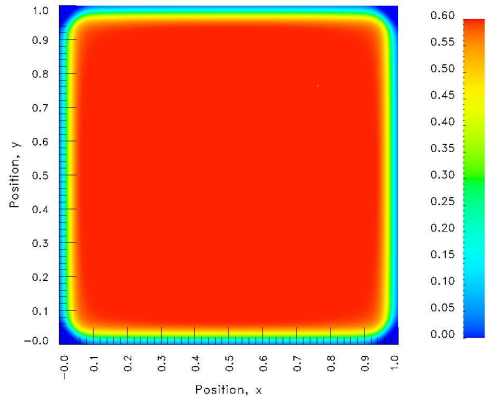

(e) $t = 0.20$

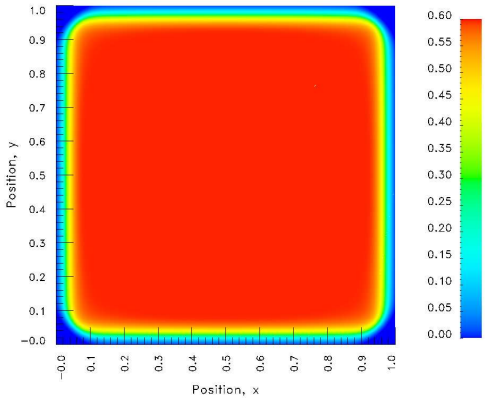

(f) $t = 0.25$

Figure 5.29: Evolution of Latent heat for liquid to solid phase change in $\mathbb{R}^2$: $\Delta t = 0.0025$, for $0 \leq t \leq 0.02$ and $\Delta t = 0.01$ for $t \geq 0.02$

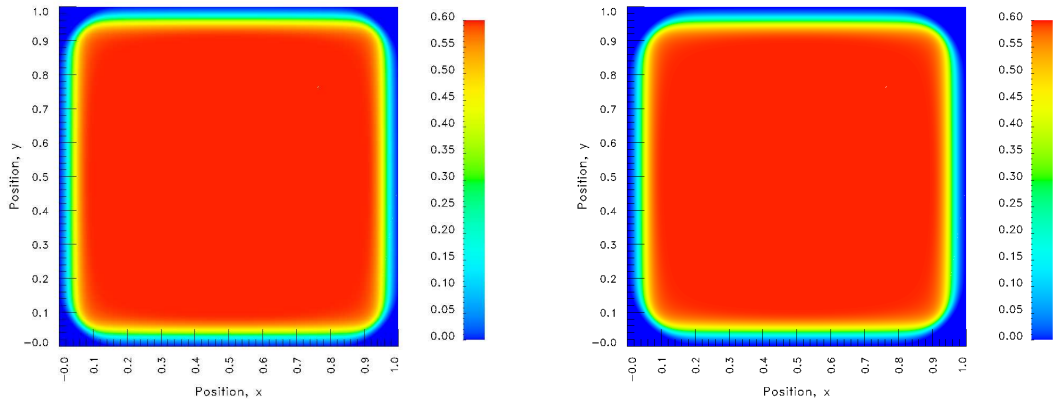

(a) $t = 0.30$

(b) $t = 0.35$

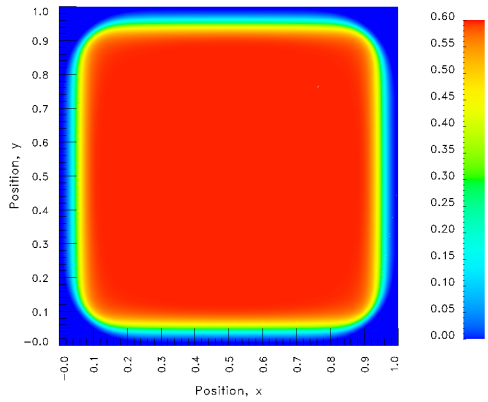

(c) $t = 0.40$

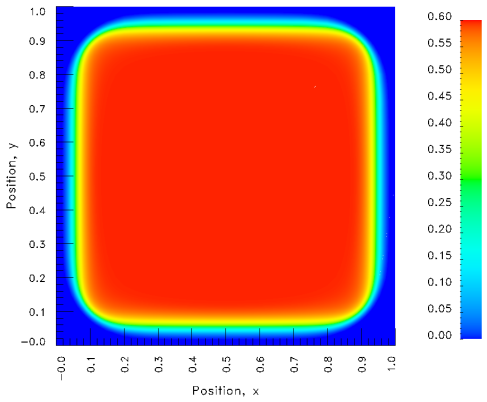

(d) $t = 0.45$

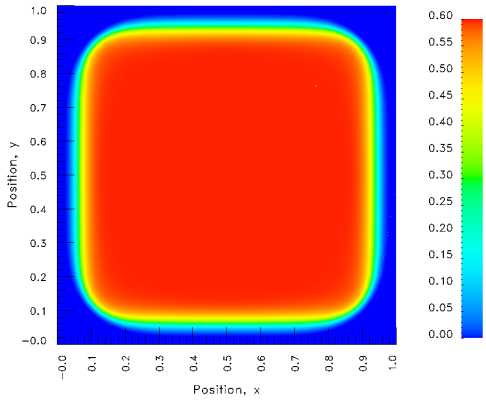

(e) $t = 0.50$

Figure 5.30: Further evolution of Latent heat for liquid to solid phase change in $\mathbb{R}^2$: $\Delta t = 0.0025$, for $0 \leq t \leq 0.02$ and $\Delta t = 0.01$ for $t \geq 0.02$

5.4.2 Solid-Liquid phase change in $\mathbb{R}^2$

Here we also consider a two dimensional domain in $\mathbb{R}^2$ consisting of a one unit square. A schematic of the domain, boundary conditions, initial conditions and reference quantities are shown in figure 5.31. A constant heat flux is applied to each boundary, except for the first time step in which the heat flux changes continuously from zero at $t = 0$ to the constant value at $t = \Delta t$.

The graded discretization for the $[1\times1]$ spatial domain is same as in section 5.4.1, shown in figure 5.26, with details of regions A, B, C and D in Table 5.1. All four boundaries maintain uniform heat flux $q = -0.1$ (heating). Evolution is computed (50 time steps) using p-level of 3 in space and time with $\Delta t = 0.01$. For this discretization, the C^{00} local approximations with p=3 yield I of $O(10^{-6})$ or lower, confirming good accuracy of the solution. $|g_i|_{max} \leq 10^{-6}$ is used for convergence check of the Newton's linear method. For most time increments Newton's linear method with line search converges in 5-10 iterations.

The evolution of the temperature and latent heat for $0 \leq t \leq 0.05$ and $0.10 \leq t \leq 0.5$ are shown in figures 5.32 - 5.35. Initiation of the liquid solid front occurs smoothly and propagates without oscillations. The study demonstrates the strength of the work in simulating moving fronts in $\mathbb{R}^2$ without front tracking techniques. This model problem also can not be simulated using phase field and sharp interface models due to the same reason as in the case of model problems in $\mathbb{R}^1$. Quarter symmetry of the evolution is quite obvious from the evolutions in Figures 5.32 - 5.35. The transition region width for these numerical studies consist of $[T_s, T_l] = [-0.004, 0.004]$.

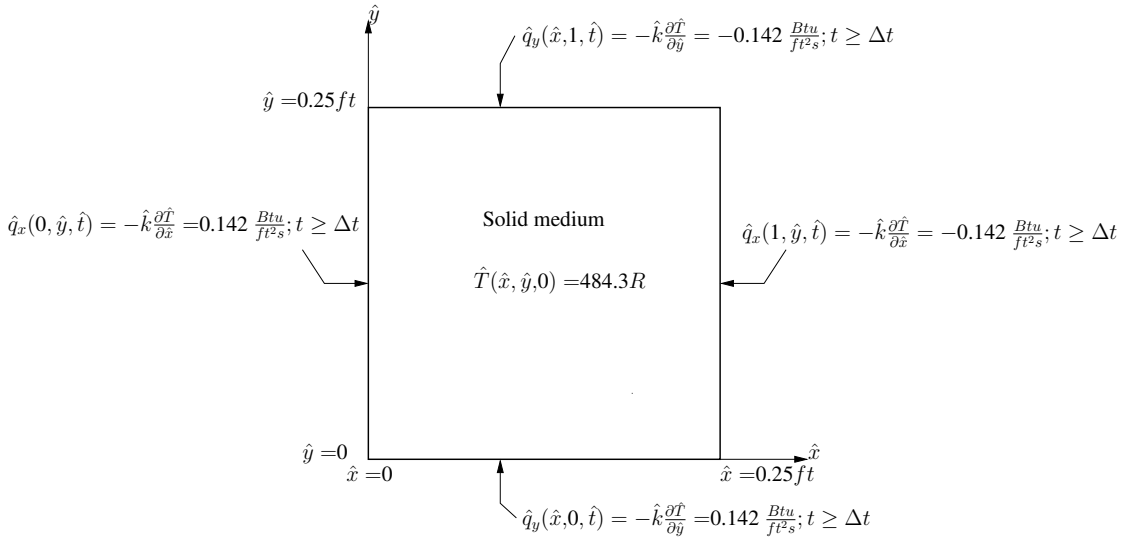

(a) Physical spatial domain

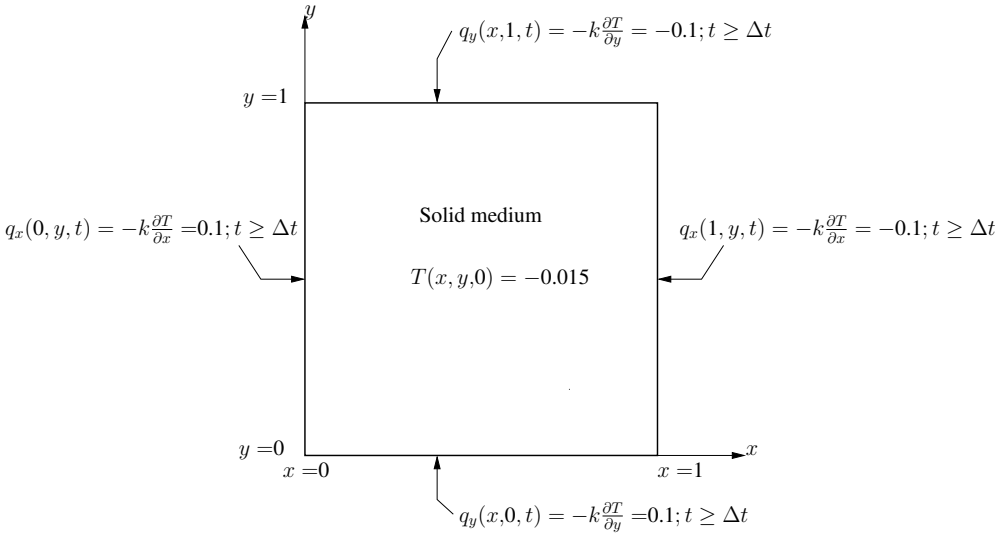

(b) Dimensionless spatial domain

Reference quantities: $\rho_0 = \hat{\rho}_s$, $k_0 = \hat{k}_s$, $c_{p0} = \hat{c}_{ps}$, $L_0 = 0.25ft$

$T_0 = (32^\circ F + 459.67) = 491.67\ R$, $L_{f0} = c_{p0}T_0 = 240.72Btu/lbm$, $q_0 = 1.42Btu/ft^2\ s$

, $t_0 = L_0^2\rho_0 c_{p0}/k_0 = 4.899 \times 10^3\ s$, $\Delta t = 0.01$; $\Delta \hat{t} = 49.0s$

Figure 5.31: Schematics and reference quantities for liquid-solid phase change in $\mathbb{R}^2$

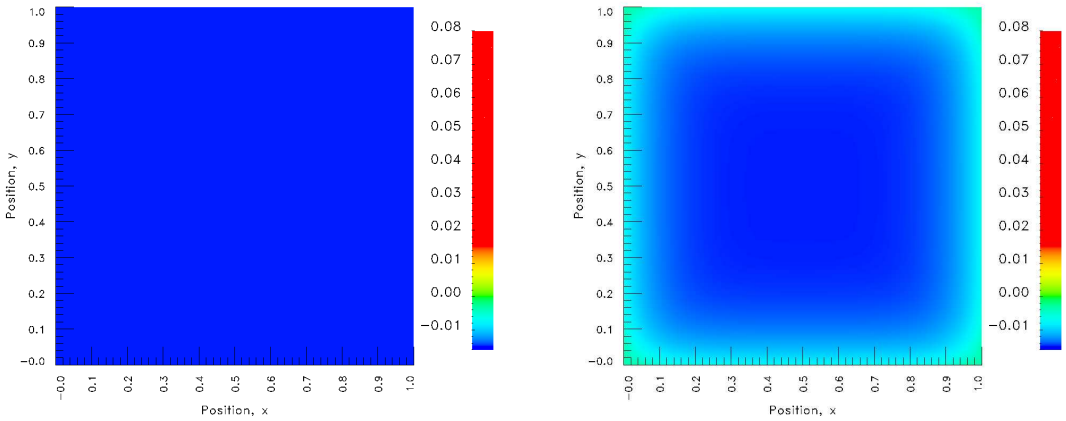

(a) Initial Condition

(b) $t = 0.01$

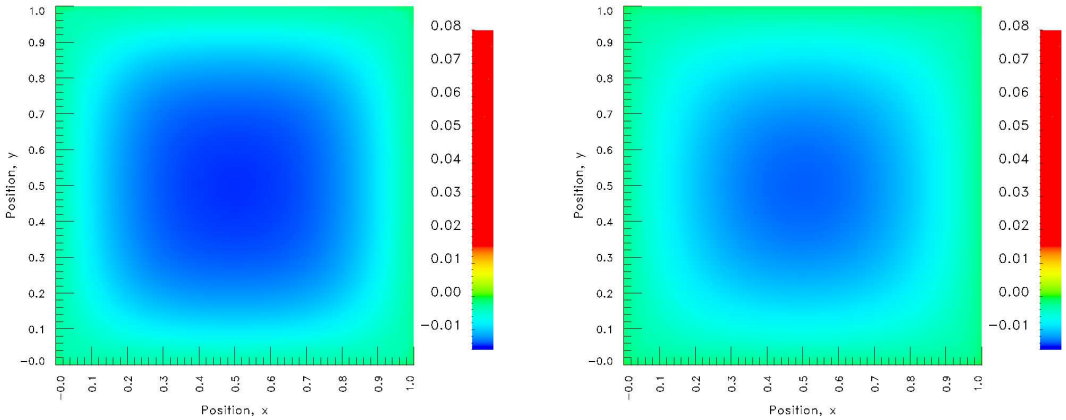

(c) $t = 0.02$

(d) $t = 0.03$

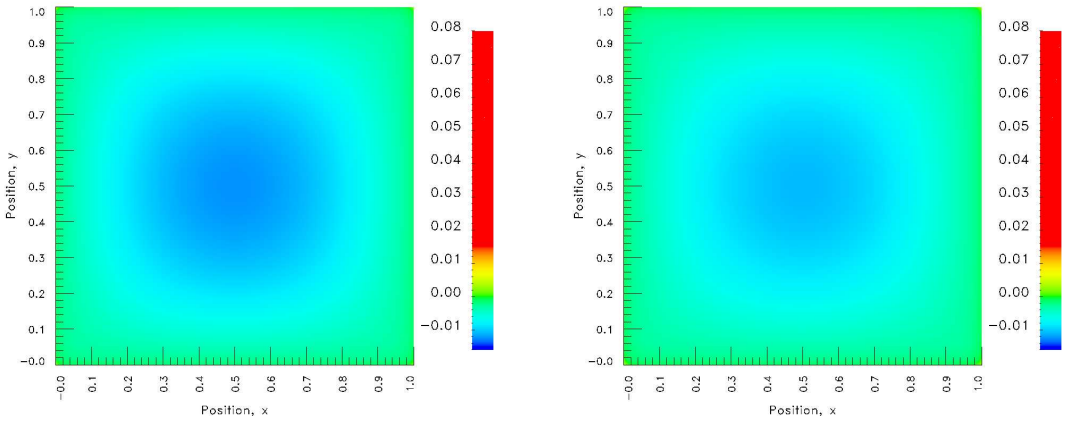

(e) $t = 0.04$

(f) $t = 0.05$

Figure 5.32: Evolution of Temperature for solid to liquid phase change in $\mathbb{R}^2$: $\Delta t = 0.01$

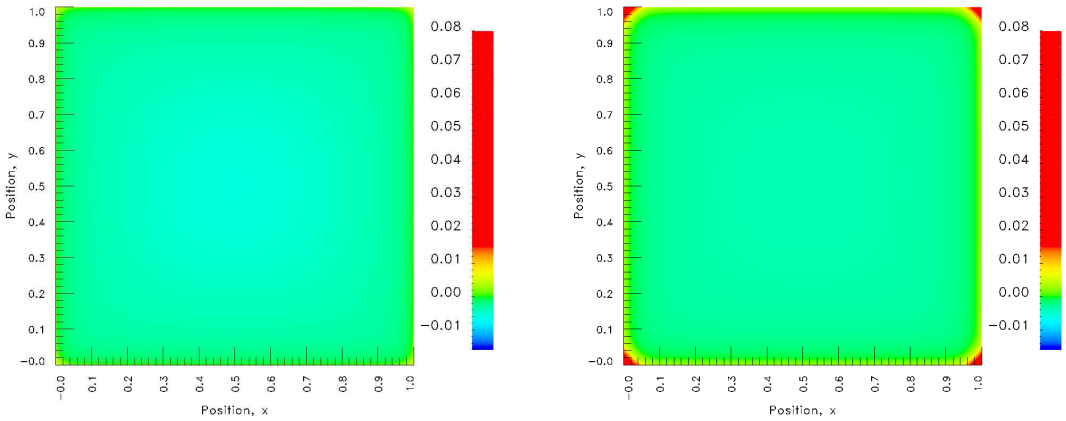

(a) $t = 0.10$

(b) $t = 0.20$

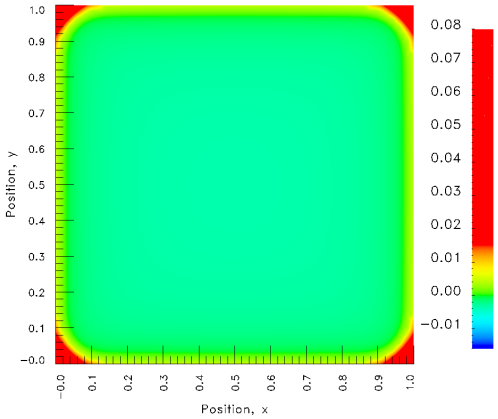

(c) $t = 0.30$

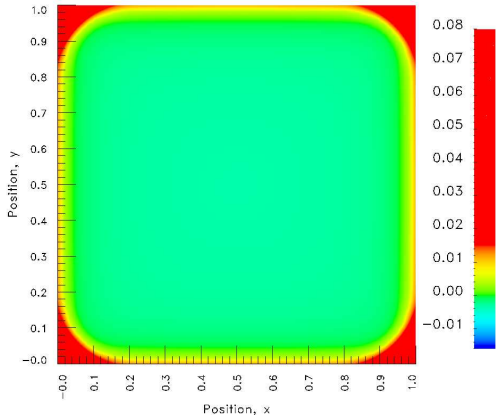

(d) $t = 0.40$

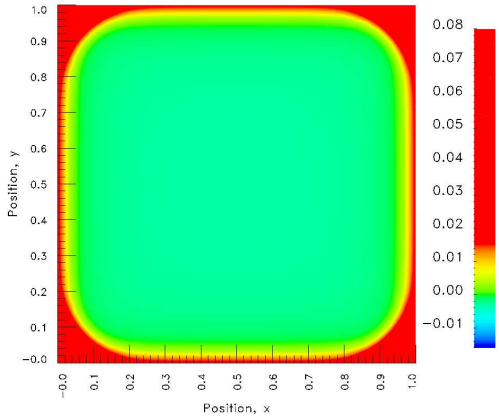

(e) $t = 0.50$

Figure 5.33: Further evolution of Temperature for solid to liquid phase change in $\mathbb{R}^2$: $\Delta t = 0.01$

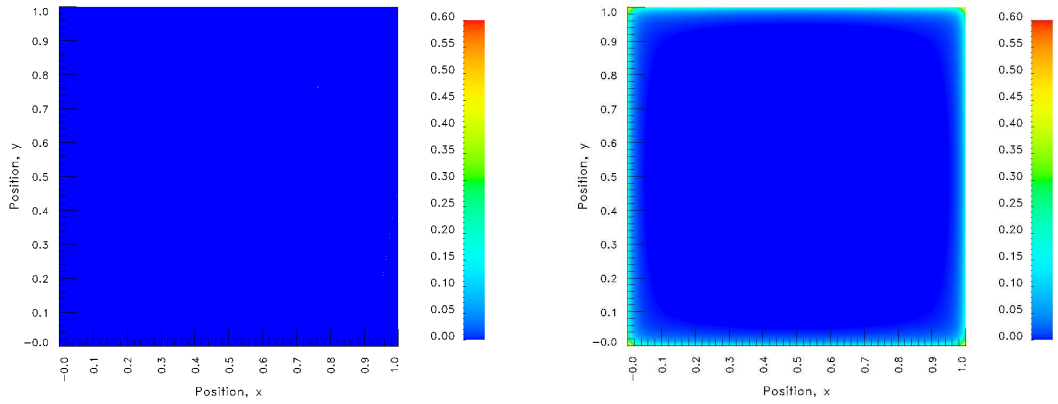

(a) Initial Condition

(b) $t = 0.05$

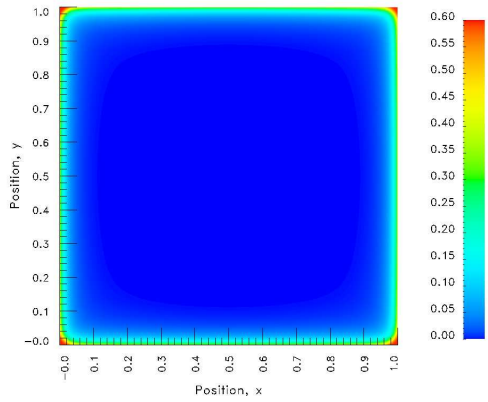

(c) $t = 0.10$

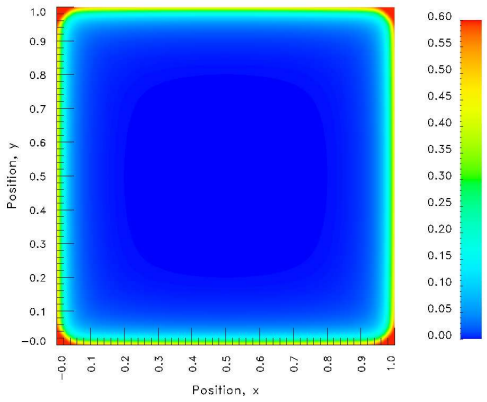

(d) $t = 0.15$

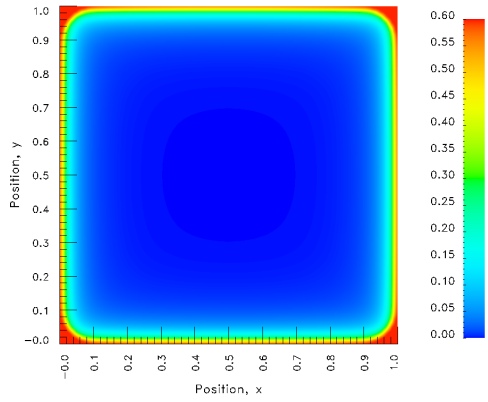

(e) $t = 0.20$

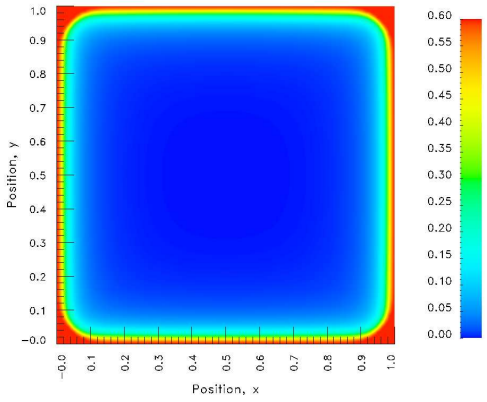

(f) $t = 0.25$

Figure 5.34: Evolution of Latent heat for solid to liquid phase change in $\mathbb{R}^2$: $\Delta t = 0.01$

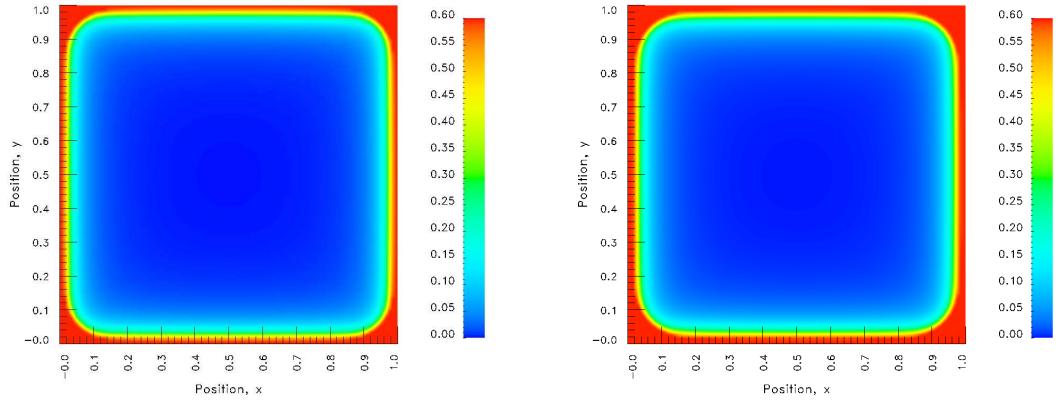

(a) $t = 0.30$

(b) $t = 0.35$

(c) $t = 0.40$

(d) $t = 0.45$

(e) $t = 0.50$

Figure 5.35: Further evolution of Latent heat for solid to liquid phase change in $\mathbb{R}^2$: $\Delta t = 0.01$

Chapter 6

Numerical simulation of phase change using mathematical models in Eulerian description

6.1 Introduction

In this chapter we consider numerical simulation of phase change processes using mathematical model in Eulerian description. As mentioned earlier in Chapter 1 and 3, the Eulerian descriptions are necessary to study phase change in processes in which the medium is flowing (non zero velocity field). Flow between parallel plates with cooling of plate(s) i.e. heat removal is a classical problem that requires a mathematical model in Eulerian description.

The mathematical model consists of continuity equation, momentum equation, energy equation and constitutive equations in contrast to Lagrangian descriptions (with zero ve-

locity field and zero stress field assumptions) in which case we only have a single non-linear PDE in temperature, i.e. energy equation. In principle, the numerical simulation of non-linear PDEs describing evolution [9, 36] is straight forward using STLSP provided the mathematical models contain precise description of the desired physics. The development of the mathematical model for phase change in Eulerian description has been presented in Chapter 3. Even though this mathematical model is not in precise agreement with the mixture theories [1–3], however we believe it captures sufficient aspects of the phase change physics to warrant numerical investigations. A simple model problem such as flow between parallel plates of a newtonian fluid with partial cooling (heat removal) of plate(s) is used to address many of the issues that are encountered in simulating phase change processes in Eulerian descriptions. In the following we present some remarks and discussion to develop focus in the numerical experiments or investigations leading to phase change simulations in $\mathbb{R}^2$.

Remarks and discussion:

(1) Since in the solid and the liquid phases all transport properties are assumed constant, the mathematical model consisting of continuity, momentum equations and the constitutive model using deviatoric Cauchy stress tensor can be used to obtain the solution of the velocity field and the deviatoric Cauchy stress tensor. Once the velocity field and the deviatoric Cauchy stress tensor are known, the energy equation can be used to obtain the temperature field. This suggests that the energy equation can be considered decoupled from the rest of the mathematical model. Perhaps we could argue the possibility of weak coupling between the energy equation and the rest of the mathematical model in solid and liquid phases.

(2) In the transition region all transport properties are a function of temperature, hence the energy equation is strongly coupled with the rest of the mathematical model.

(3) The argument presented in remark (1) can also be viewed differently. Presence of velocity field and the deviatoric Cauchy stress tensor in the energy equation suggests that the energy equation is in fact coupled with the rest of the mathematical model. Thus, it should be possible to consider the entire mathematical model consisting of continuity, momentum equations, energy equation and the constitutive equations for the stress tensor and heat vector as a coupled system of PDEs in simulating the solutions numerically regardless of the phase. We pursue this approach in the present work. That is, we consider the entire mathematical model consisting of continuity, momentum equations, energy equation and the constitutive laws for the deviatoric stress tensor and heat vector for all phases. As an example for phase change processes in $\mathbb{R}^2$ we have velocities $\bar{u}$, $\bar{v}$, pressure $\bar{p}$, stresses ${}_d\bar{\sigma}^{(0)}_{xx}$, ${}_d\bar{\sigma}^{(0)}_{yy}$, ${}_d\bar{\sigma}^{(0)}_{xy}$, temperature $\bar{T}$, and heat fluxes $\bar{q}_x$ and $\bar{q}_y$ as nine dependent variables in nine partial differential equations. This model (described in section 3.2) obviously has closure.

(4) In the numerical studies we consider developing flow between parallel plates as a model problem. The fluid (water) is assumed to be newtonian. Upon phase change the solid medium (ice) is assumed to be hypoelastic. Details of the mathematical model are presented in section 4.3.2 and are not repeated for the sake of brevity.

(5) Initially, we present some preliminary numerical studies to demonstrate that essential elements of the physics of phase change is a flowing medium with non zero stress field are in fact present in the proposed mathematical model. These studies are followed by a numerical simulation of the phase change in $\mathbb{R}^2$. Developing flow of

water between parallel plates with applied heat flux (cooling) at the lower plate is used as a model problem.

Change of notation:

For the sake of simplicity, certain changes in notations are made in this chapter.

- The overbar symbol ($^{-}$) used in previous chapters to differentiate from Lagrangian descriptions, is omitted for convenience, since all formulations in this chapter are in Eulerian descriptions.
- Subscripts 1 and 2 or x_1 and x_2 used for the dependent and independent variables refer to the their Cartesian components. We replace x_1 and x_2 by x and y or in some cases by 1 and 2.
- The velocity components v_1, v_2 or v_x, v_y are replaced by u and v.

6.2 Numerical studies

We consider the following numerical studies:

(a) Numerical simulation of viscous dissipation for flow between parallel plates.

(b) Numerical studies including viscous dissipation and externally applied heat flux on isolated portions of the plates (symmetric) for flow between parallel plates.

(c) Consequence of using divergence free velocity field for solid medium as opposed to pressure constraint equation.

(d) Numerical simulation of phase change in $\mathbb{R}^2$ for flow between parallel plates as a model problem.

6.2.1 Numerical simulation of viscous dissipation: flow between parallel plates (no phase change)

In this numerical study we consider numerical simulation of viscous dissipation for flow between parallel plates. Figures 6.1(a) and 6.1(b) show schematics and boundary conditions. At the inlet: $T = 0$, velocity is fully developed, $u = g(y)$, $v = 0$ and $p = 0$. Both plates are stationary and insulated ($u = 0$, $v = 0$, $q_y = 0$). At outflow ${}_d\sigma_{xx}^{(0)} = 0$. Figure 6.2 shows the spatial discretization of the x, y domain. We obtain numerical solutions for this model problem as a boundary value problem as well as a initial value problem (using $\Delta t = 50.0$). Local approximations of class C^0 are used with p-level of 3 for both the BVP as well as the IVP. Computed evolutions of temperature at the outflow (T versus y at $x = 0.5$) and the lower plate (T versus x at $y = 0.0$) and a comparison with the BVP solution are shown in figures 6.3 and 6.4. Evolutions are smooth and the stationary state of the temperature evolution agrees with the BVP solution precisely. Figure 6.5 shows plots of the velocity field during evolution which remain unaffected as expected. The residual functional I of the order of $O(10^{-12})$ and $|g_i|_{max}$ of the order of $O(10^{-7})$ for all time increments ensure good accuracy of the evolution and the solution of the BVP. This study shows that numerical simulations of viscous dissipation in processes without externally applied heat flux is simulated quite accurately.

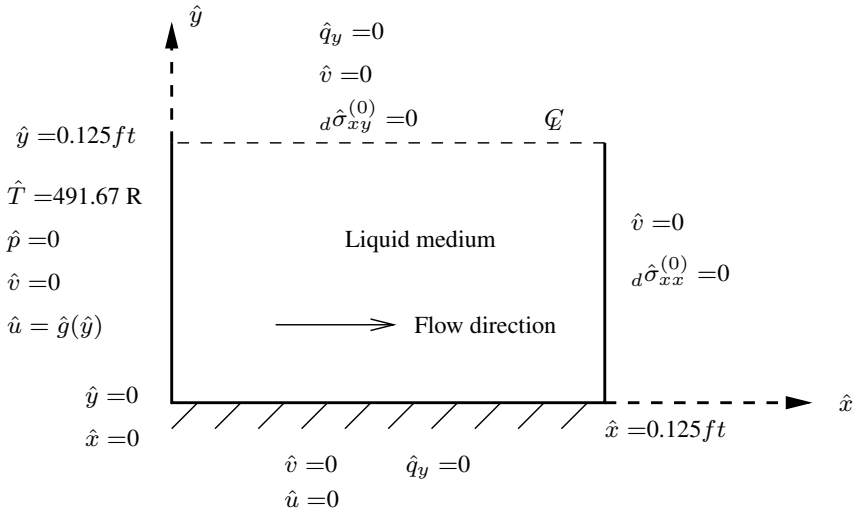

(a) Physical spatial domain

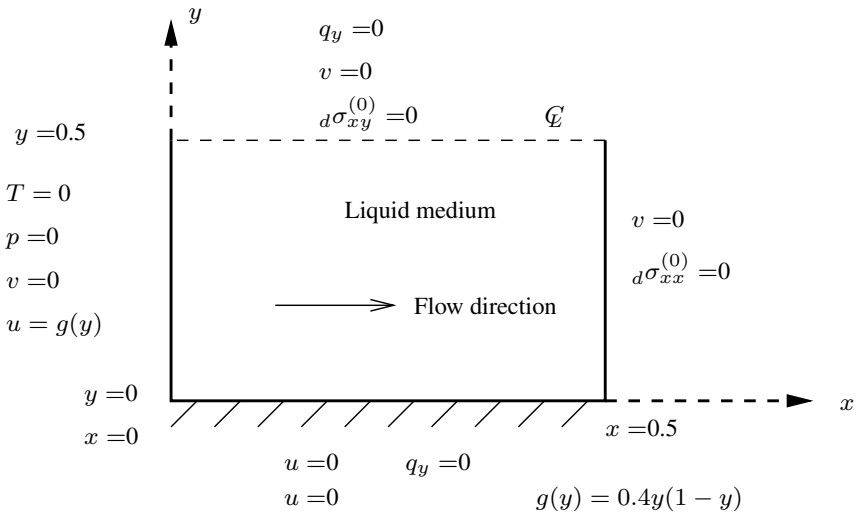

(b) Dimensionless spatial domain

Reference quantities: $\rho_0 = \hat{\rho}_s$, $k_0 = \hat{k}_s$, $c_{p0} = \hat{c}_{ps}$, $L_0 = 0.25ft$, $v_0 = 1.0ft/s$ $T_0 = (32^\circ F + 459.67) = 491.67\ R$, $t_0 = 0.25\ s$, $q_0 = 1.42Btu/ft^2\,s$, $\Delta t = 50.0$, $\Delta\hat{t} = 12.5s$, $\mu_0 = \hat{\mu}$, $\tau_0 = E_0 = \rho_0 v_0^2 = 57.16lbm/ft\,s^2$

Figure 6.1: Schematics and reference quantities for viscous dissipation for flow between parallel plates

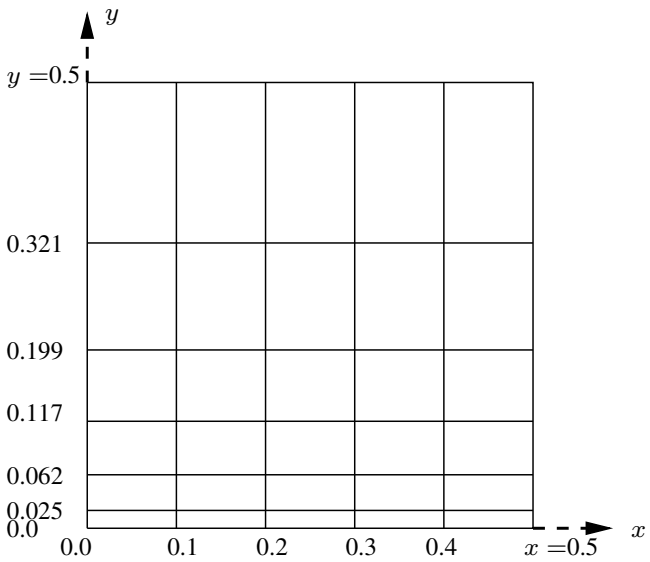

Figure 6.2: Spatial discretization

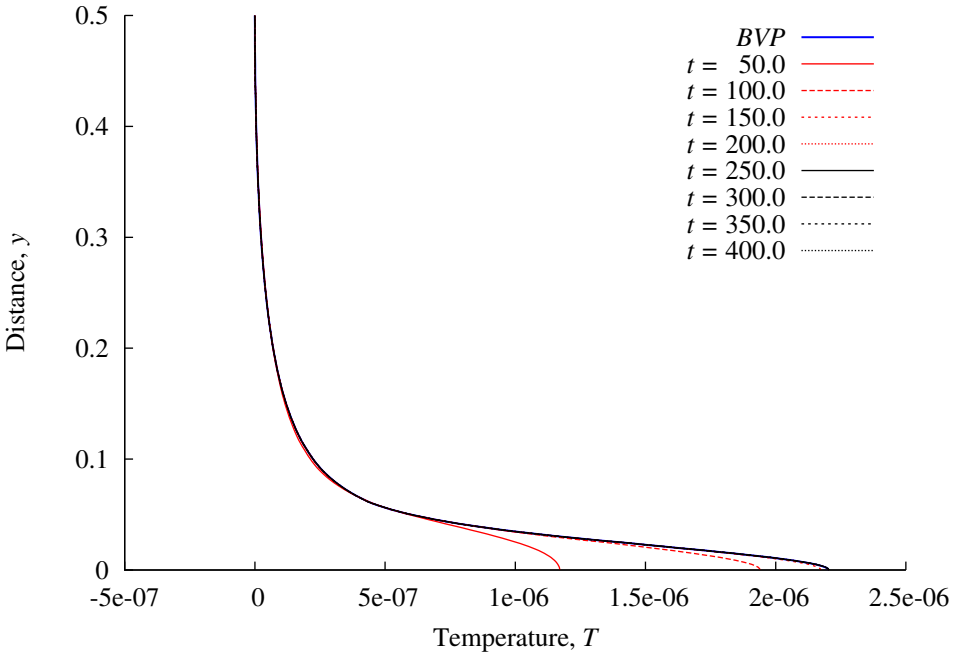

Figure 6.3: Temperature T versus y at outlet ($x = 0.5$), only viscous dissipation

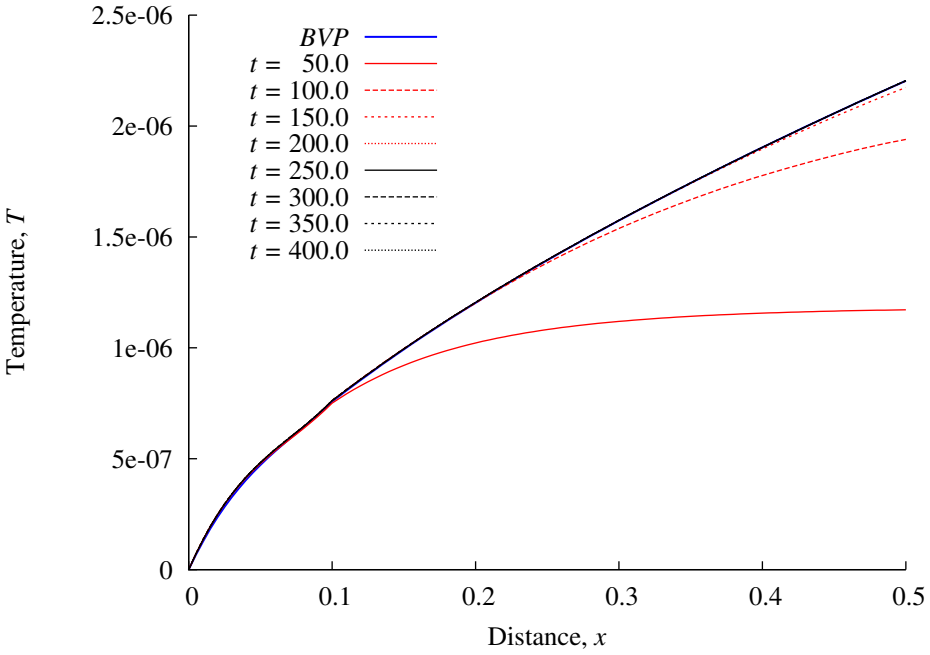

Figure 6.4: Temperature T versus x at lower plate ($y = 0.0$), only viscous dissipation

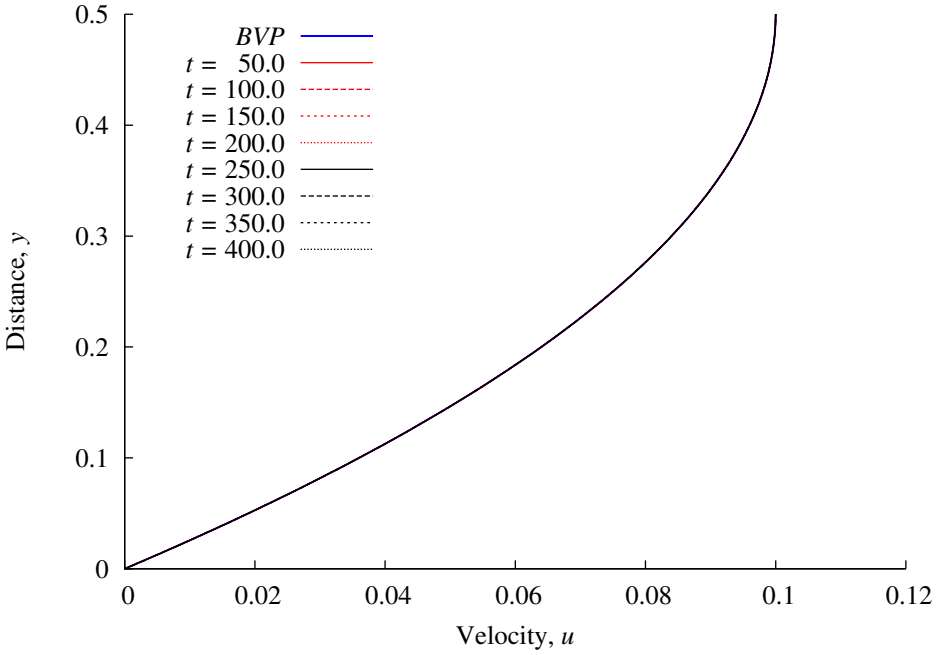

Figure 6.5: Velocity u versus y at ($x = 0.5$), only viscous dissipation

6.2.2 Numerical study including viscous dissipation and externally applied heat flux: flow between parallel plates (no phase change)

In this study we consider the same model problem as in section 6.2.1 but with externally applied heat flux. A bicubic in x heat flux (cooling) centered at $x = 0.2$ and cubic in t is applied to both plates (figure 6.6). The schematics and discretization are same as is section 6.2.1 (figures 6.1(a), 6.1(b) and 6.2). In the numerical studies we consider $q_{y,max}$ of 10^{-4}, 10^{-3}, 10^{-2} and 10^{-1} for the BVP, and $q_{y,max}$ of 10^{-4} and 10^{-3} for the IVP.

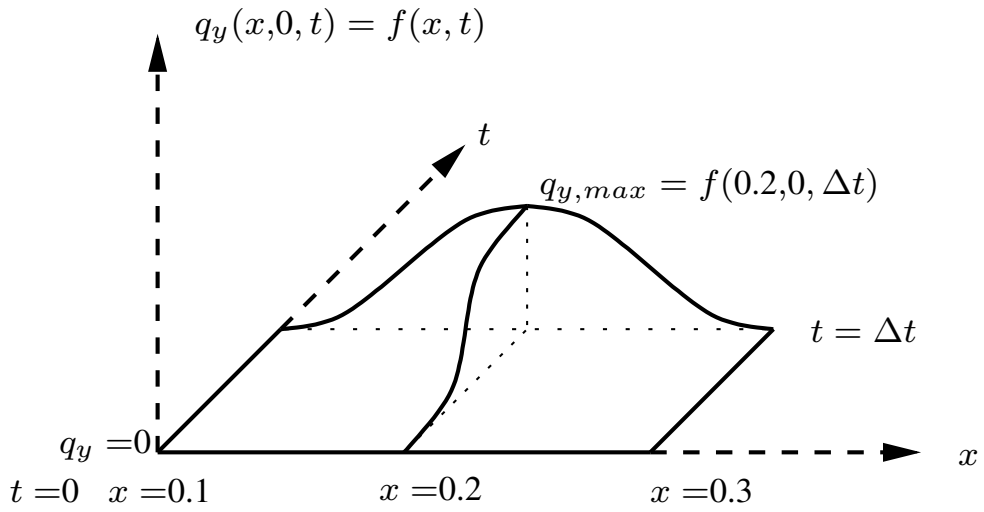

Figure 6.6: Details of Heat flux $q_y(x, 0, t) = f(x, t)$ at the plates (figure shows lower plate, $y = 0$)

BVP

Figures 6.7 to 6.10 show plots of velocity u at $x = 0.2$ for different values of $q_{y,max}$ and at p-levels of 3, 5, 7 and 9. Plots of the temperature at the outflow and lower plate ($y = 0.0$) for the same p-levels are shown in figures 6.7 to 6.10. These studies demonstrate

that as $q_{y,max}$ increases (well beyond viscous dissipation) progressively higher p-levels are required if the discretization is kept fixed. If we keep $p = 3$ fixed, then of course mesh refinement will be needed for accurate results. These studies confirm that the velocity field and the temperature field are uncoupled but both can be simulated using a combined single mathematical model that includes energy equation and the heat flux.

IVP

In this section we consider same configuration and details as for BVP but consider numerical solutions of the evolution using different values of $q_{y,max}$ and compare the stationary state of the evolution with the solution of the corresponding BVP. Figures 6.15(a) and 6.15(b) show evolution of temperature T at the outflow and at the plate ($y = 0$) for p-level of 3 and comparisons with solutions of the corresponding BVP for $q_{y,max} = 10^{-4}$. Plots of the velocity field at the outflow and $x = 0.2$ are shown in figure 6.16. Decoupling between the temperature field and the velocity field is quite clear. Stationary state of the evolution agrees well with the solution of the BVP.

Similar studies for $q_{y,max} = 10^{-3}$ are shown in figures 6.17 to 6.18 for $p = 3$. The results for $q_{y,max} = 10^{-3}$ are reasonable but not as good as for $q_{y,max} = 10^{-4}$. Further numerical studies conducted for $q_{y,max} > 10^{-3}$ confirm that for this fixed grid discretization at $p = 3$, the computed solution progressively deteriorate with increasing $q_{y,max}$. As shown for BVP this situation is easily corrected by increasing p-level. The same holds for the IVP as well.

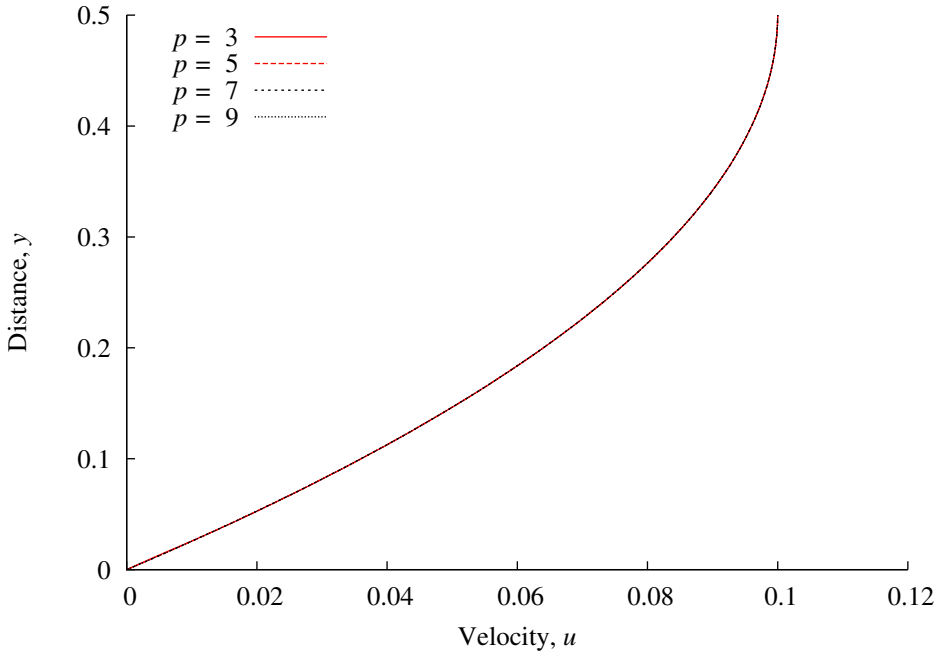

Figure 6.7: Velocity u versus y at center of disturbance ($x = 0.2$) for $q_{y,max} = 10^{-4}$, BVP various p-levels

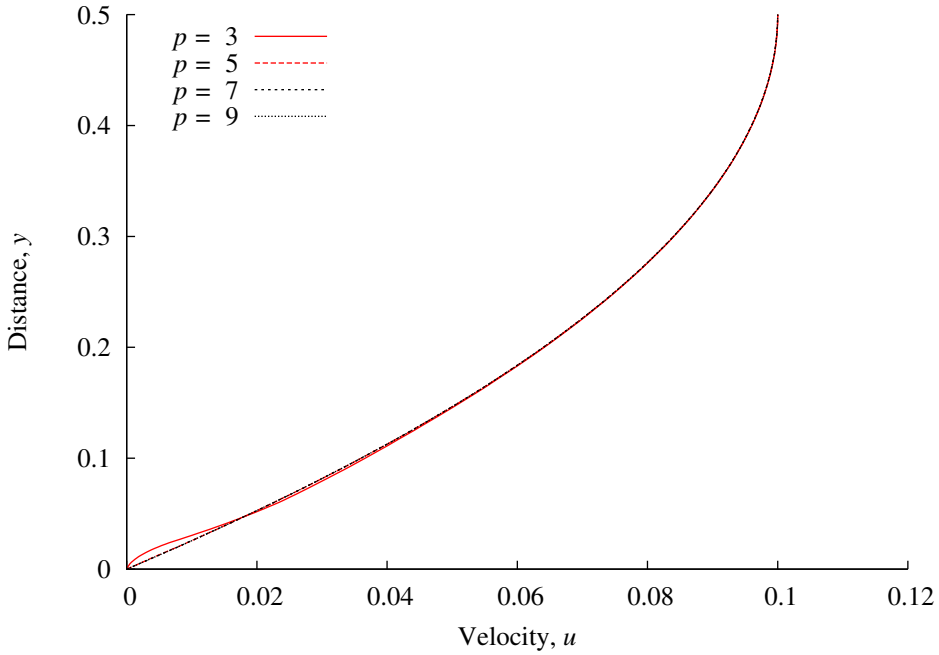

Figure 6.8: Velocity u versus y at center of disturbance ($x = 0.2$) for $q_{y,max} = 10^{-3}$, BVP various p-levels

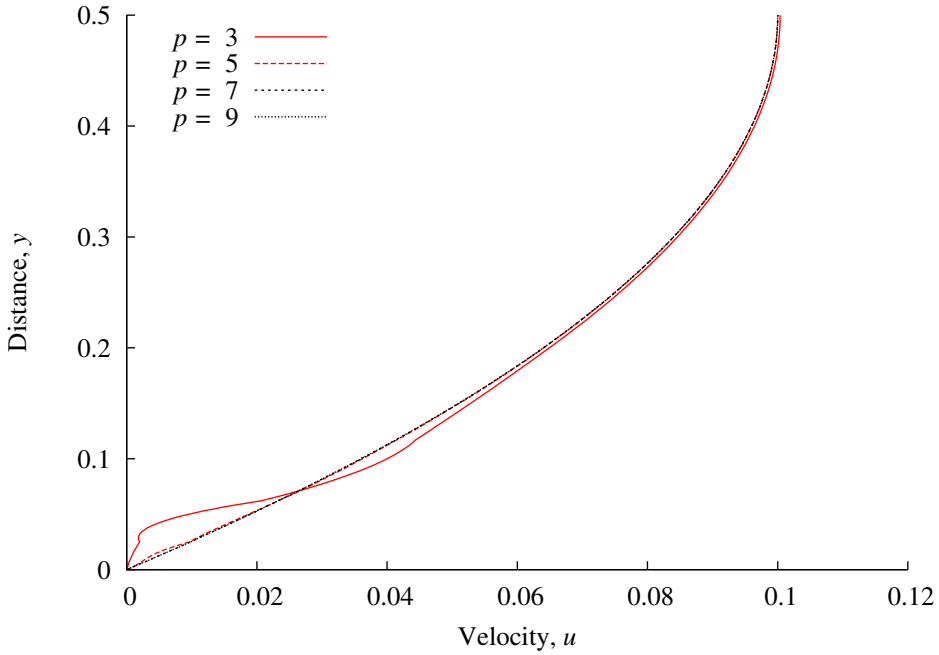

Figure 6.9: Velocity u versus y at center of disturbance ($x = 0.2$) for $q_{y,max} = 10^{-2}$, BVP various p-levels

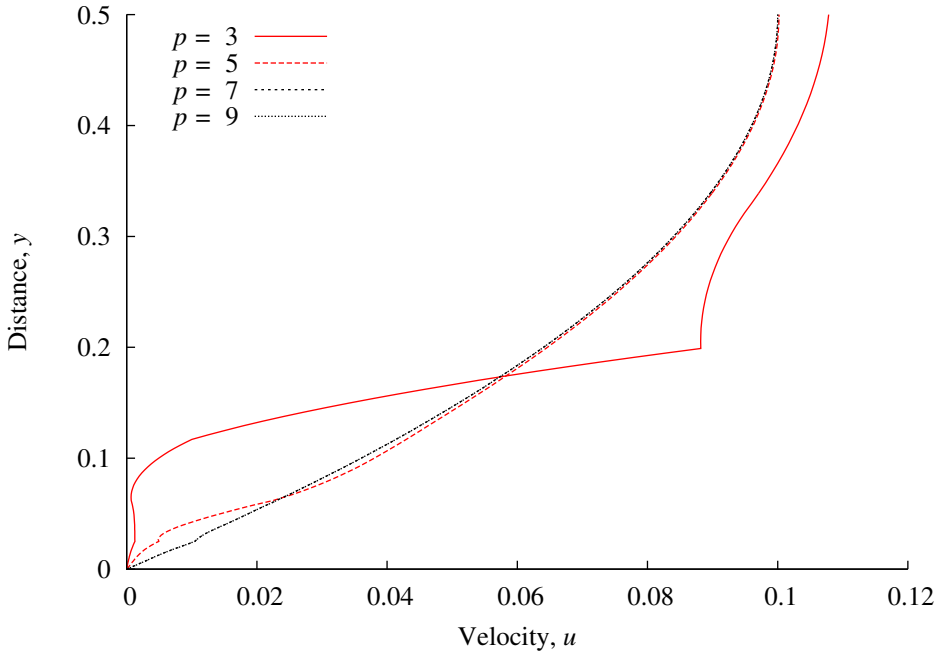

Figure 6.10: Velocity u versus y at center of disturbance ($x = 0.2$) for $q_{y,max} = 10^{-1}$, BVP various p-levels

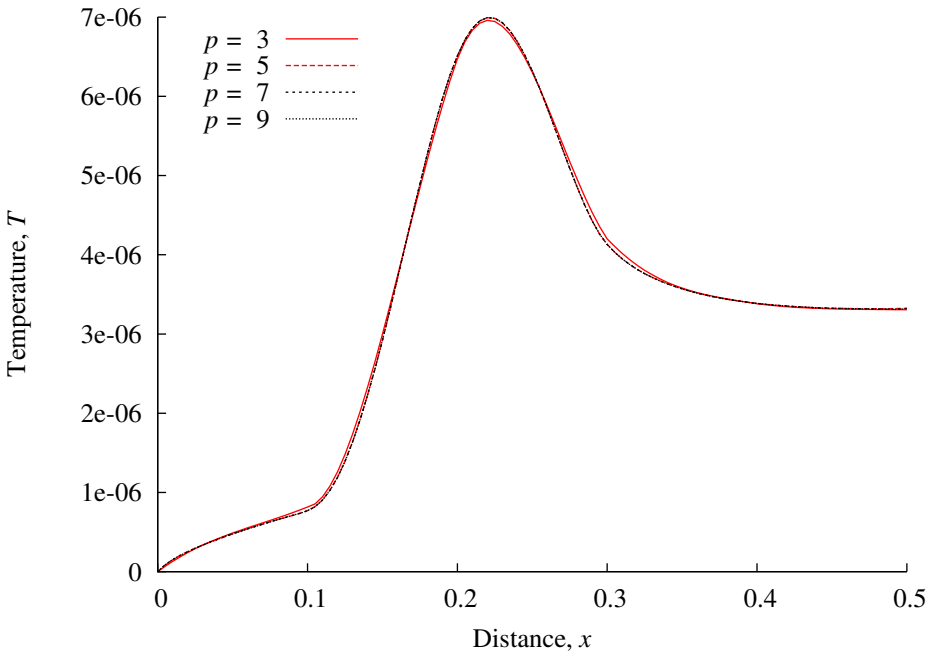

(a) Temperature T versus x at lower plate ($y = 0.0$)

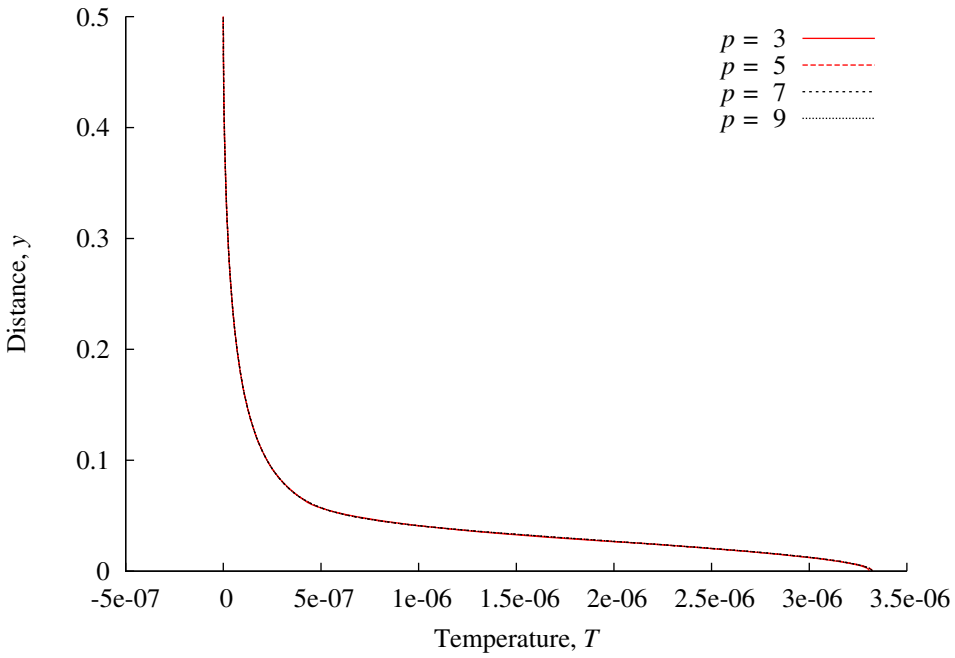

(b) Temperature T versus y at outlet ($x = 0.5$)

Figure 6.11: Temperature T for $q_{y,max} = 10^{-4}$, BVP various p-levels

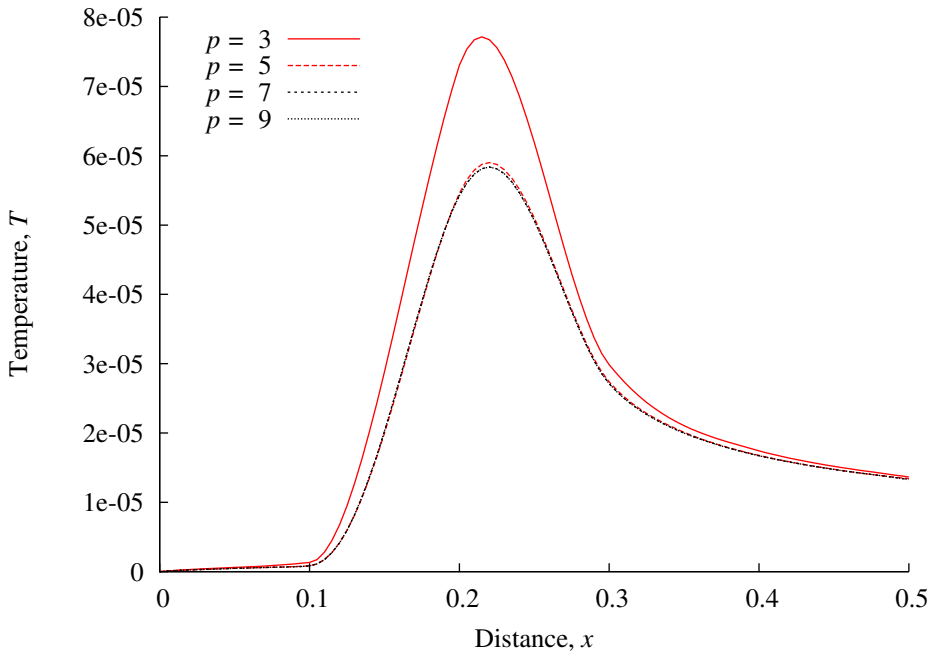

(a) Temperature T versus x at lower plate ($y = 0.0$)

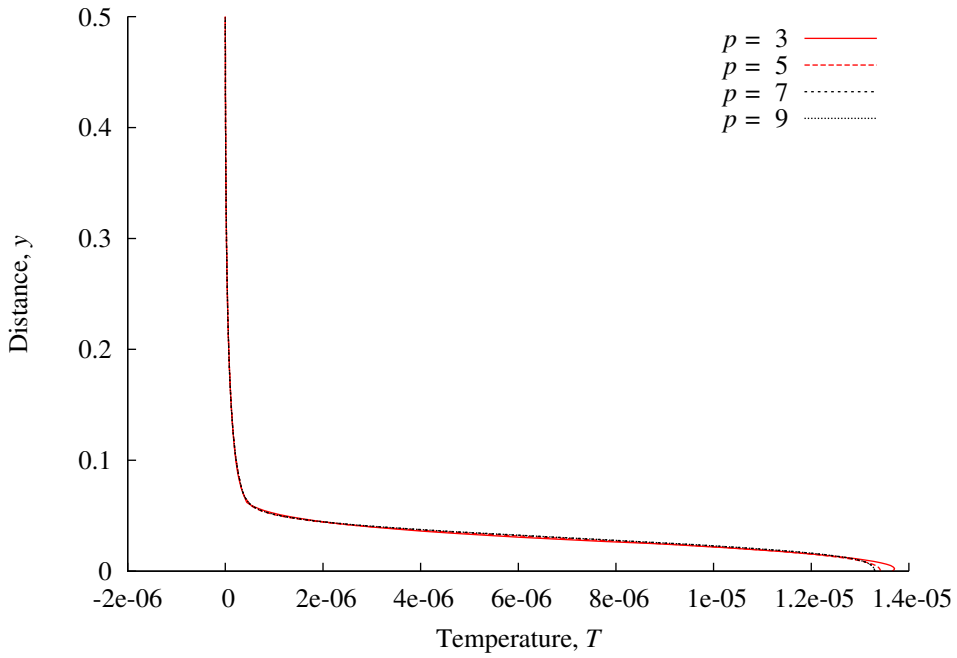

(b) Temperature T versus y at outlet ($x = 0.5$)

Figure 6.12: Temperature T for $q_{y,max} = 10^{-3}$, BVP various p-levels

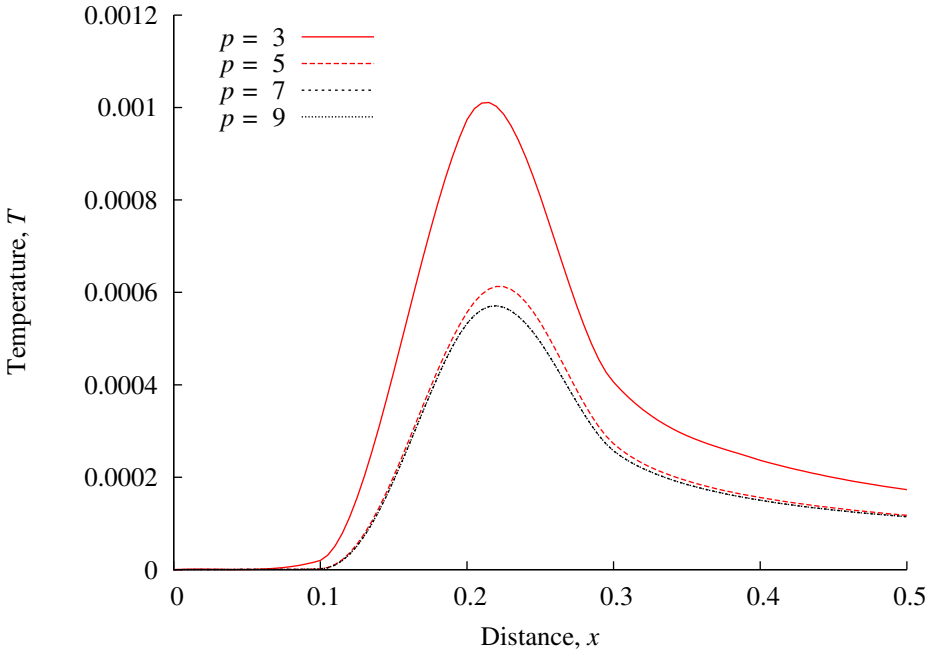

(a) Temperature T versus x at lower plate ($y = 0.0$)

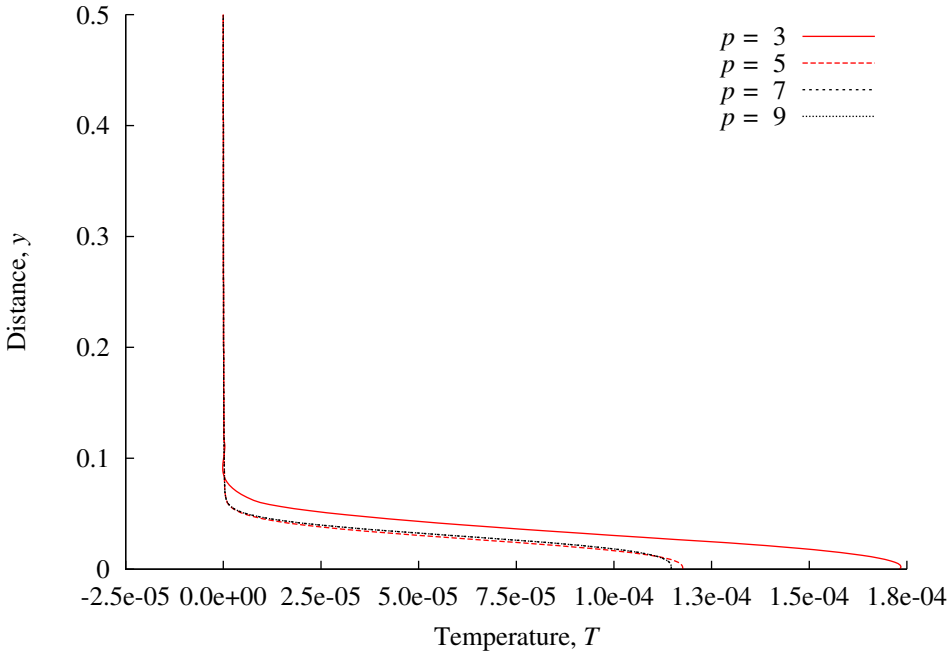

(b) Temperature T versus y at outlet ($x = 0.5$)

Figure 6.13: Temperature T for $q_{y,max} = 10^{-2}$, BVP various p-levels

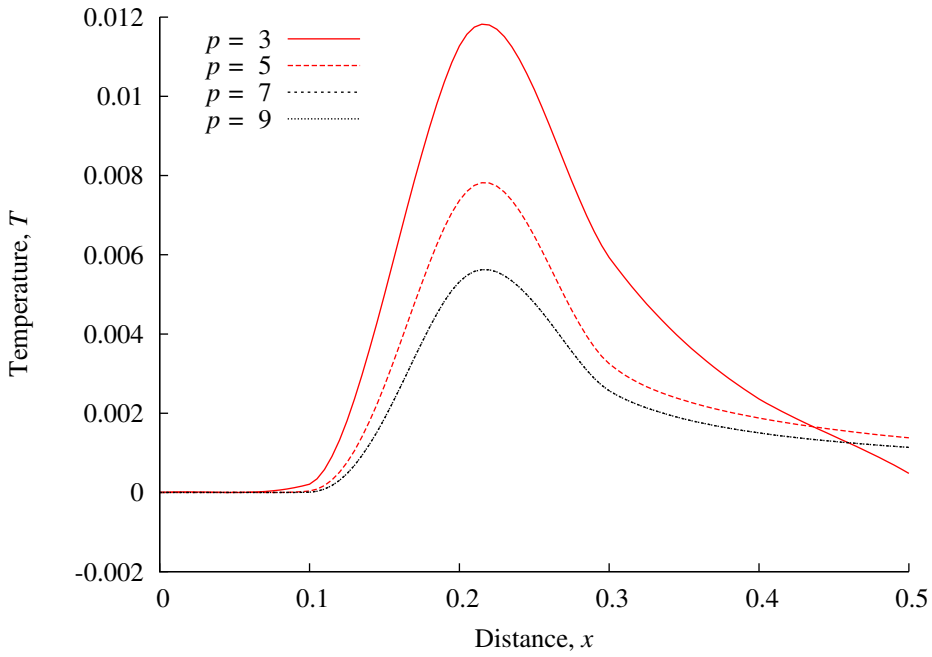

(a) Temperature T versus x at lower plate ($y = 0.0$)

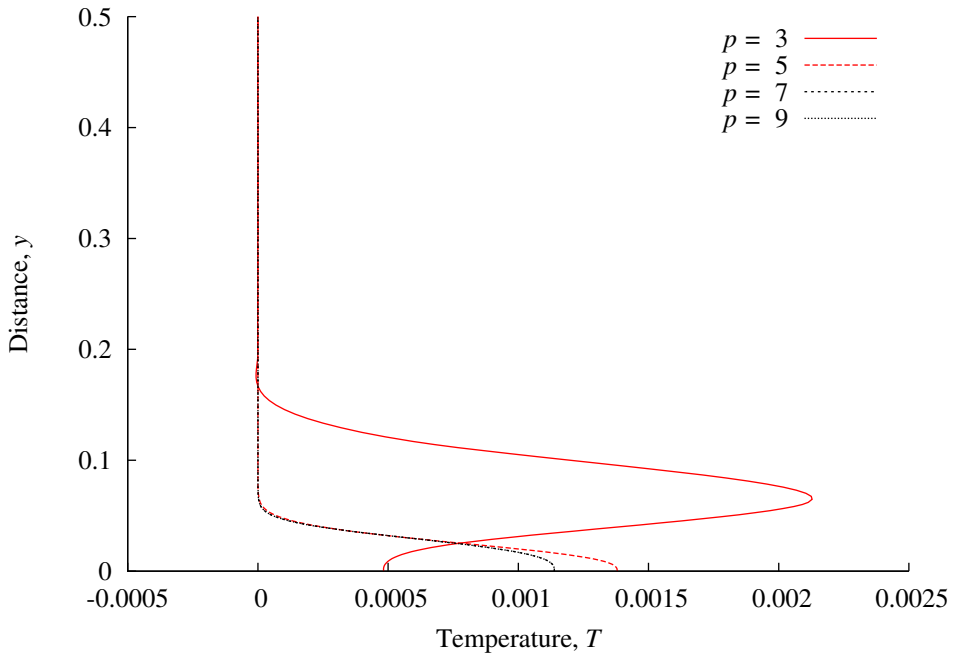

(b) Temperature T versus y at outlet ($x = 0.5$)

Figure 6.14: Temperature T for $q_{y,max} = 10^{-1}$, BVP various p-levels

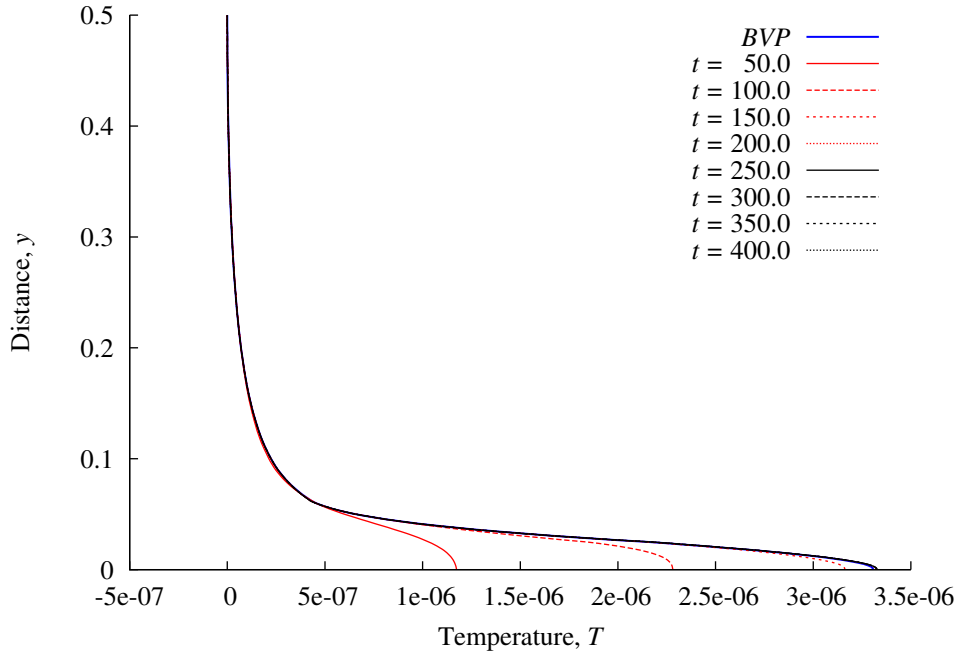

(a) Temperature T versus y at outlet ($x = 0.5$)

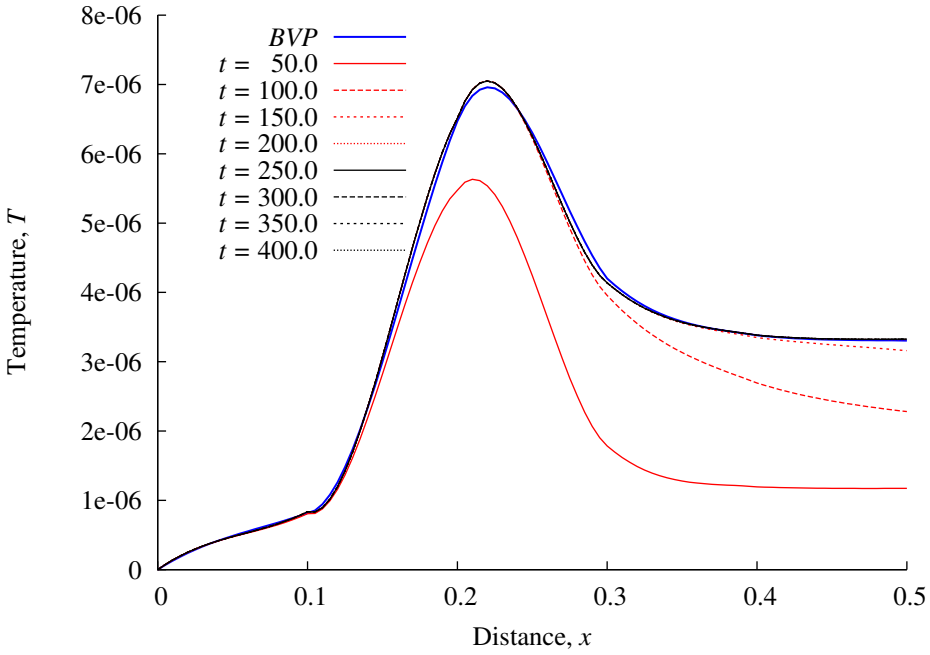

(b) Temperature T versus x at the lower plate ($y = 0.0$)

Figure 6.15: Temperature T for $q_{y,max} = 10^{-4}$, BVP and IVP, p=3

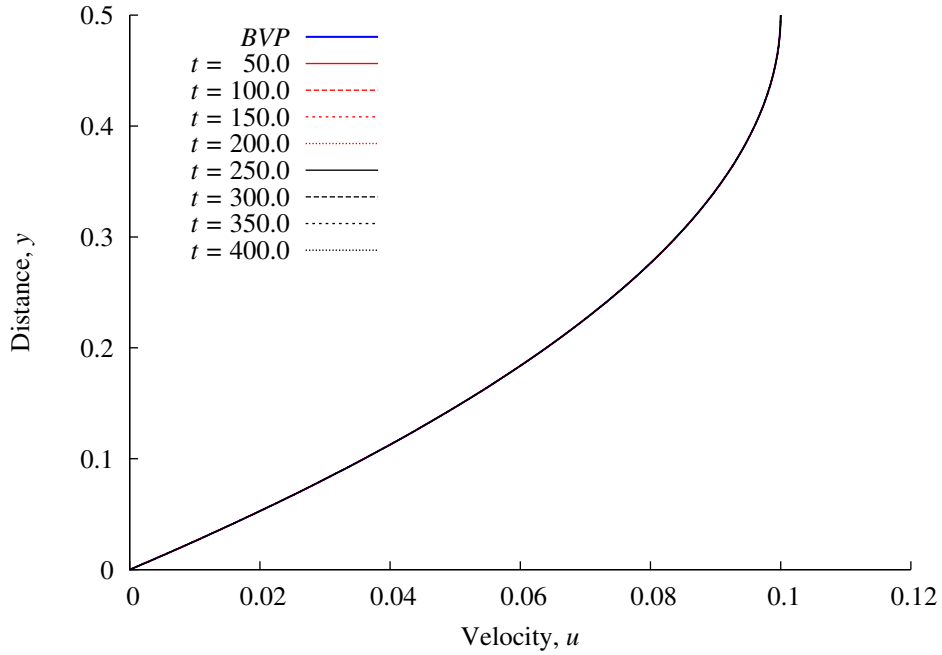

(a) Velocity u versus y at outlet ($x = 0.5$)

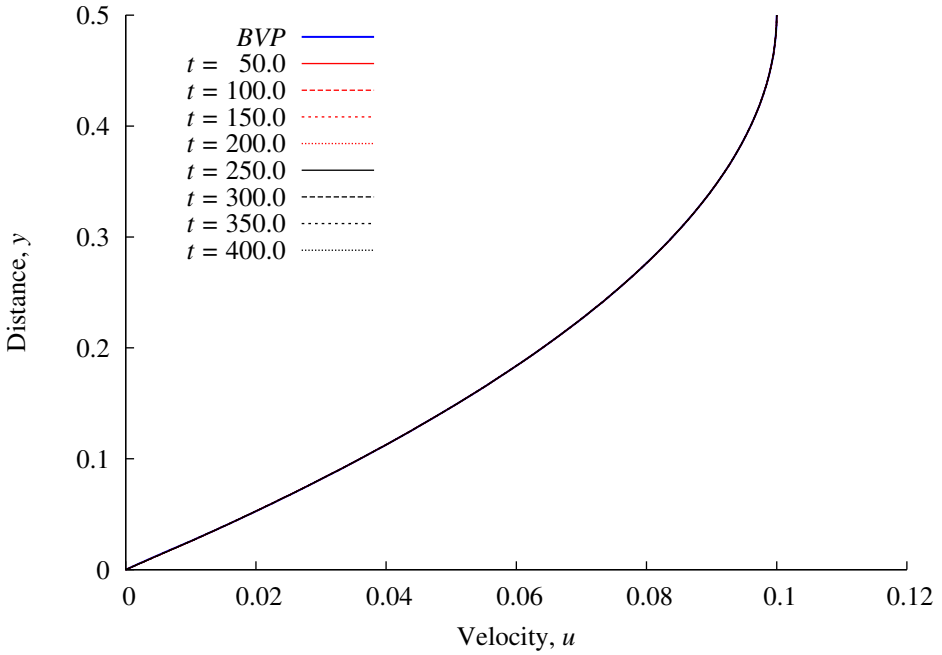

(b) Velocity u versus y at the center of the disturbance ($x = 0.2$)

Figure 6.16: Velocity u for $q_{y,max} = 10^{-4}$, BVP and IVP, p=3

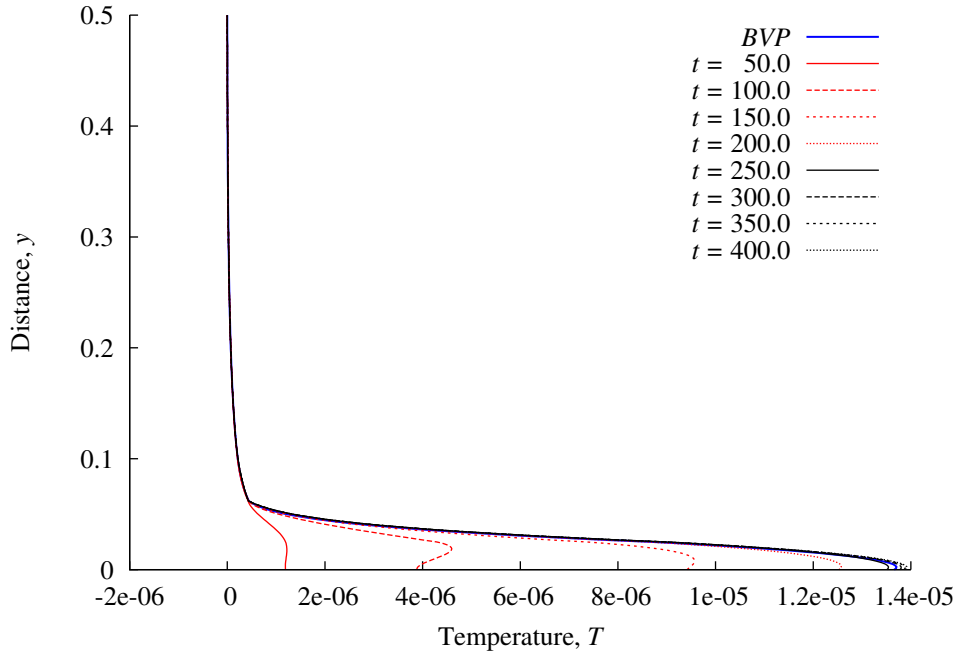

(a) Temperature T versus y at outlet ($x = 0.5$)

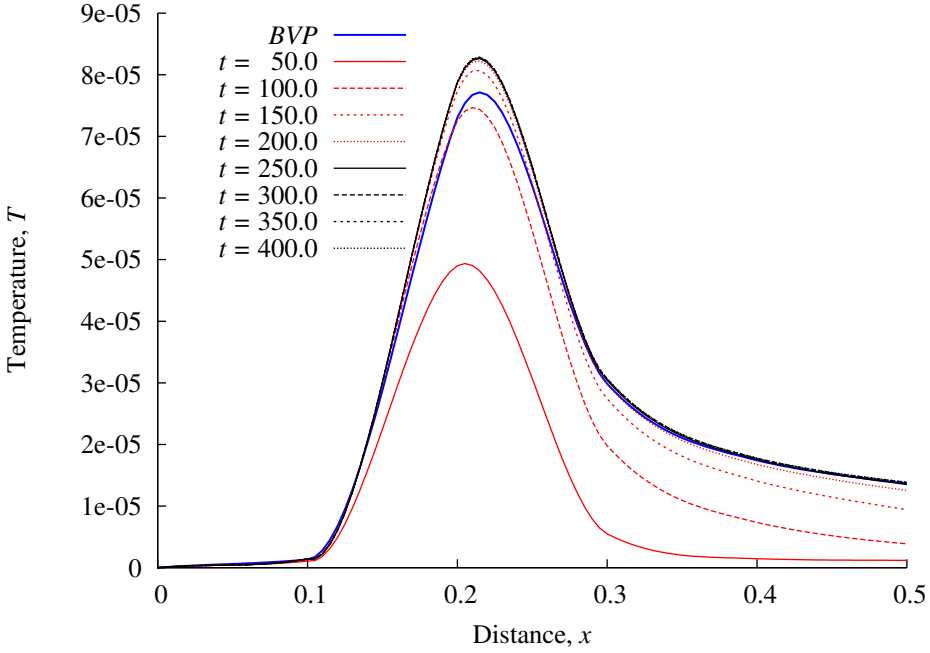

(b) Temperature T versus x at the lower plate ($y = 0.0$)

Figure 6.17: Temperature T for $q_{y,max} = 10^{-3}$, BVP and IVP, p=3

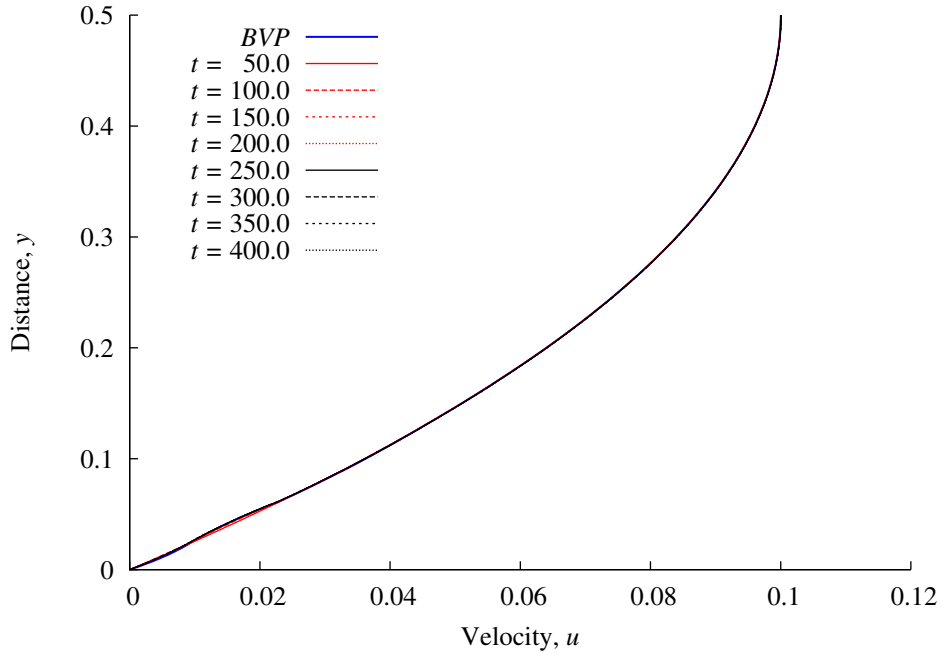

(a) Velocity u versus y at outlet ($x = 0.5$)

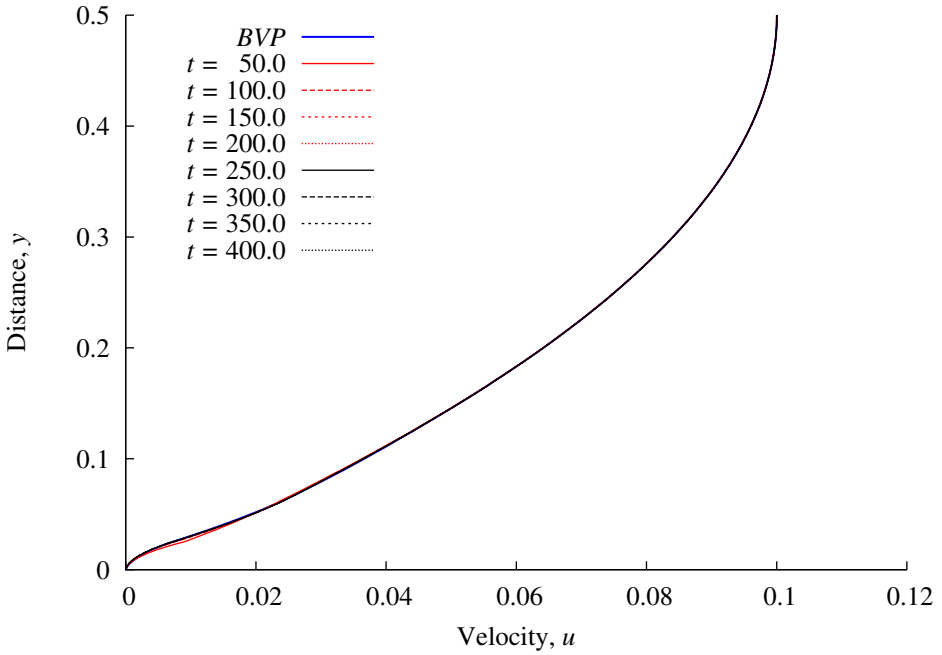

(b) Velocity u versus y at the center of the disturbance ($x = 0.2$)

Figure 6.18: Velocity u for $q_{y,max} = 10^{-3}$, BVP and IVP, p=3

6.2.3 Consequence of using divergence free velocity field for solid medium

In the development of the mathematical model for solid phase, we showed that in the Eulerian description for solid matter the continuity equation must be replaced with the pressure constraint equation. This due to the fact that for hypoelastic solids, mechanical pressure is mean normal stress. In this section we present a simple numerical study to demonstrate that a failure in doing so can result in erroneous deformation field or may even prohibit computations due to lack of convergence when solving non-linear systems of algebraic equations. We consider $\bar{\Omega} = [0,1] \times [0,0.5] \subset \mathbb{R}^2$, a solid medium (ice) shown in figure 6.21. We use a (20×12) graded discretization of $\bar{\Omega}$ shown in figure 6.20. Schematics are shown in figures 6.21(a) and 6.21(b). The properties of ice are given in section 5.2. We use the following reference quantities.

$$\rho_0 = \hat{\rho}_s \ ; \ k_0 = \hat{k}_s \ ; \ c_{p0} = \hat{c}_{ps} \ ; \ L_0 = 0.25ft \ ; \ v_0 = 1.0ft/s \ ; \ q_0 = 1.42Btu/ft^2\, s$$

$$T_0 = (32^\circ F + 459.67) = 491.67 \ R \ ; \ t_0 = 0.25 \ s \ ; \ \Delta t = 50.0 \ ; \ \Delta \hat{t} = 12.5s$$

$$\mu_0 = \hat{\mu} \ ; \ \tau_0 = E_0 = \rho_0 v_0^2 = 57.16lbm/ft\, s^2$$

The boundary at $y = 0$ is subjected to heat flux (heating) as shown in figure 6.19 (bicubic in x and cubic in t). Evolution is computed for one increment of time with $p = 3$, $\Delta t = 200.0$, $\Delta \hat{t} = 50.0s$ using: the mathematical model containing continuity equation and the mathematical model in which continuity equation is replaced by the pressure constraint equation (see mathematical model at Chapters 3 and 4 in sections 3.2 and 4.3.2). When using pressure constraint equation, the Newton's linear method with line search converges in two iterations with $I = 0(10^{-5})$ and $|g_i|_{max} = 0(10^{-6})$ indicating good accuracy of the evolution. When using continuity equation in the mathematical model, the Newton's linear method with line search fails to converge. After 10 iterations $I = 0(10^{-1})$ and

($|g_i|_{max} = 0(10^5)$). Using more iterations make I and g values worse than those after 10 iterations. Figures 6.22-6.26 show plots of velocity u versus y; velocity v versus y; temperature T versus y; heat flux q_x versus y and heat flux q_y versus y at $x = 0.5$ for the two mathematical models. In case of the continuity equation, numerical results are at the end of the 10^{th} iteration (unconverged). From figures 6.22(a), 6.22(b), 6.23(a) and 6.23(b) we note that even when the velocities are extremely small, they are smooth and well behaved when pressure constraint equation is used. Plots of temperature, and heat fluxes (q_x and q_y) clearly show erroneous nature of the evolution resulting from the use of the mathematical model containing the continuity equation.

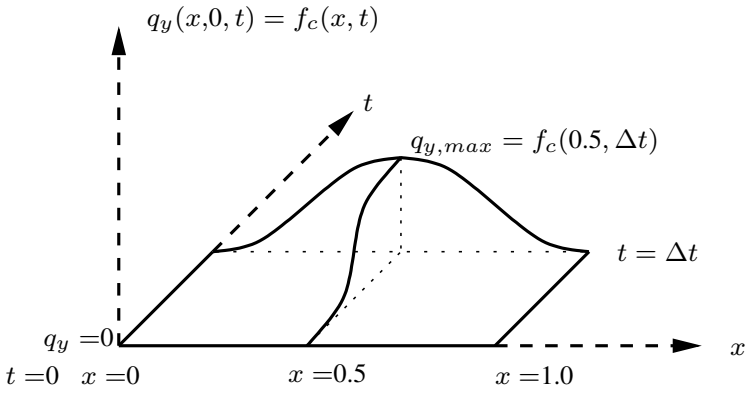

Figure 6.19: Details of Heat flux $q_y(x, 0, t) = f(x, t)$ at the lower boundary ($y = 0$)

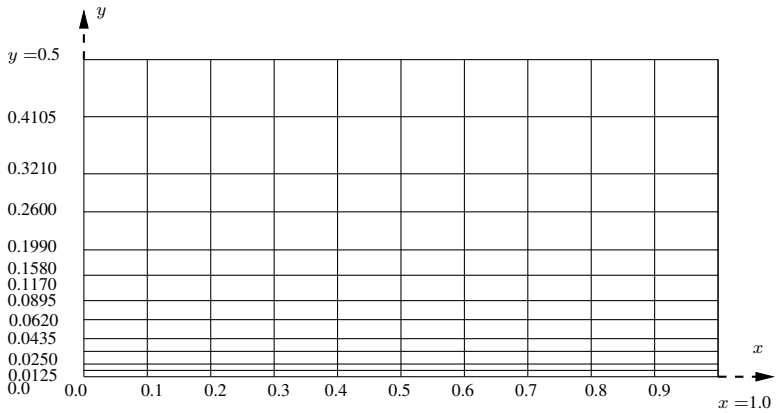

Figure 6.20: Spatial discretization for hypoelastic solid problem

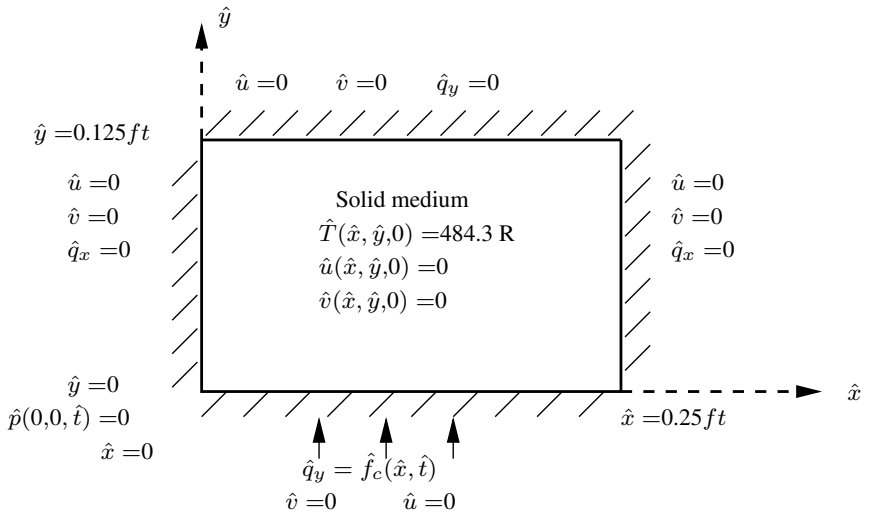

(a) Physical spatial domain

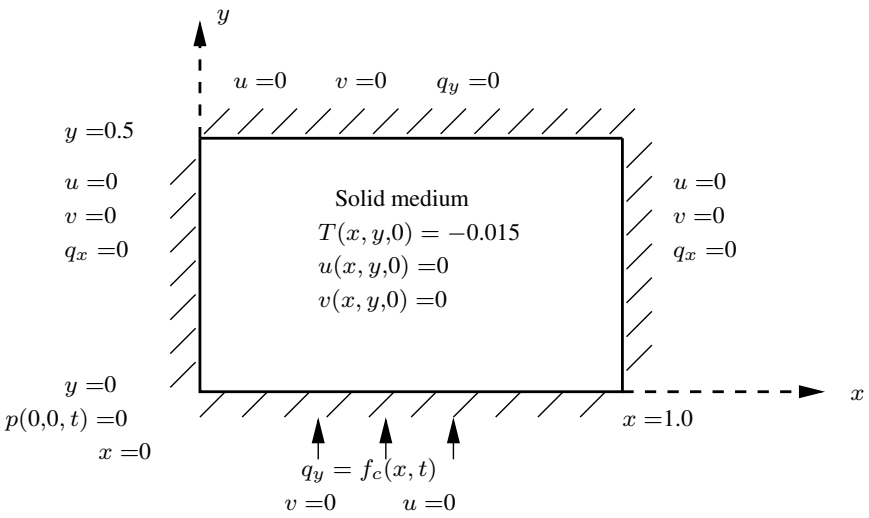

(b) Dimensionless spatial domain

Figure 6.21: Schematics for heat transfer in hypoelastic solid

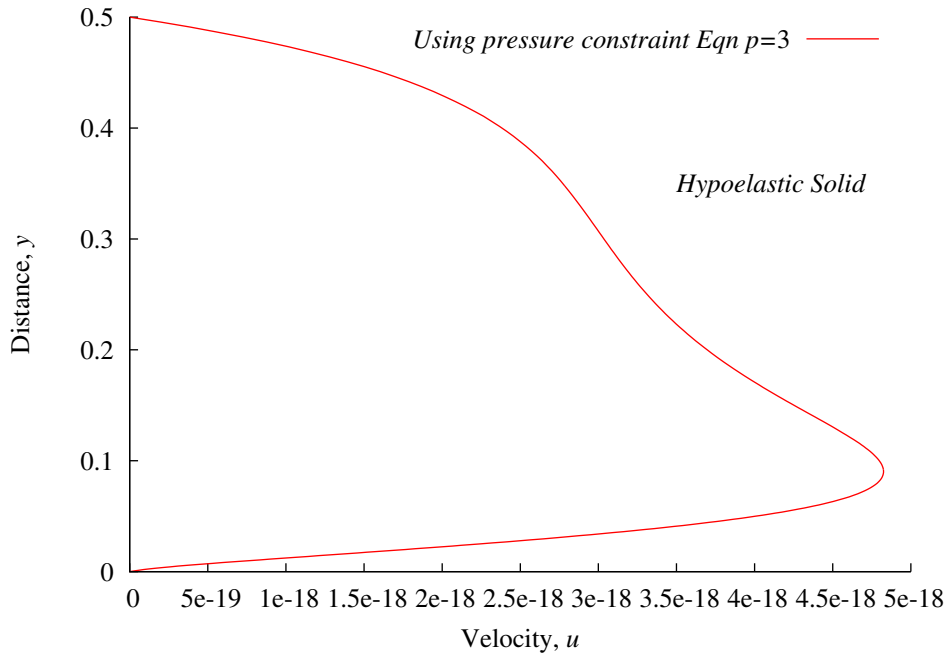

(a) Velocity u versus y at center of disturbance ($x = 0.5$), using pressure constraint equation

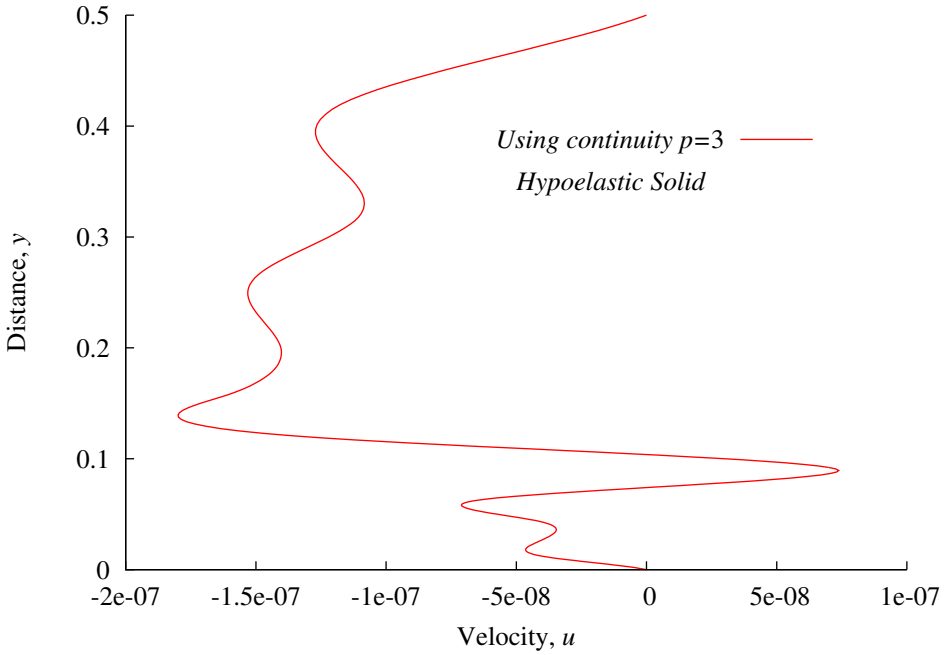

(b) Velocity u versus y at center of disturbance ($x = 0.5$), using continuity

Figure 6.22: Comparison of Velocity u versus y at center of disturbance ($x = 0.5$)

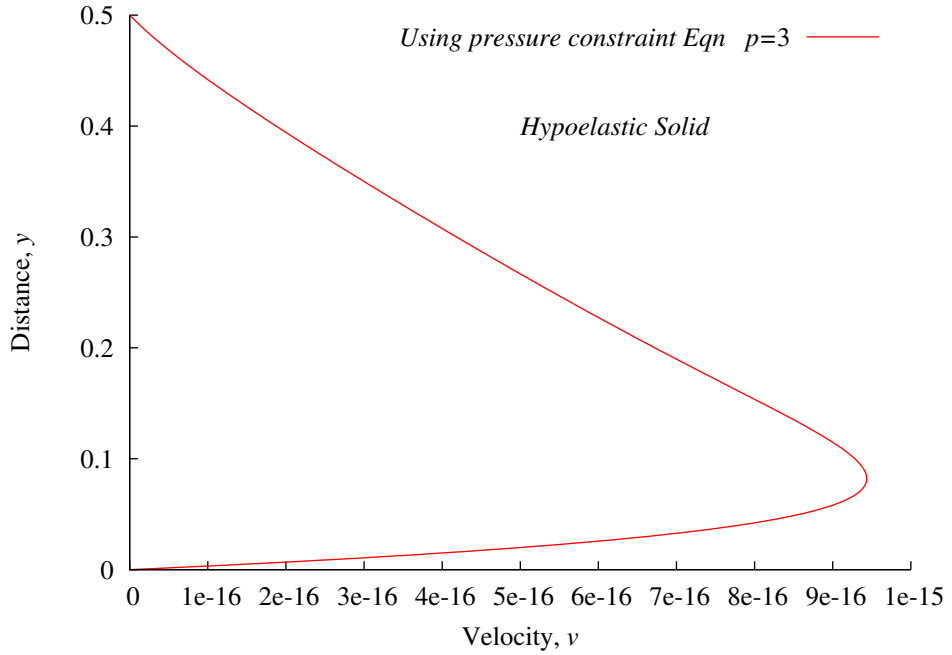

(a) Velocity v versus y at center of disturbance ($x = 0.5$), using pressure constraint equation

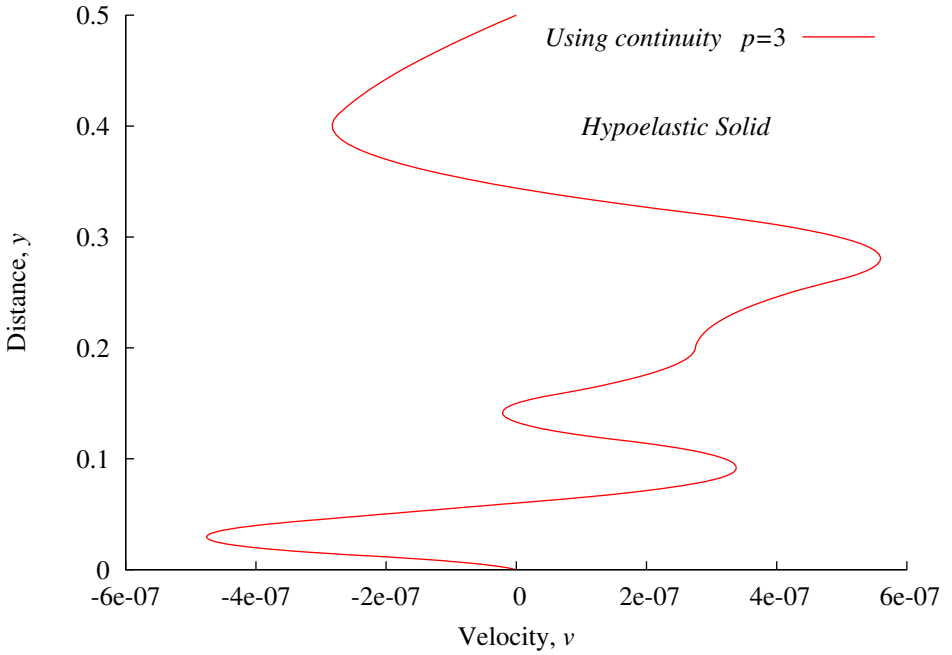

(b) Velocity v versus y at center of disturbance ($x = 0.5$), using continuity

Figure 6.23: Comparison of Velocity V versus y at center of disturbance ($x = 0.5$)

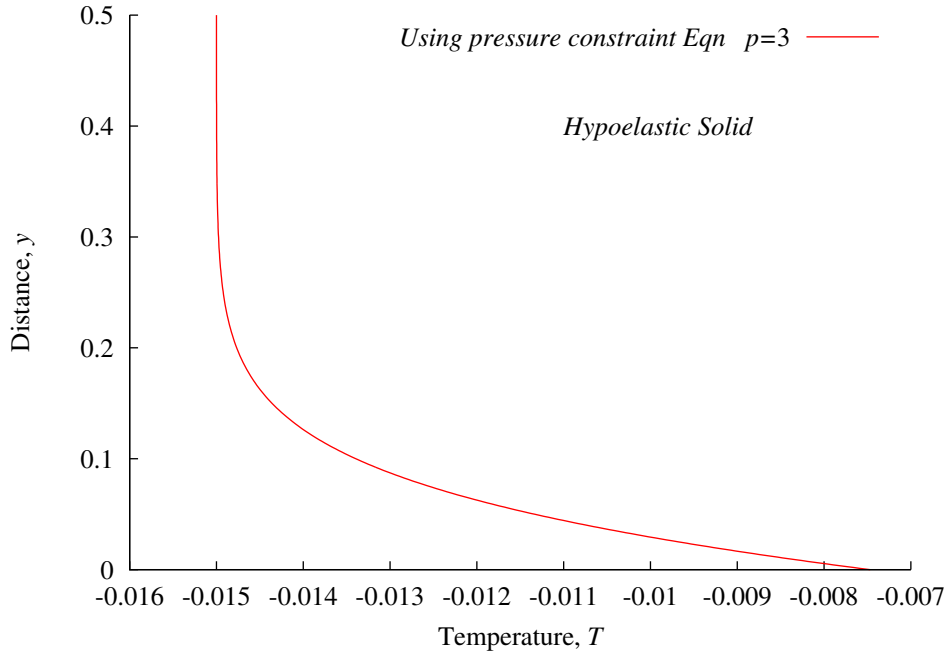

(a) Temperature T versus y at center of disturbance ($x = 0.5$), using pressure constraint equation

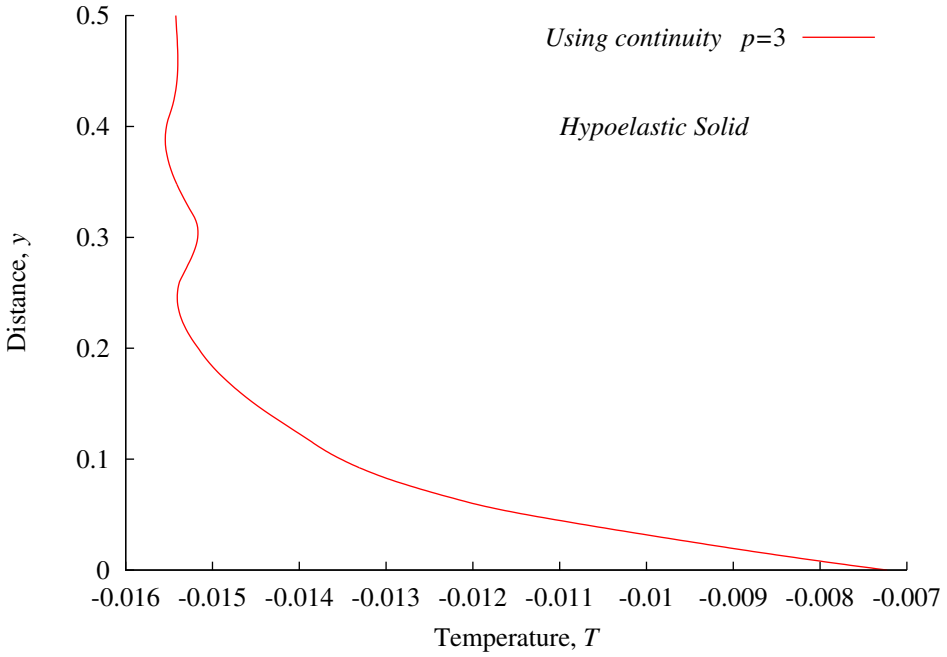

(b) Temperature T versus y at center of disturbance ($x = 0.5$), using continuity

Figure 6.24: Comparison of Temperature T versus y at center of disturbance ($x = 0.5$)

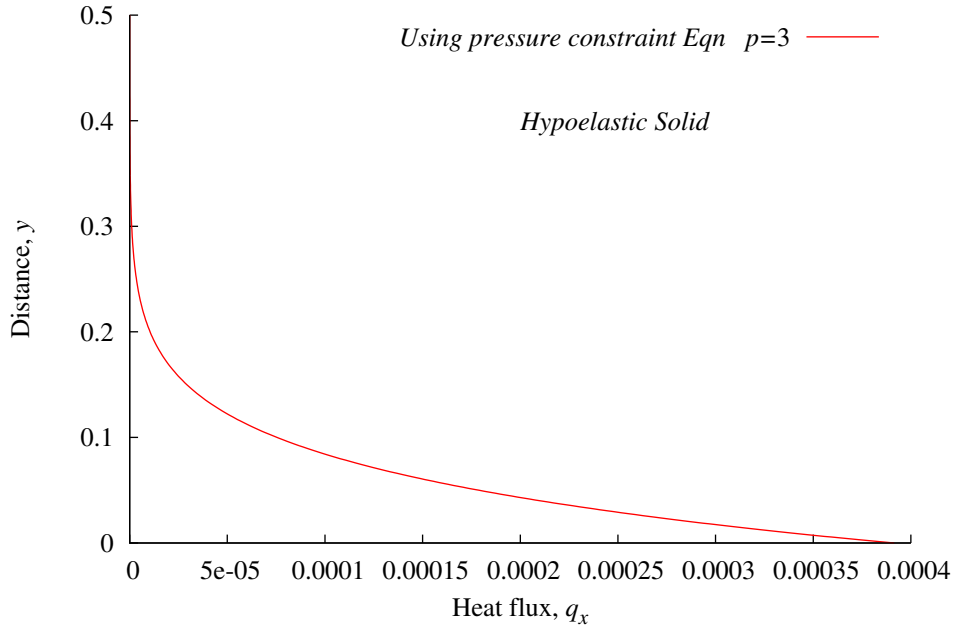

(a) Heat flux q_x versus y at center of disturbance ($x = 0.5$), using pressure constraint equation

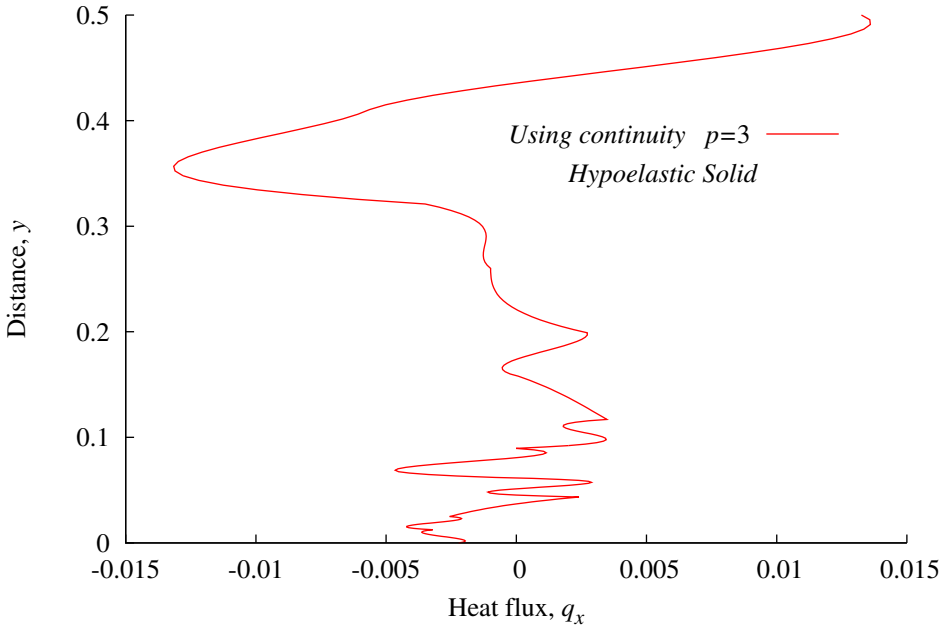

(b) Heat flux q_x versus y at center of disturbance ($x = 0.5$), using continuity

Figure 6.25: Comparison of Heat flux q_x versus y at center of disturbance ($x = 0.5$)

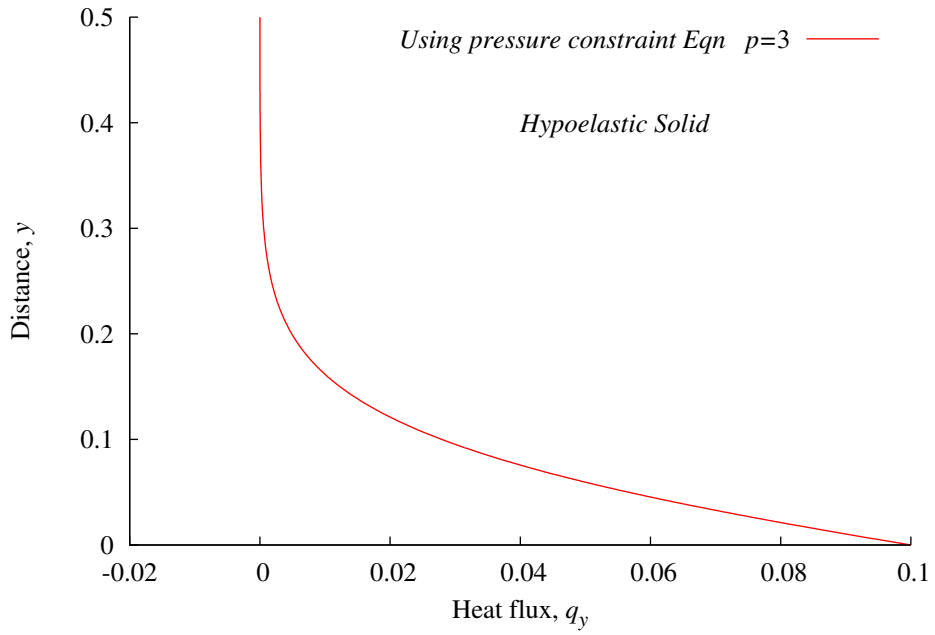

(a) Heat flux q_y versus y at center of disturbance ($x = 0.5$), using pressure constraint equation

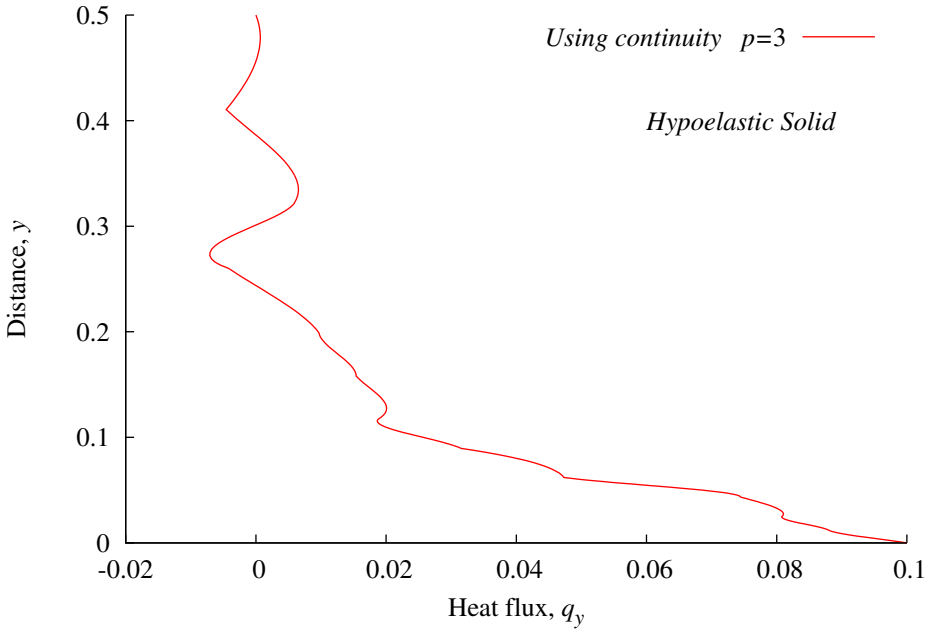

(b) Heat flux q_y versus y at center of disturbance ($x = 0.5$), using continuity

Figure 6.26: Comparison of Heat flux q_y versus y at center of disturbance ($x = 0.5$)

6.2.4 Numerical studies for liquid-solid phase change in $\mathbb{R}^2$: flow between parallel plates

In this section we present some preliminary numerical studies for liquid-solid phase change in $\mathbb{R}^2$. We consider flow between parallel plates as a model problem. Schematics of the computational domain (in physical space and dimensionless space), boundary conditions are shown in figures 6.28. The medium is water at $t = t_0 = 0$ (initial configuration) with temperature $\hat{T} = 499.05\ R$, $T = 0.015$. Velocity field at inlet is fully developed flow i.e. $u(0, y, 0) = 0.4y(1 - y)$ with maximum $u_{max} = 0.1$, $\hat{u}_{max} = 0.1 ft/s$ at $y = 0.5$ and $v(0, y, 0) = 0$. The transport properties of water and ice are given in section 5.2. We use the following reference quantities.

$$\rho_0 = \hat{\rho}_s\ ;\ k_0 = \hat{k}_s\ ;\ c_{p0} = \hat{c}_{ps}\ ;\ L_0 = 0.25 ft\ ;\ v_0 = 1.0 ft/s\ ;\ q_0 = 1.42 Btu/ft^2\, s$$

$$T_0 = (32^\circ F + 459.67) = 491.67\ R\ ;\ t_0 = 0.25\ s\ ;\ \Delta t = 50.0\ ;\ \Delta \hat{t} = 12.5 s$$

$$\mu_0 = \hat{\mu}\ ;\ \tau_0 = E_0 = \rho_0 v_0^2 = 57.16 lbm/ft\, s^2$$

The transition zone is taken to be $[T_s, T_l] = [-0.003, 0.003]$. We consider a (40×6) graded discretization of the spatial domain $\bar{\Omega} = [0.0, 4.0] \times [0.0, 0.5]$. Both plates are subjected to bicubic heat flux q_y (cooling) centered at $x = 1.0$ over 0.2 unit length with $q_{y,max} = -0.1$ (peak value at $x = 1.0$). Evolution is computed using $p = 3$ (both in space and time) with $\Delta t = 50.0$ (corresponding to $\Delta \hat{t} = 12.5$ seconds).

Discussion of results and Remarks

Plots of temperature T versus x at $y = 0$ for various values of time during the evolution are shown in figure 6.29(a). Graphs of temperature T versus y at $x = 1.0$ for various values

of time are also shown in figure 6.29(b). Figures 6.30(a) and 6.30(b) show plots of velocity u versus y at $x = 1.0$ during the evolution. Graphs of latent heat L_f versus y at $x = 1.0$ for various values of time are presented in figure 6.31. Carpet plot of T at $t = 500$ (end of tenth time step) for the whole spatial domain is shown in figure 6.32. A closeup of the carpet plot for temperature at $t = 500$ near $x = 1.0$ is shown in figure 6.33. Figure 6.34 shows carpet plot of velocity u at $t = 500$. Figure 6.35 shows carpet plot of velocity v at $t = 500$. A closeup of the carpet plot of velocity v near $x = 1.0$ is shown in figure 6.36.

From the temperature values in figures 6.29(a) and 6.29(b) we note that phase change is initiated between the fourth and fifth time step. As evolution continues to proceed beyond the fifth time step, temperature values continue to reduce in the zone where heat is extracted (in the neighborhood of $x = 1.0$) resulting in the growth of the transition region. Plots of velocity u versus y at $x = 1.0$ in figures 6.30(a) and 6.30(b) (center of the heat extraction zone) are perhaps most illustrative of the phase change process. Due to phase change i.e. solidification, the velocity field diminishes in the neighborhood of the plate and eventually becomes zero. Growth of zero velocity u it the y direction with continued evolution confirms growth of phase transition region from liquid to solid phase. We remark that some lack smoothness and minor deviations are due to lack of mesh refinement and use of lower p-levels (p=3). From the carpet plots of temperature T at $t = 500$ we clearly observe substantially reduced temperature in the vicinity of $x = 1.0$. Carpet plot of velocity u also confirms existence of zero u velocity region in the vicinity of $x = 1.0$ that progressively diminishes as we move down stream from the location $x = 1.0$. Carpet plots of v at $t = 500$ in figures 6.35 and 6.36 are also quite illustrative of the existence of phase change i.e. solidification (with zero u and v velocities) at $x = 1.0$ and in its vicinity. We observe that peak values of v velocity occurs upstream of $x = 1.0$ and away from the plate

confirming that flow is encountering obstacle in the path due to solidification. Negative v velocity past $x = 1.0$ also confirms the obstacle i.e. solidification in the path of the flow near $x = 1.0$.

The numerical studies confirm that the mathematical model proposed in this thesis incorporates physics of phase change and is capable of initiating the phase transition and its growth upon further evolution. Low I and g values ($O(10^{-6})$) confirm good accuracy of the computed evolution.

From the velocity plot in figure 6.30(a) we note that mesh refinement as well as higher p-levels are necessary for more accurate evolution during initial stages so that evolution for large values of time showing formation and propagation of complete front can be simulated with reasonable accuracy. Even with such a coarse mesh and low p-level the results confirm that the mathematical model is adequate to simulate phase-change in Eulerian description.

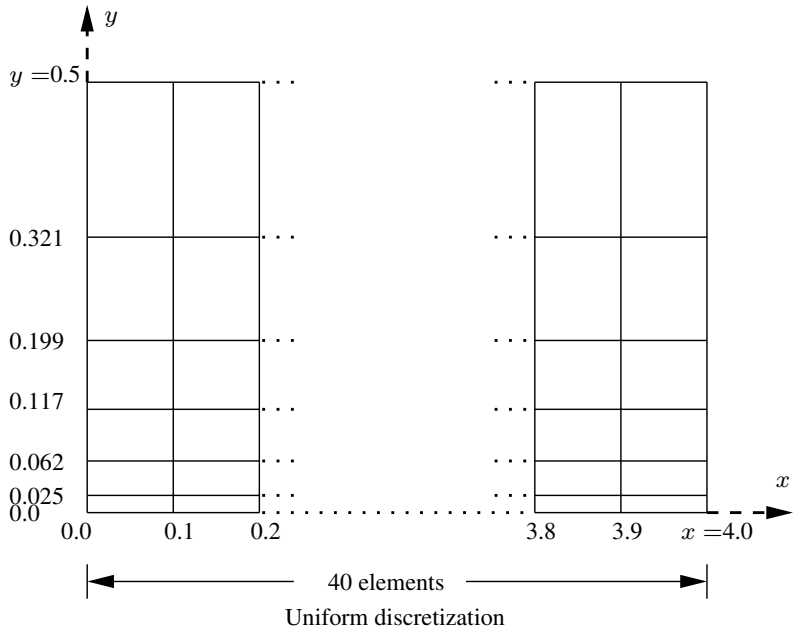

Figure 6.27: Spatial discretization for phase change: flow between parallel plates

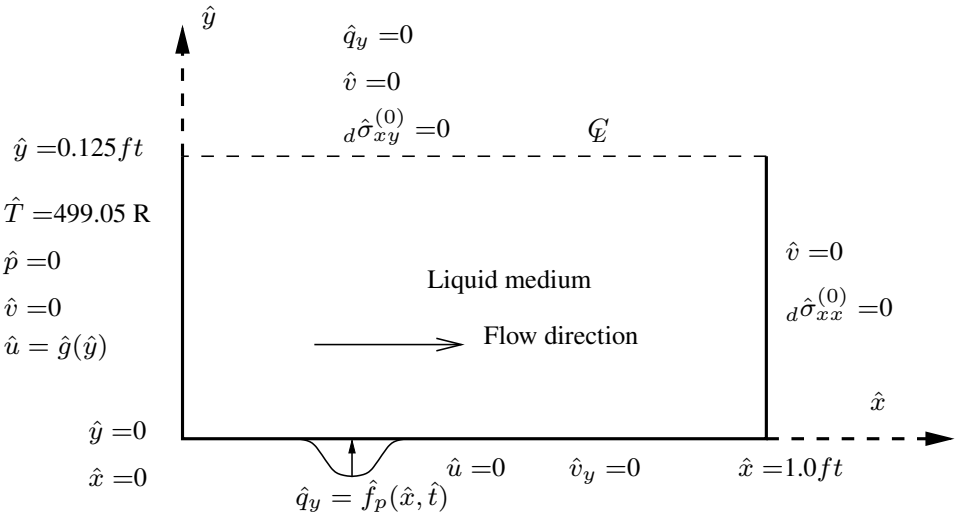

(a) Physical spatial domain

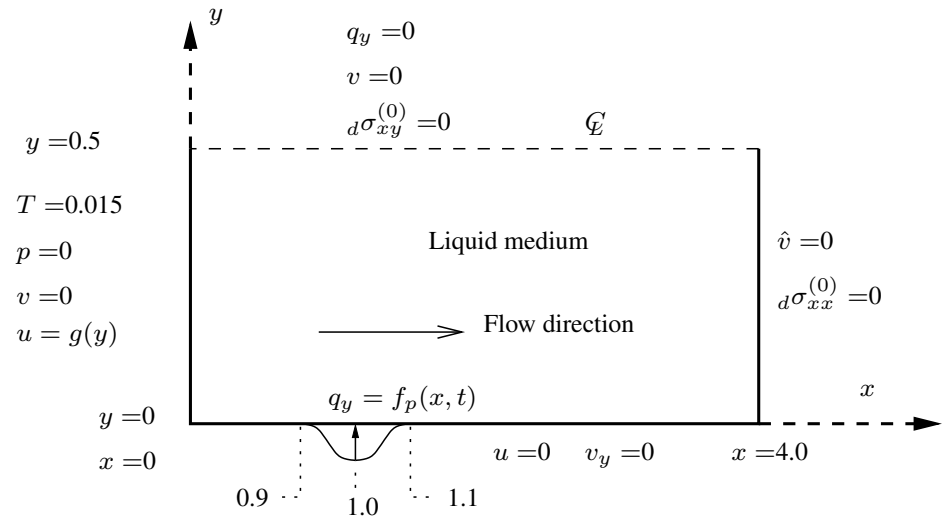

(b) Dimensionless spatial domain

Figure 6.28: Schematics and reference quantities for phase change: flow between parallel plates

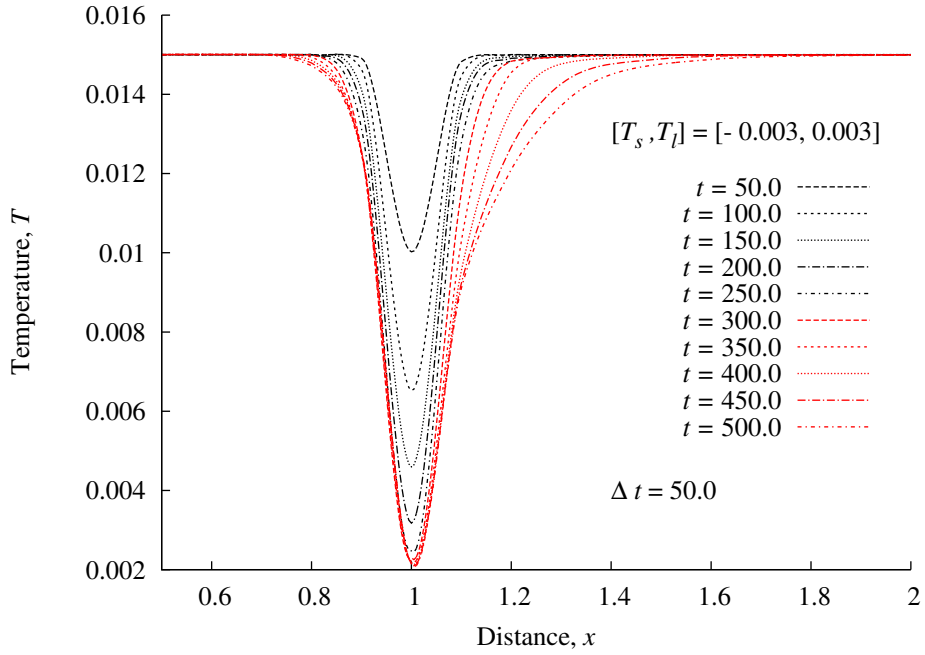

(a) Temperature T versus x at $y = 0.0$

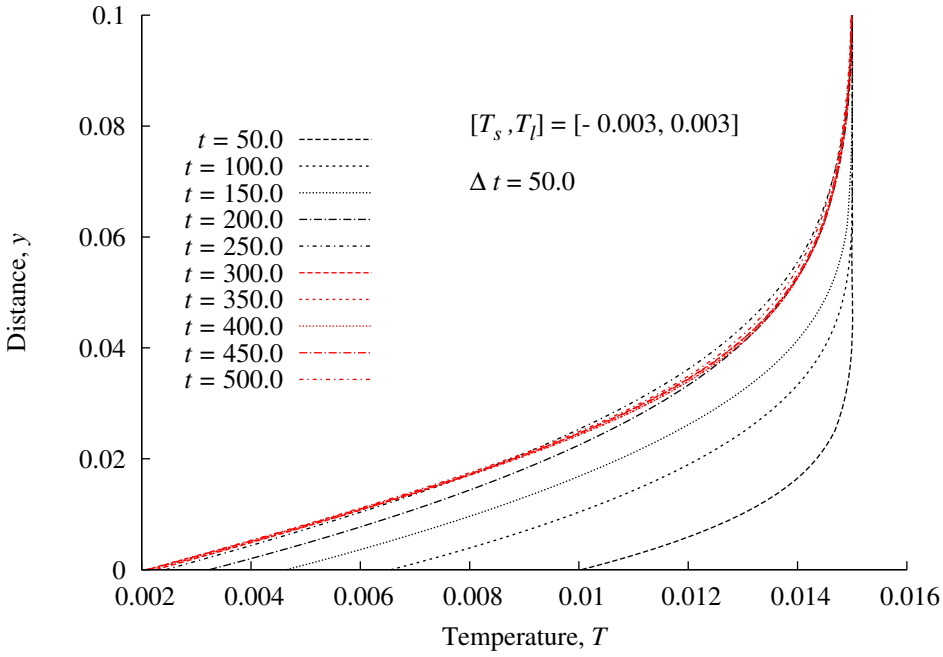

(b) Temperature T versus y at $x = 1.0$

Figure 6.29: Temperature for liquid to solid phase change between parallel plates

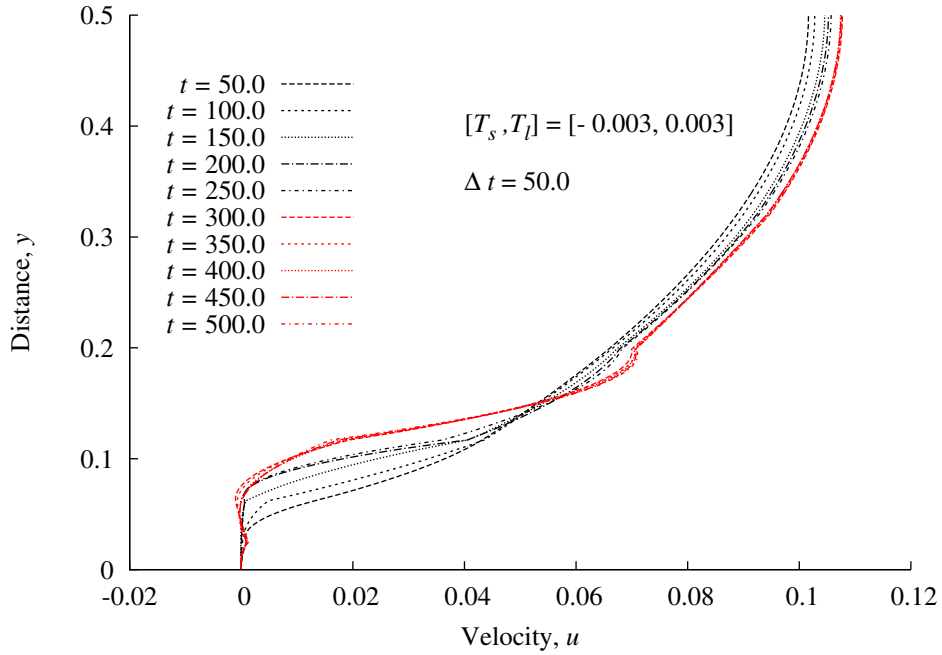

(a) Velocity u versus y at $x = 1.0$

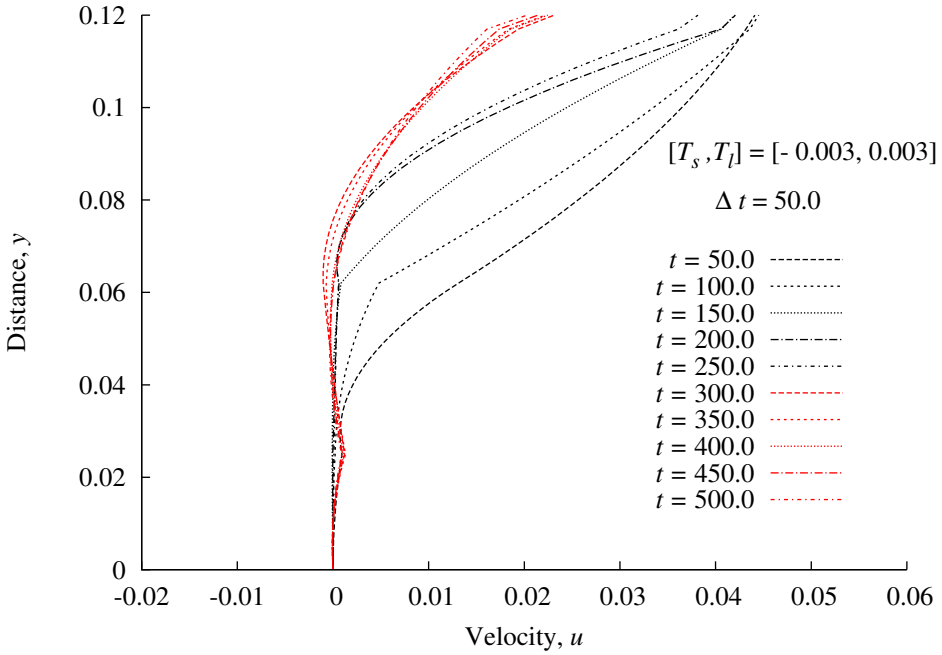

(b) Closeup of Velocity u versus y at $x = 1.0$

Figure 6.30: Velocity u versus y at $x = 1.0$

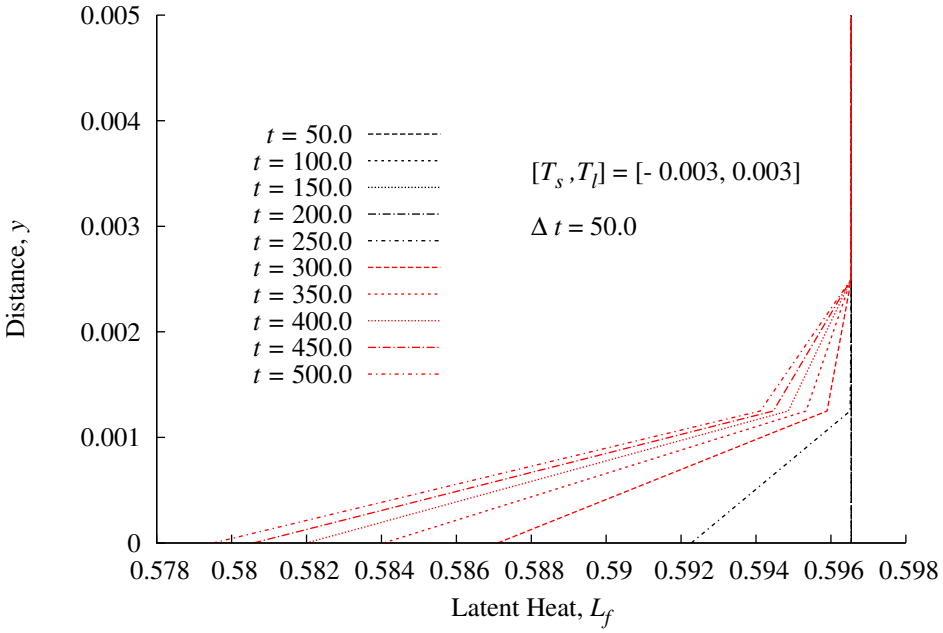

Figure 6.31: Latent heat L_f versus y at $x = 1.0$

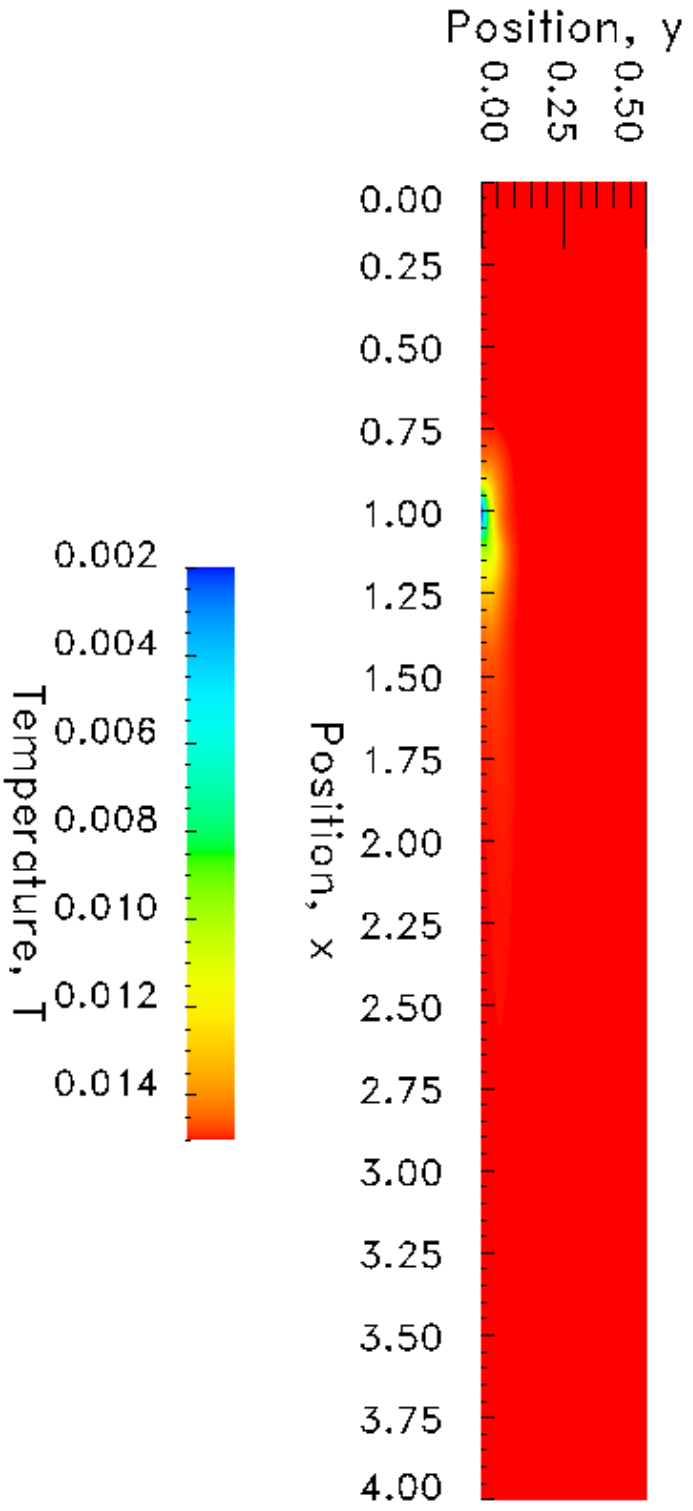

Figure 6.32: Temperature T at $t = 500.0$, end of tenth time step

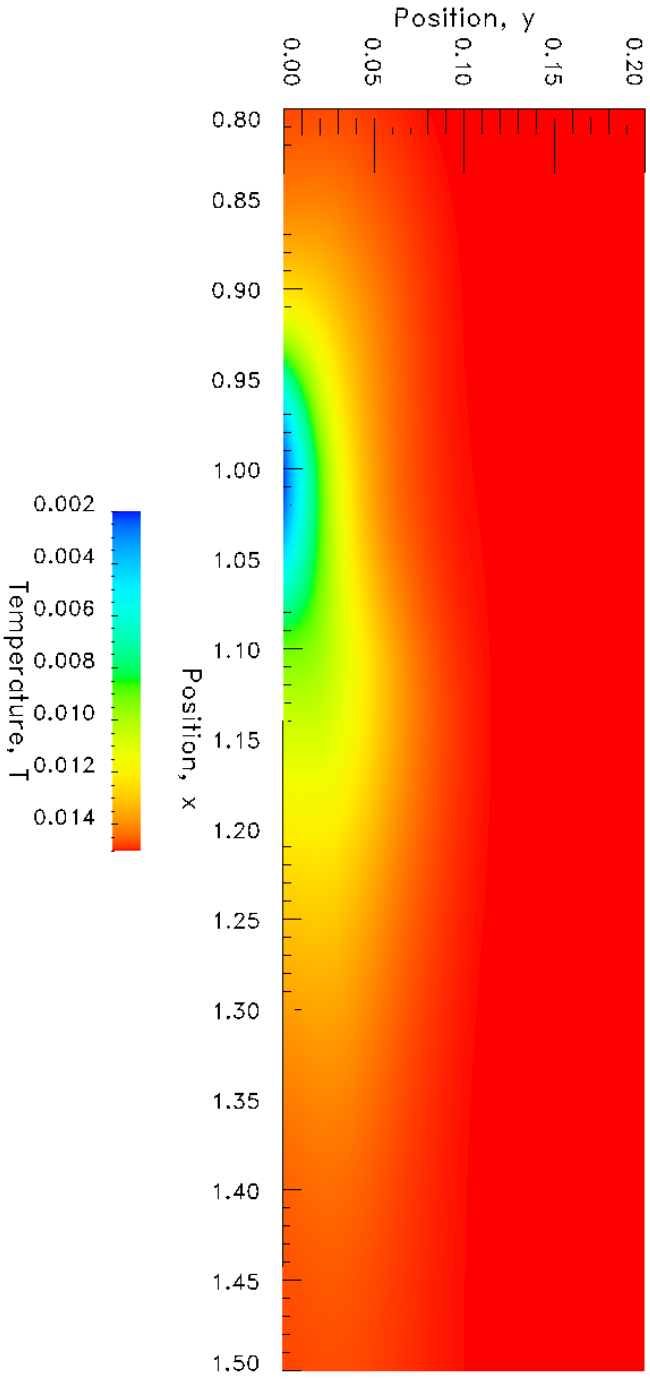

Figure 6.33: Closeup of Temperature T at $t = 500.0$, end of tenth time step

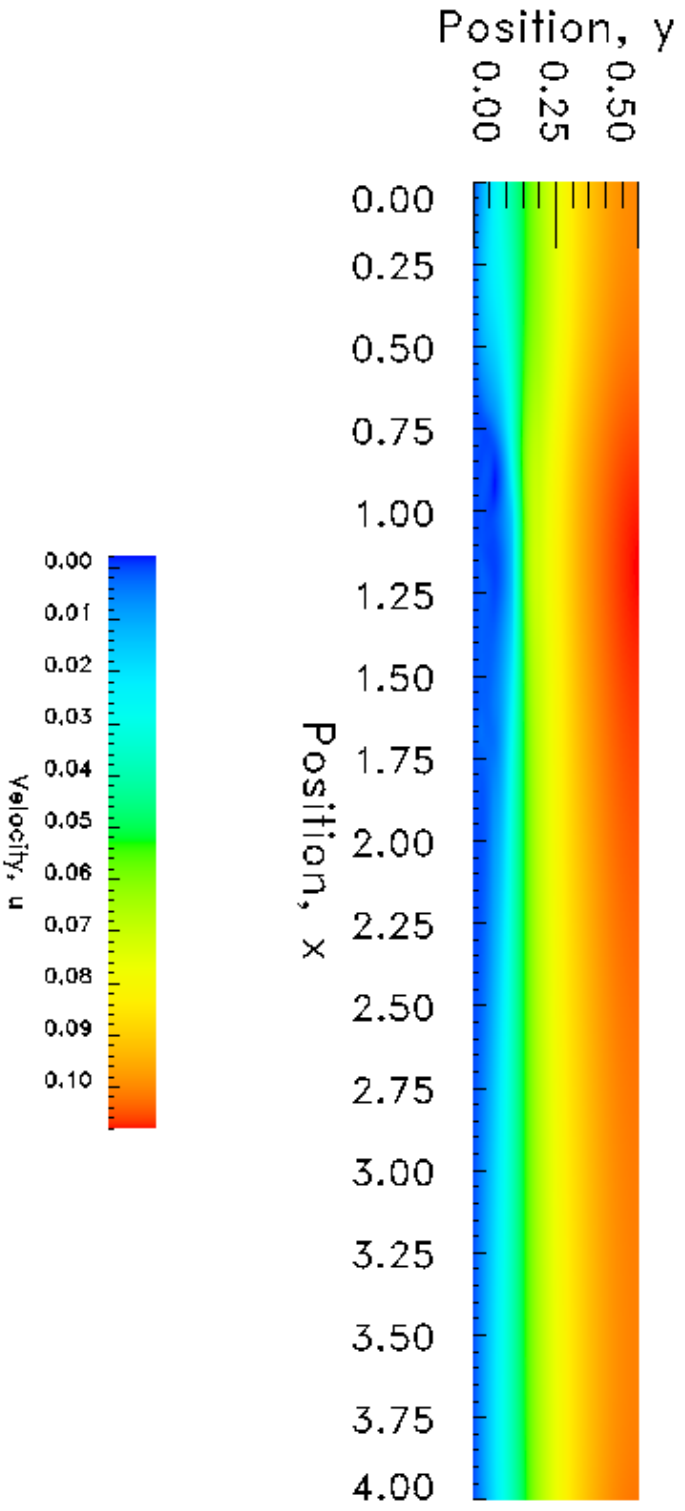

Figure 6.34: Velocity u at $t = 500.0$, end of tenth time step

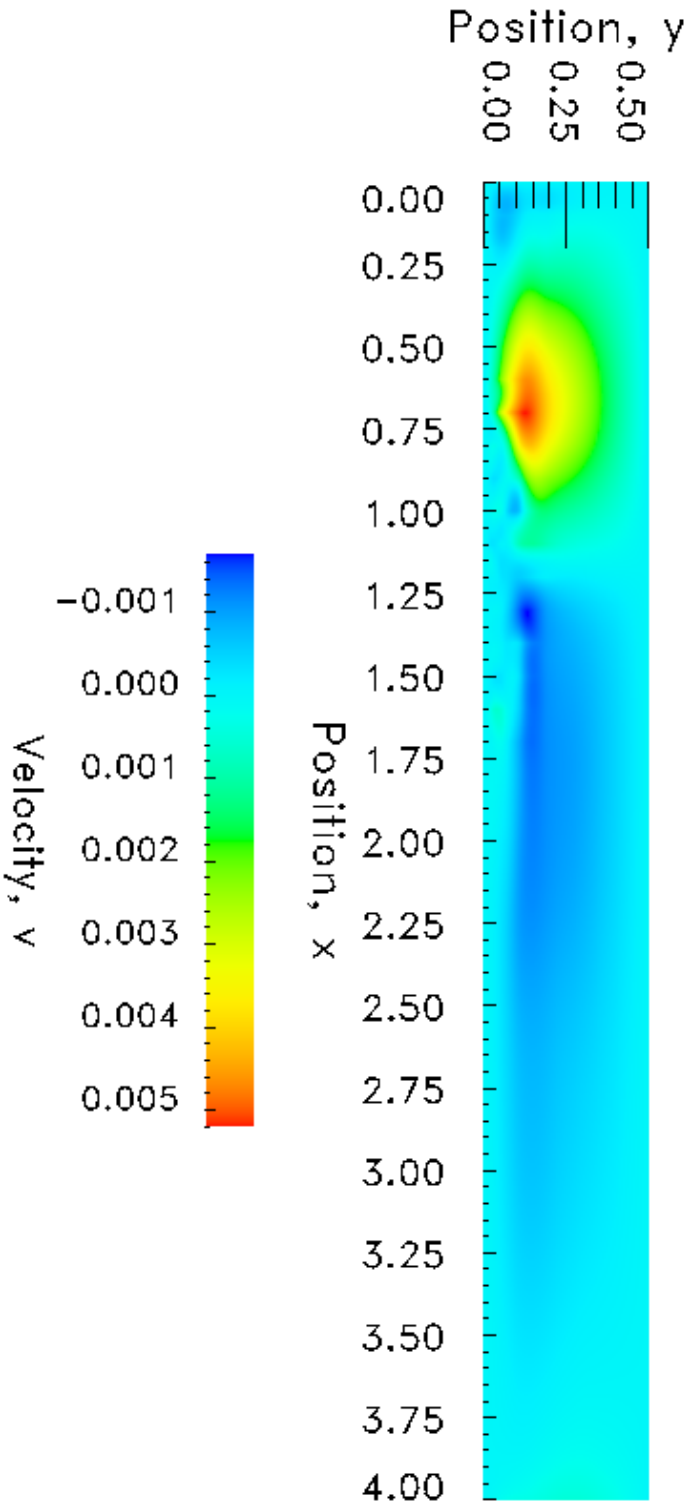

Figure 6.35: Velocity v at $t = 500.0$, end of tenth time step

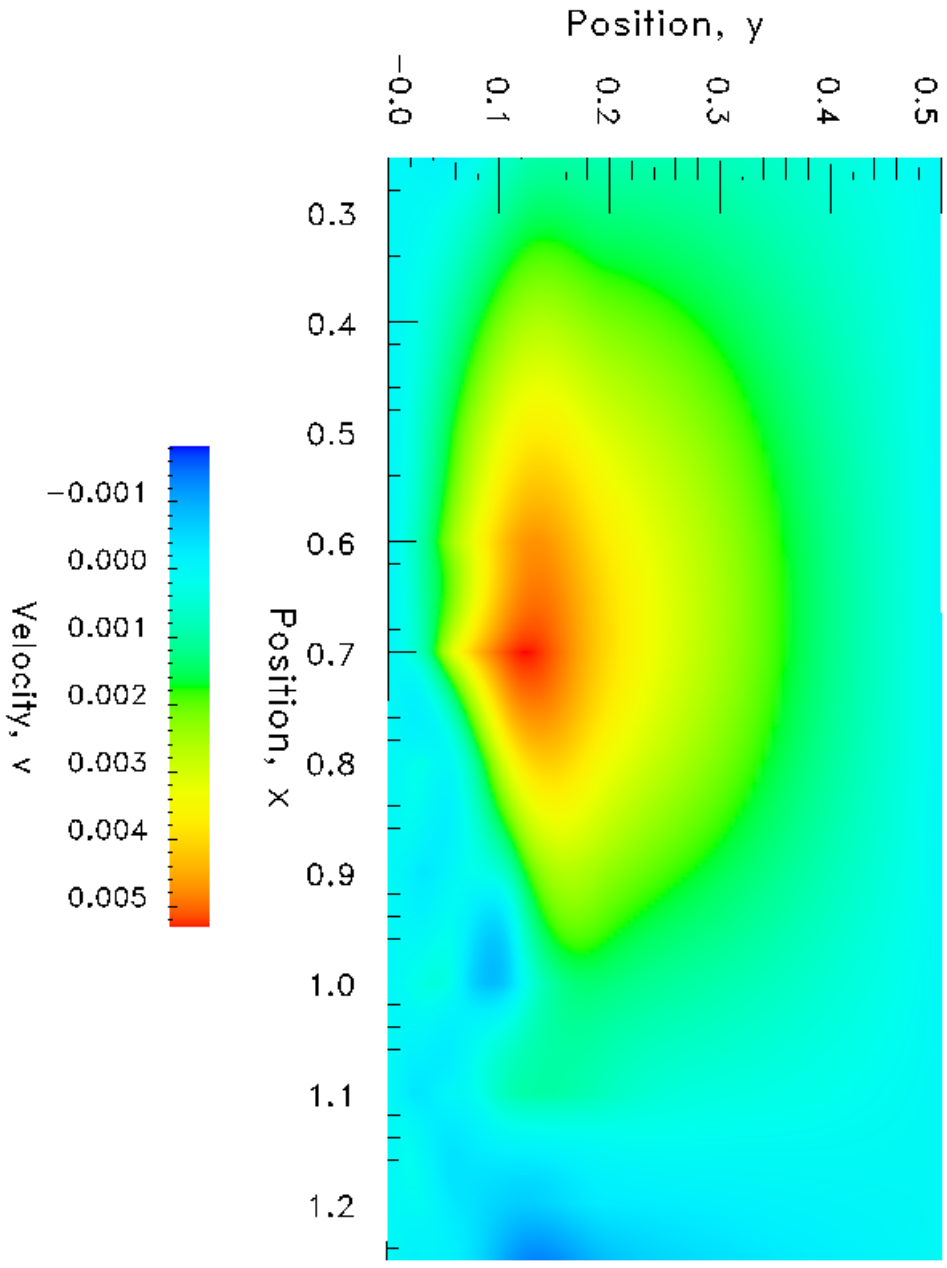

Figure 6.36: Closeup of Velocity v at $t = 500.0$, end of tenth time step

Chapter 7

Summary and Conclusions

In this thesis numerical simulation of liquid-solid or solid-liquid phase change phenomena have been presented in $\mathbb{R}^1$ and $\mathbb{R}^2$ using a smooth interface approach. Summary of this work and some conclusions drawn from this work are presented in this chapter. The mathematical models of the phase-change physics are constructed in Lagrangian description with the assumptions of homogeneous and isotropic medium, no flow, and free boundaries as well as in Eulerian descriptions in which velocity field and stress field are not zero.

In Lagrangian descriptions, continuity and the momentum equations are identically satisfied. Thus, only the first law of thermodynamics (energy equation), Fourier heat conduction law and the physics of phase change form the basis for deriving the mathematical model of phase change phenomena. The energy equation is expressed in terms of specific total energy and heat conduction. Fourier heat conduction law and the specific total energy, expressed in terms of internal energy and latent heat are substituted in the energy equation to derive a single non-linear PDE in temperature containing up to second order derivatives of the temperature with respect to spatial coordinates but only the first order derivatives of

the temperature with respect to spatial coordinates but only the first order derivatives of the temperature and latent heat with respect to time. Specific heat c_p, density ρ, thermal conductivity k and the latent heat of fusion L_f are all assumed to be functions of temperature. The physics of phase change is incorporated through a smooth interface between the two phases. We assume that the phase change occurs over a small temperature range $[T_s, T_l]$ referred to as the interface or transition region. In the transition region ρ, c_p, k and L_f are assumed to be continuous and differentiable functions of temperature. Outside the transition region, ρ, c_p and k have their respective values in the solid or liquid phases. Using $L_f = L_f(T)$, the time derivative of L_f in the energy equation is replaced by the derivative of the latent heat with respect to temperature and the time derivative of temperature. This yields the final form of the energy equation as a single non-linear diffusion equation in the temperature. Hence the location of the interface separating the two phases, its initiation from commencement of the evolution and the propagation of the interface location in the spatial domain during evolution are all intrinsic in this mathematical model. The energy equation in temperature can also be recast as a system of first order PDEs using temperature and heat flux(es) as dependent variables. This may be convenient in finite element processes when the numerical solution of lower class are sought. L_f is not used as a dependent variable as in reference [23].

When using this mathematical model, no special methods are required for tracking the front. In sharp interface and phase field models, specification of the interface separating the two phases is essential as initial condition i.e. these models can not simulate initiation of the interface. In the present mathematical model, formation of the transition region from the commencement of the evolution and the two phases separated by the transition region upon further evolution is inherent in the mathematical model. It is well known that sharp

interface model incorporating singular solutions are numerically most difficult without excessive upwinding that destroys the sharp fronts. The phase field models on the other hand require a priori knowledge of a potential that is highly dependent on the application in addition to ICs defining the interface location at the commencement of the evolution. None of these restrictions, limitations and assumptions are present in the mathematical model considered here in the Lagrangian descriptions.

In Eulerian description, the mathematical model consists of continuity, momentum equations, energy equation and the constitutive equations for deviatoric Cauchy stress tensor and heat flux. The liquid phase (water) is assumed to be Newtonian fluid with constant transport properties except in the transition region in which all transport properties are a continuous and differentiable functions of temperature. The solid phase (ice) is assumed to be a hypoelastic solid with constant material properties except in the transition zone in which we assume these to be continuous and differentiable functions of temperature. In the solid phase, continuity is replaced with the pressure constraint equation. When deriving momentum and energy equations in the transition region we assume the matter to be homogeneous and isotropic with variable material properties. The continuity equation in the transition region is considered to be the sum of divergence free velocity field and pressure constraint equation with volume fractions determined based on the temperature T between T_s and T_l. Similar volume fraction rule is applied to the constitutive equation for deviatoric stress in the transition region. Fourier heat conduction law is assumed to hold in the transition region. This mathematical model can be derived as a system of PDEs in terms of velocities, pressure, deviatoric Cauchy stress and temperature or as system of first order PDEs by introducing heat flux(es) as dependent variables.

The numerical solutions of non-linear PDEs in both Lagrangian and Eulerian descrip-

tions are obtained using space-time least squares finite element method in ***h,p,k*** framework [6, 8, 9, 36–39]. Space-time least squares finite element processes yield unconditionally stable computations during the entire evolution regardless of the choice of h and p. The algebraic systems contain symmetric and positive definite coefficient matrices. The least squares functional I and its proximity to zero is an absolute measure of error in the computed evolution without the knowledge of a theoretical solution. This is an extremely important and intrinsic feature of the computational methodology used in the present work. The evolution described by the IVP is computed for an increment of time using a space-time strip (in $\mathbb{R}^1$) and a space-time slab (in $\mathbb{R}^2$) with time marching. We time march only when the least squares functional for the current increment of time is sufficiently close to zero. Thus, within the framework of computational infrastructure used here 'time accurate' evolutions are possible. The least squares functional values for all four model problems used in the present work are ensured to be sufficiently low during the entire evolution. This establishes good accuracy of the evolutions and their very close proximity to 'time-accurate' evolutions.

In the model problems in $\mathbb{R}^1$, phase change in Lagrangian descriptions, at the commencement of the evolution we either have a solid phase or a liquid phase. The numerical studies conducted using $C^{11}(\bar{\Omega}^e_{xt})$ local approximations demonstrate formation of the transition region, its propagation during evolution leading to two phases separated by the transition region. The studies demonstrate that the thin transition region does not diffuse during evolution (establishing lack of numerical dispersion in the computational method used in this work). ρ, c_p, k and L_f have their respective values in the solid and liquid phases. In the transition region, ρ, c_p, k and L_f are continuous and differentiable and are assumed to be a polynomial of fifth degree in temperature. Numerical studies are also presented to

demonstrate that the width $[T_s, T_l]$ of the transition region does not influence the location of interface marked by the center of $[T_s, T_l]$. However, spatial discretization is influenced by this choice. Phase change numerical studies (solid-liquid, liquid-solid) in $\mathbb{R}^2$ using first order system of PDEs in Lagrangian descriptions with $C^{00}(\bar{\Omega}^e_{xt})$ local approximations show formation of rather complete transition region and its propagation. Low values of I and g during evolution confirm good accuracy of the computed solutions. Due to smoothness of the evolution $C^{00}(\bar{\Omega}^e_{xt})$ local approximations perform satisfactorily.

Investigations are presented using mathematical model in the Eulerian description (first order systems of PDEs with $C^{00}(\bar{\Omega}^e_{xt})$ local approximations). Flow between parallel plates has been used as a model problem. We summarize the findings in the following.

(*i*) In a process without externally applied heat flux, viscous dissipation is simulated easily and accurately for relatively coarse discretization using only p-level of 3. The velocity field and the temperature field remain uncoupled.

(*ii*) In the presence of viscous dissipation and externally applied heat flux, finer discretization and higher p-levels are needed to obtain converged evolutions. The converged solutions in this case also confirm that velocity field and the temperature field remain uncoupled.

(*iii*) In the solid phase the continuity equation must be replaced with pressure constraint equation. This is essential due to the fact that for hypoelastic solid matter the mechanical pressure is the mean normal Cauchy stress. Numerical studies confirm that using continuity equation results in failure in obtaining numerical solutions.

(*iv*) Phase change for flow of water between parallel plates with partially cooled plates

clearly demonstrates:

(a) Initiation of transition region

(b) Velocity field progressively approaching zero as the evolution proceeds towards solid phase.

(c) Relatively coarse mesh and $p = 3$ used in this study are highly inadequate to demonstrate complete formation of the transition region and its propagation in the y direction. But the validity of the mathematical model and the computational infrastructure is demonstrated clearly.

(d) Unfortunately due to limited computational resources, numerical studies with highly graded and refined discretization with higher p-levels are not possible at present but are planned in near future.

Surana et.al. [6, 9, 40, 42, 43] has demonstrated the benefits of using a single PDE in temperature employing approximations in higher order spaces. This can be done easily.

In summary, the work presented in this thesis has the following important features: (i) Derivations of the mathematical models in Lagrangian and Eulerian descriptions. (ii) Incorporating the phase-change physics through a transition region in which ρ, c_p, k, and L_f are continuous and differentiable, thereby avoiding singular nature of the evolution as in case of sharp approach. (iii) The mathematical models permit initiation of the interface i.e. transition region which can not be done in the other two methods used commonly for phase change problems. (iv) The models permit variable transport properties. (v) No special techniques are needed to track the solid-liquid or liquid-solid fronts as these features are intrinsic in the mathematical models. (vi) Computational infrastructure ensures unconditionally stable computations during the entire evolution and provides a computed

measure of the solution accuracy which enables computations of time accurate evolutions. The mathematical models in Eulerian description permitting the study of phase change phenomena in flowing medium with constrained boundaries resulting in non-zero velocity and stress field is of extreme practical importance. The mathematical model presented here has some assumptions but is able to describe the phase change physics adequately. Further refinement of the mathematical model in Eulerian description and numerical studies with refined discretizations and higher p-levels are currently in progress in CML.

Bibliography

[1] K. R. Rajagopal and L. Tao. *Mechanics of Mixtures*. World Scientific, River Edge, NJ, 1995.

[2] M. Massoudi, A. Briggs, and C. C. Hwang. Flow of a dense particulate mixture using a modified form of the mixture theory. *Particulate Science and Technology*, 17:1–27, 1999.

[3] Mehrdad Massoudi. Constitutive relations for the interaction force in multicomponent particulate flows. *International Journal of Non-Linear Mechanics*, 38:313–336, 2003.

[4] John W. Cahn and John E. Hilliard. Free energy of a nonuniform system. i. interfacial free energy. *The Journal of Chemical Physics*, 28(2):1015–1031, 1958.

[5] Lev D. Landau, Evgenij Michailovič Lifšic, and Lev P. Pitaevskij. *Statistical Physics: Course of Theoretical Physics*. Pergamon Press plc, London, 1980.

[6] K.S. Surana and J.N. Reddy. *Mathematics of computations and finite element method for initial value problems*. Book manuscript in progress, 2012.

[7] T. Belytschko and T.J.R. Hughes. *Computational Methods in Mechanics*. North Holland, 1983.

[8] B.C. Bell and K.S. Surana. A space-time coupled p-version lsfef for unsteady fluid dynamics. *International Journal of Numerical Methods in Engineering*, 37:3545–3569, 1994.

[9] K.S. Surana, J.N. Reddy, and S. Allu. The k-version of finite element method for initial value problems: mathematical and computational framework. *International Journal of Computational Methods in Engineering Science and Mechanics*, 8:123–136, 2007.

[10] J. Stefan. *Ober einige Probleme der Theorie der Warmeleitung*. Sitzungsber. Akad. Wiss. Wien, Math.-Naturwiss. Kl., 1889.

[11] L.I. Rubinstein. *The Stefan Problem*. American Mathematical Society, Providence, twenty seventh edition, 1994.

[12] H.S. Carslaw and J.S. Jaeger. *Conduction of Heat in Solids*. Oxford University Press, New York, second edition, 1959.

[13] K. Krabbenhoft, L. Damkilde, and M. Nazem. An implicit mixed enthalpy-temperature method for phase-change problems. *Heat Mass Transfer*, 43:233–241, 2007.

[14] Sin Kim, Min Chan Kim, and Won-Gee Chun. A fixed grid finite control volume model for the phase change heat conduction problems with a single-point predictor-corrector algorithm. *Korean J. Chem. Eng.*, 18(1):40–45, 2001.

[15] V.R. Voller, M. Cross, and N. C. Markatos. An enthalpy method for convection/diffusion phase change. *International Journal for Numerical Methods in Engineering*, 24(1):271–284, 1987.

[16] R. A. Lambert and R. H. Rangel. Solidification of a supercooled liquid in stagnation-point flow. *International Journal of Heat and Mass Transfer*, 46(21):4013–4021, 2003.

[17] Nabeel Al-Rawahi and Gretar Tryggvason. Numerical simulation of dendritic solidification with convection: Two-dimensional geometry. *Journal of Computational Physics*, 180(2):471–496, 2002.

[18] E. Pardo and D. C. Weckman. A fixed grid finite element technique for modelling phase change in steady-state conduction–advection problems. *International Journal for Numerical Methods in Engineering*, 29(5):969–984, 1990.

[19] D. M. Anderson, G. B. McFadden, and A. A. Wheeler. A phase-field model of solidification with convection. *Physica D: Nonlinear Phenomena*, 135(1-2):175–194, 2000.

[20] Y. Lu, C. Beckermann, and J.C. Ramirez. Three-dimensional phase-field simulations of the effect of convection on free dendritic growth. *Journal of Crystal Growth*, 280(1-2):320–334, 2005.

[21] C. Beckermann, H. J. Diepers, I. Steinbach, A. Karma, and X. Tong. Modeling melt convection in phase-field simulations of solidification. *Journal of Computational Physics*, 154(2):468–496, 1999.

[22] Curtis M. Oldenburg and Frank J. Spera. Hybrid model for solidification and convection. *Numerical Heat Transfer Part B: Fundamentals*, 21:217–229, 1992.

[23] Michael Truex. Numerical simulation of liquid-solid, solid-liquid phase change using finite element method in ***h,p,k*** framework with space-time variationally consistent integral forms. Master's thesis, University of Kansas, Department of Mechanical Engineering, July 2010.

[24] Y. Ding, J.A. Gear, and K.N. Tran. A finite element modeling of thermal conductivity fabrics embedded with phase change material. *Heat Mass Transfer*, 43:233–241, 2007.

[25] G. Caginalp. Stefan and hele-shaw type models as asymptotic limits of the phase-field equations. *Phys. Rev. A*, 39:5887–5896, Jun 1989.

[26] M. Fabbri and V.R. Voller. The phase-field method in sharp-interface limit: A comparison between model potentials. *Journal of Computational Physics*, 130:256–265, 1997.

[27] Karan S. Surana, Ma Yongting, Albert Romkes, and J. N. Reddy. Development of mathematical models and computational framework for multi-physics interaction processes. *Mechanics of Advanced Materials & Structures*, 17(7):488 – 508, 2010.

[28] Karan S. Surana, Ma Yongting, Albert Romkes, and J. N. Reddy. The rate constitutive equations and their validity for progressively increasing deformation. *Mechanics of Advanced Materials & Structures*, 17(7):509 – 533, 2010.

[29] K.S. Surana and J.N. Reddy. *Continuum Mechanics*. Book manuscript in progress, 2012.

[30] K.S. Surana, D. Nuñez, J.N. Reddy, and A. Romkes. Rate constitutive theory for ordered thermoelastic solids. *Annals of Solid and Structural Mechanics (under review)*, 2012.

[31] M. Gelfand and S.V. Foming. *Calculus of Variations*. Dover, New York, 2000.

[32] S.G. Mikhlin. *Variational methods in mathematical physics*. Pergamon Press, New York, 1964.

[33] J.N. Reddy. *Functional analysis and variational methods in applied mechanics*. McGraw-Hill, New York, 1986.

[34] J.N. Reddy. *Energy principles and variational methods in applied mechanics*. John Wiley, New York, 2002.

[35] C. Johnson. *Numerical solution of partial differential equations by finite element method*. Cambridge University Press, 1987.

[36] K.S. Surana, S. Allu, J.N. Reddy, and P.W. Tenpas. Least squares finite element processes in *hpk* mathematical framework for non-linear conservation law. *International Journal of Numerical Methods in Fluids*, 57(10):1545–1568, 2008.

[37] D.L. Winterscheidt and K.S. Surana. p-version least squares finite element formulation for two dimensional incompressible fluid flow. *International Journal of Numerical Methods in Fluids*, 18:43–69, 1994.

[38] B.C. Bell and K.S. Surana. p-version least squares finite element formulation of two dimensional incompressible non-newtonian isothermal and non-isothermal fluid flow. *International Journal of Numerical Methods in Fluids*, 18:127–167, 1994.

[39] D.L. Winterscheidt and K.S. Surana. p-version least squares finite element formulation for burgers equation. *International Journal for Numerical Methods in Engineering*, 36:3629–3646, 1993.

[40] K.S. Surana, A. Ahmadi, and J.N. Reddy. k-version of finite element method for non-self-adjoint operators in bvp. *International Journal of Computational Engineering Science*, 4(4):737–812, 2003.

[41] K. S. Surana, L. R. Anthoni, S. Allu, and J. N. Reddy. Strong and weak form of governing differential equations in least squares finite element processes in hpk framework. *International Journal of Computational Methods in Engineering Science and Mechanics*, 9:1–24, 2008.

[42] K.S. Surana, A. Ahmadi, and J.N. Reddy. k-version of finite element method for non-linear differential operators in bvp. *International Journal of Computational Engineering Science*, 5(1):133–207, 2004.

[43] K.S. Surana, A. Ahmadi, and J.N. Reddy. k-version of finite element method for self-adjoint operators in bvp. *International Journal of Computational Engineering Science*, 3(2):155–218, 2002.